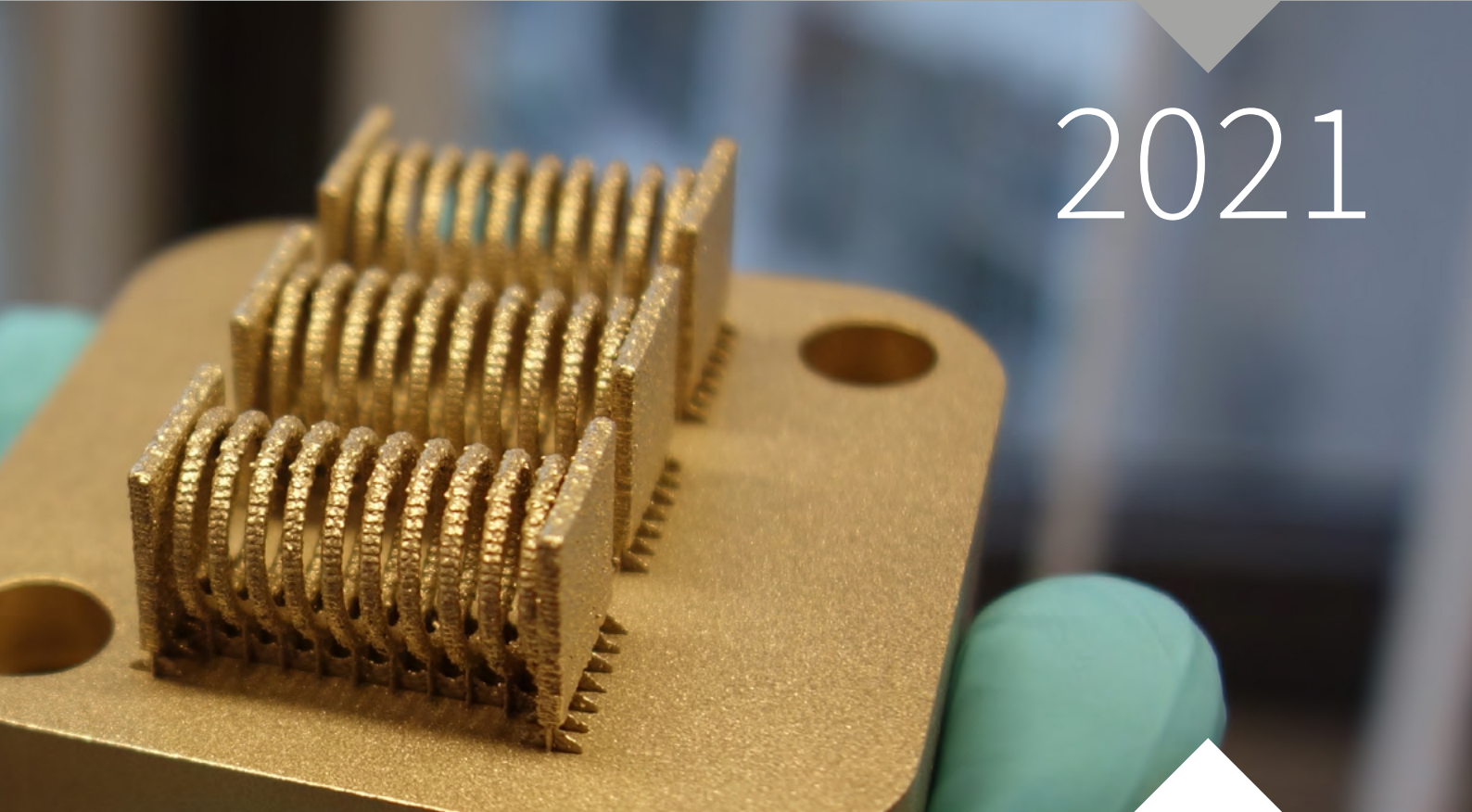


Jahresbericht Annual Report

2021



Das Bild auf dem Umschlag zeigt additiv gefertigte Zugfederprototypen zur Veranschaulichung des Einweg-Formgedächtniseffekts bei einer kupferbasierten Formgedächtnislegierung. Foto: Tobias Gustmann

The cover picture shows additively manufactured tension spring for illustrating the one way-shape memory effect of a copper-based shape memory alloy.

Photo: Tobias Gustmann

Liebe Leserinnen und Leser,

große Erwartungen haben das Jahr 2021 geprägt. Wissenschaft war gefragt. Im Zusammenhang mit der Pandemie und im Umgang mit dem Klimawandel wurde sie im Wechsel gefeiert und kritisiert. Auch bei der Suche nach einem nachhaltigen Lebensstil ist sie unablässig gefordert. Die großen Aufgaben unserer Zeit bestimmen unsere Denkrichtung und wir fragen uns zu Recht: Wie können und wie wollen wir unsere Zukunft gestalten?

Neben der gewohnten Auswahl an Forschungsbeiträgen beleuchten wir daher in diesem Heft insbesondere, wo wir Potential für eine nachhaltige Materialforschung erkannt haben und an welcher Stelle wir einen Beitrag für eine ressourcenschonende und generationsgerechte Zukunft leisten. Wir möchten all unseren Förderern und Partnern danken, die uns eine exzellente Forschung, innovative Methodik und die Ausbildung der nächsten Generation ermöglichen.

Bleiben Sie neugierig und gesund!

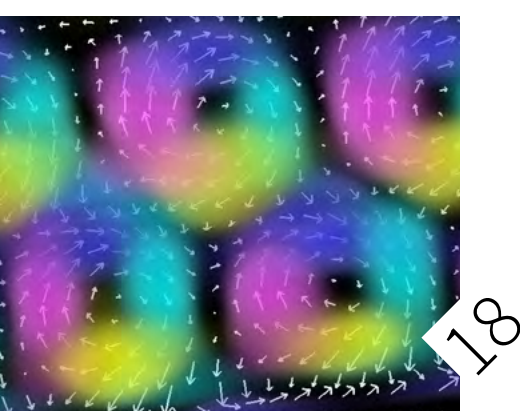


Juliane Schmidt, Kaufmännische Direktorin und Prof. Dr. Bernd Büchner, Wissenschaftlicher Direktor.
Juliane Schmidt, Administrative Director and Prof. Dr. Bernd Büchner, Scientific Director.

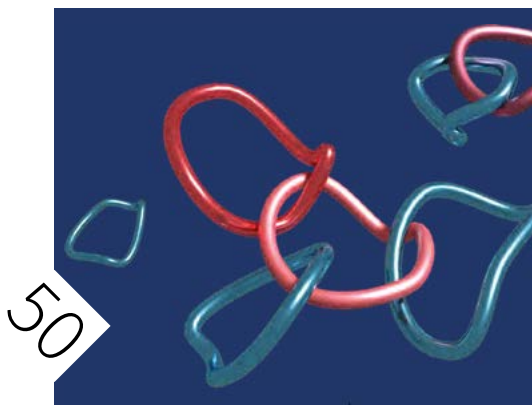


Inhalt Contents

- 4 **Jahresrückblick 2021**
Review 2021
- 10 **Unser Forschungsprogramm**
Our Research Program
- 12 **Schwerpunkt 2021: Nachhaltigkeit**
Focus 2021: Sustainability
- 18 **Wissenschaftliche Beiträge**
Research Highlights
- 18 **Forschungsgebiet 1: Funktions-Quanten-Materialien**
Research Area 1: Functional Quantum Materials
- 20 *Unveiling the three-dimensional magnetic texture of skyrmion tubes*
- 24 *Saving energy by voltage control of ferrimagnets*
- 28 *Kitaev exchange in a geometrically frustrated cobaltate*
- 32 *Creating ferroic micropatterns through geometrical transformation*
- 36 **Forschungsgebiet 2: Funktion durch Nanoskaligkeit**
Research Area 2: Function through size
- 38 *Towards tellurium-free thermoelectric modules for power generation from low-grade heat*
- 42 *Miniaturized microcoils for NMR spectroscopy with high resolution and sensitivity*
- 46 *Medical imaging of microrobots: From *in vitro* to *in vivo**



- 50 Forschungsgebiet 3: Quantenphänomene im Nanomaßstab
Research Area 3: Quantum Effects at the Nanoscale
- 52 *Self-assembled monolayers of fullerene-based single-molecule magnets on graphite and graphene*
- 56 *2D topological quantum magnets and bosonization duality for massless Dirac fermions*
- 60 *Electric circuits access a new regime of topology*
- 64 *Origami perovskite microtube cavity for programmable three-dimensional lasing*
- 68 Forschungsgebiet 4: Vom Material zum Produkt
Research Area 4: Towards Products
- 70 *Environmentally friendly cathode materials for cost-effective Lithium-ion batteries*
- 74 *Laser powder bed fusion of ductile Cu-Al-Mn shape memory alloys - From general processing to functional parts*
- 78 *Additive manufactured low modulus Ti-Nb with tailored microstructure for load-bearing bone implants*
- 82 *Elite electrons*
- 86 **Organigramm**
Organization Chart
- 88 **Zahlen und Fakten**
Facts and Figures



Jahresrückblick 2021

Auch 2021 war ein Jahr mit pandemiebedingten Herausforderungen, Hindernissen und Behelfslösungen. Anhaltende Reise- und Kontaktbeschränkungen zwangen Konferenzen, Seminare, neue Begegnungen und hitzige Diskussionen in Online-Formate, die nur ein schwacher Ersatz für das Gefühl des Dabeiseins sind. Das führt uns deutlich vor Augen, wie wichtig der persönliche Austausch und die Kommunikation von Mensch zu Mensch sowohl unter den Fachleuten als auch mit der Öffentlichkeit für den wissenschaftlichen Betrieb sind.

Am gravierendsten haben wir diese Einschränkung bei der turnusmäßigen Evaluierung durch den Senat der Leibniz-Gemeinschaft erlebt. Dabei wird alle sieben Jahre von einer internationalen Expertenkommission geprüft, ob die Voraussetzungen für eine gemeinsame Bund-Länder-Förderung des Instituts weiterhin gegeben sind. Diese bestehen im Wesentlichen in der wissenschaftlichen Exzellenz, der überregionalen Bedeutung der Forschung und im gesamtstaatlichen wissenschaftspolitischen Interesse. Pandemiebedingt musste die Evaluierung des IFW am 6. Juli 2021 in einem Ersatzverfahren als rein virtuelle Veranstaltung durchgeführt werden. Das bedeutet, dass weder Posterdiskussionen und Laborbesichtigungen noch Gespräche mit Mitarbeiterinnen und Mitarbeitern möglich waren, um die Qualität unserer Arbeit festzustellen. Das Verfahren stützte sich lediglich auf die schriftlichen Unterlagen und auf ein zweistündiges Online-Gespräch mit der Institutsleitung. Umso mehr freut es uns, dass die Gesamtleistung des Instituts und insbesondere die Forschungsleistungen weiterhin als erfolgreich und herausragend bewertet werden. Auch das strategische Konzept zur mittel- und langfristigen Weiterentwicklung des IFW wird prinzipiell unterstützt, inklusive der Pläne zur strategischen Erweiterung unseres Instituts.

Review of 2021

2021 was another year of pandemic-related challenges, obstacles and workarounds. Continued travel and contact restrictions forced conferences, seminars, new meetings, and heated discussions into online formats that are poor substitutes for the feeling of taking part on-site. This makes us realize the importance of face-to-face interaction and communication, both among professionals and with the public, to the scientific enterprise.

We have experienced this restriction most seriously during the regular evaluation by the Senate of the Leibniz Association. Every seven years, an international commission of experts examines whether the conditions for joint federal and state funding of the institute continue to be met. These are essentially scientific excellence, the supra-regional importance of the research and the national scientific policy interest. Due to the pandemic, the evaluation of the IFW on July 6, 2021 had to be held as a purely virtual event in a substitute procedure. This means that there were no poster discussions, no laboratory visits and no meetings with staff members possible to determine the quality of our work and to experience the spirit at the institute. The procedure was based only on the written documents and on a two-hour online conversation with the institute's management. We are all the more pleased that the overall performance of the institute and in particular its research achievements continue to be rated as successful and outstanding. The strategic concept for the medium and long-term further development of the IFW is also supported in principle, including the plans for the strategic enlargement of the IFW.

With joint appointment procedures of professorships, we are setting an important course for future both for research at IFW and for cooperation with universities. In 2021, we were able to make good progress with the appointment

Mit der gemeinsamen Berufung von Professoren werden naturgemäß wichtige Weichen für die zukünftige Forschung am IFW, aber auch für die Kooperation mit den Universitäten gestellt.

2021 konnten wir die Berufungsverfahren für zwei freie Direktorenstellen und zwei zusätzliche W2-Positionen in unterschiedlichen Stadien gut vorantreiben. Das gemeinsame Verfahren zur Besetzung der W2-Stiftungsprofessur für Elektronenoptik an der Fakultät Physik der TU Dresden steht kurz vor dem Abschluss. Wir dürfen hoffen, dass diese Professur, die mit einer Forschungsgruppenleiter-Position am IFW verbunden ist, in der ersten Jahreshälfte 2022 besetzt sein wird. Auch im Verfahren zur Besetzung der W3-Professur für Materialchemie, verbunden mit der Institutsleitung des IFW-Instituts für Komplexe Materialien, erwarten wir eine Ruferteilung im Laufe des Jahres 2022.

procedures for two vacant director positions and two additional W2 positions at different stages. The joint procedure for filling the W2 endowed professorship “Electron optics” at the Faculty of Physics of TU Dresden is about to be completed. We may expect that this W2 professorship, which is combined with a research group leader position at IFW, will be filled in the first half of 2022. In the appointment procedure for the W3 professorship “Materials chemistry”, combined with the director position at the IFW Institute for Complex Materials, we also expect a call to be issued in the course of 2022.

After Prof. Dr. Oliver Schmidt left the IFW in September 2021, the Board of directors initiated a discussion process to fill the vacant director position. Both the Scientific Advisory Board of the IFW and the Faculty of Electrical Engineering

In den beiden Bereichen Materialchemie und Elektronenoptik stehen neue Berufungen auf dem Plan.
New appointments are pending in the fields of materials chemistry and of electron optics.



Nachdem Prof. Dr. Oliver Schmidt das IFW im September 2021 verlassen hat, hat das Direktorium einen Diskussionsprozess zur Neubesetzung der frei gewordenen Direktorenstelle angestoßen. Dabei haben sowohl der Wissenschaftliche Beirat des IFW als auch die Fakultät Elektrotechnik und Informationstechnik der TU Dresden wertvollen Input geleistet, für den wir sehr dankbar sind. Ein weiteres Berufungsverfahren wurde 2021 mit der TU Bergakademie Freiberg gestartet. Dabei geht es um die gemeinsame Besetzung der W2-Professur für Entwicklung und Funktionalisierung metallischer Werkstoffe, verbunden mit einer Forschungsgruppenleiter-Position am IFW. Auch hier sind wir optimistisch, dass die Stelle binnen eines Jahres besetzt sein wird. Eine weitere Angelegenheit, die uns in 2021 intensiv beschäftigt hat, war der geplante Neubau eines Forschungsgebäudes. Mit dem Neubauprojekt sollen weitere Laborflächen insbesondere für die anwendungsnahe Forschung entstehen und zusätzliche Arbeitsplätze für die Mitarbeiterinnen und Mitarbeiter des IFW geschaffen werden. Nachdem unser Neubauprojekt 2021 zweimal seinen geplanten Standort gewechselt hat, hoffen wir nun mit dem Grundstück an der Nöthnitzer Straße den optimalen Bauplatz gefunden zu haben. In diesem Prozess hat sich die Möglichkeit eröffnet, den IFW-Neubau mit dem Bauvorhaben des Exzellenz-Clusters ct.qmat auf einem gemeinsamen Baufeld zu kombinieren und gemeinsam zu realisieren. Noch sind nicht alle Hürden genommen, aber wir treiben das Vorhaben weiter voran und sind zuversichtlich, vielleicht schon in einem Jahr den ersten Spatenstich feiern zu können.

Als Leibniz-Institut wird das IFW je zur Hälfte von Bund und Land finanziert. Zusätzlich eingeworbene Drittmittel stellen nicht nur eine wesentliche Erweiterung dieser Grundförderung dar, sondern sind auch ein wichtiger Maßstab für unsere Leistungs- und Wettbewerbsfähigkeit. In dieser Hinsicht war das IFW 2021 sehr erfolgreich, was sich nicht zuletzt darin äußert, dass wir 2021 bei den Drittmitteleinwerbungen wieder die Marke von zehn Millionen Euro erreicht und übertroffen haben. Ein besonderer Erfolg war die Bewilligung des großen BMBF-Verbundprojektes „Quantenrepeater.Link – QR.X“. Im Verbund mit den Partnern des Konsortiums sollen erstmals mobil einsetzbare Quantenrepeater-Ge-

and Information Technology of the TU Dresden provided valuable input, for which we are very grateful. Another appointment process has started in 2021 with the TU Bergakademie Freiberg. This involves the joint filling of the W2 professorship “Development and functionalization of metallic materials”, combined with a research group leader position at IFW. Here, too, we are optimistic that the position will be filled within one year.

Another concern that kept us occupied in 2021 was the construction plan for a new research building which is intended to create additional laboratory space, especially for application-oriented research, and to create new office space for IFW employees. After the IFW building project changed its planned location twice during 2021, we now hope that the optimal building site is settled on Nöthnitzer Strasse right in the neighborhood of the IFW main building. During this process the possibility of combining the new IFW building with the construction project of the ct.qmat cluster of excellence on a joint construction site has opened up. We seized this chance and are now planning a joint construction project with ct.qmat/TU Dresden. Not all hurdles have been cleared yet, but we are quite optimistic that we will perhaps be able to celebrate the groundbreaking ceremony in a year's time. As a Leibniz Institute, IFW is funded equally by the federal and state governments. Additionally, acquired third-party funding not only represents a significant expansion of this basic funding, but is also an important benchmark for our performance and competitiveness. In this respect, the IFW was very successful in the past year, as evidenced not least by the fact that we again reached and exceeded the ten-million-euro mark in third-party funding in 2021. A particular success was the approval of the large BMBF joint project "Quantum Repeater.Link - QR.X". For the first time, mobile quantum repeater systems based on different technology platforms are being developed in cooperation with the partners of the consortium. IFW is contributing its expertise in the field of semiconductor based sources of entangled photons.

Due to the pandemic, many scientific conferences and colloquia had to switch to online platforms again in 2021. This affected, for example, the third

samtsysteme entwickelt werden, die auf unterschiedlichen Technologieplattformen basieren. Das IFW bringt dabei insbesondere die Kompetenzen auf dem Gebiet der Halbleiter-Photonenpaarquellen ein. Pandemiebedingt mussten wissenschaftliche Konferenzen und Kolloquien auch 2021 zum großen Teil auf Online-Plattformen ausweichen. Das betraf beispielsweise den dritten UKRATOP-Workshop im März und die Nature-Konferenz "Microrobots and Nanorobots for Biotechnology" im Mai.

Umso mehr freut es uns, dass im Tal zwischen zwei Pandemiewellen einige Veranstaltungen zwar mit Einschränkungen, aber doch mit echten Begegnungen stattfinden konnten, so die internationale Tagung "Frustrated Magnetism and Topology" des SFB 1143 im September und der BIOREMIA-Workshop im Oktober.

Auch die jährliche interne Programmklasur konnte Anfang November in gewohnter Form mit allen verantwortlichen Wissenschaftlerinnen und Wissenschaftlern in Meißen stattfinden. Im Ergebnis von intensiven, institutsübergreifenden Diskussionen über jüngste Forschungsergebnisse und daraus resultierenden neuen Ideen entstand ein aktualisiertes IFW-Forschungsprogramm.

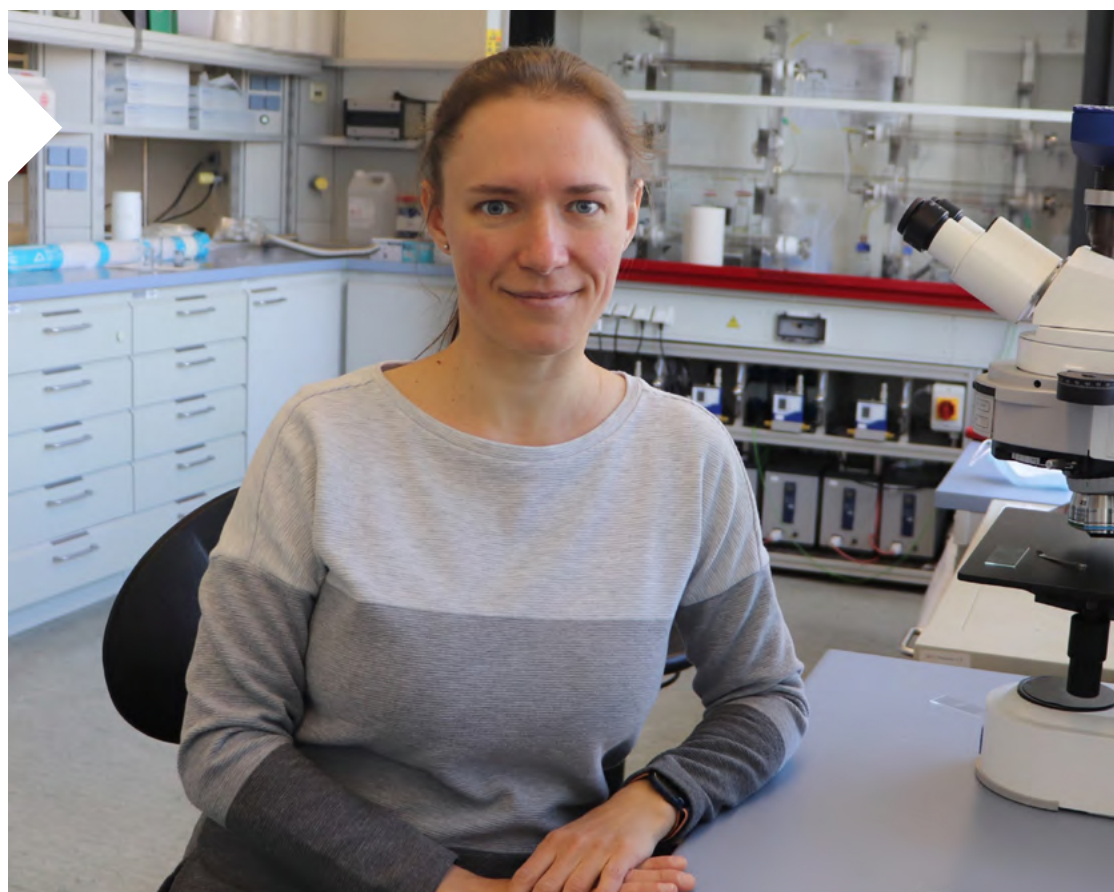
UKRATOP workshop in March and the Nature conference "Microrobots and Nanorobots for Biotechnology" in May. We are all the more pleased that in the valley between two pandemic waves some events could take place with some restrictions, but still with face-to-face meetings, such as the international meeting "Frustrated Magnetism and Topology" of the SFB 1143 in September and the BIOREMIA workshop in October.

The annual internal IFW program meeting could also be held in the usual form with all responsible scientists. As a result of intensive, cross-institute discussions on the latest research results and the resulting new ideas, an updated IFW research program was developed. Based on the proven foundation of the three pillars Quantum - Nano - Function, we have given more space to the development of materials and technologies for a sustainable and climate-neutral future. With the 2023/24 program budget, this aspect will also be made more visible to the outside world, among other things by renaming Research Area 4 "Sustainable Materials and Technologies".

Despite the restrictions imposed by the pandemic, we made great efforts during 2021 to maintain the

Im Mai 2021 war unsere Wissenschaftlerin Dr. Yulia Krupskaya "Physikerin der Woche". Seit dem Jahr 2018 stellt der Arbeitskreis Chancengleichheit der Deutschen Physikalischen Gesellschaft e. V. (DPG) wöchentlich Physikerinnen in Deutschland oder deutsche Physikerinnen im Ausland und deren Forschung vor.

Since 2018, the working group on equal opportunities of the German Physical Society (DPG) highlights weekly women in physics in Germany or German women in physics abroad. In May 2021, our scientist Dr. Yulia Krupskaya and her research were presented in this way.



Ausgehend vom bewährten Fundament der drei Säulen Quantum – Nano – Funktion haben wir der Entwicklung von Materialien und Technologien für eine nachhaltige und klimaneutrale Zukunft mehr Raum gegeben. Mit dem Programmbudget 2023/24 soll dieser Aspekt auch nach außen stärker sichtbar gemacht werden, u. a. durch die Umbenennung des Forschungsgebietes 4 in „Nachhaltige Materialien und Technologien“.

Trotz der Einschränkungen durch die Pandemie haben wir auch 2021 große Anstrengungen unternommen, um den Dialog mit einer breiten Öffentlichkeit aufrechtzuerhalten. Da bewährte Formate wie die Lange Nacht der Wissenschaften und die Führung von Schulklassen nicht möglich waren, haben wir neue Wege für die Öffentlichkeitsarbeit erschlossen: Erstmals haben wir ein Kinderbüchlein mit dem Titel „Heute forschen wir“ herausgegeben, waren an der App-Entwicklung „Katze Q“ beteiligt, die spielerisch in die Welt der Quantenphysik einführt und haben Videoclips über unseren Youtube-Kanal verbreitet. Auch an der gemeinsamen Dresdner Aktion „Juniordoktor“ haben wir uns wieder mit

dialogue with a broader public. As established events such as the Long Night of Science and the guided tours for school classes could not be realized, we explored new ways for public relations work: For the first time, we published a children's booklet entitled "Heute forschen wir" (Today we do research), were involved in the app development "Kitty Q", which playfully introduces the world of quantum physics, and broadcast video clips via our IFW YouTube channel. We also participated again in the joint Dresden campaign "Juniordoktor" with new offers. Some of them could or even had to be attended from home.

The training of students and young scientists remains a very important concern of our work. PhD students and undergraduates are involved in almost all scientific projects and the resulting publications. One example is the Leibniz Junior Research Group HELICAL on two-dimensional quantum materials, which started in 2021. In 2021, 23 PhD theses were successfully completed, three of them with the best possible grade summa cum laude.

Faszination Wissenschaft für Minis: Zum Internationalen Kindertag erschien unser kleines Kinderbuch "Heute forschen wir" im Pixi-Format. Darin gehen die Kinder Lara und Ben auf Entdeckungstour durch unser Forschungsinstitut. Sie lernen neben spannender Forschung auch viele unterschiedliche Menschen und Sprachen kennen. Das Büchlein kann kostenfrei unter media@ifw-dresden.de bestellt werden.

Fascinating science for kids: For International Children's Day, we published our mini children's book "Heute forschen wir" (Today we do research) in Pixi format. In this book, the children Lara and Ben go on a discovery tour through our research institute. In addition to exciting research, they also meet many different people and get to know many different languages. The booklet can be ordered for free at media@ifw-dresden.de.



neuen Angeboten für Schülerinnen und Schüler beteiligt. Einige davon konnten oder mussten auch von zu Hause aus wahrgenommen werden.

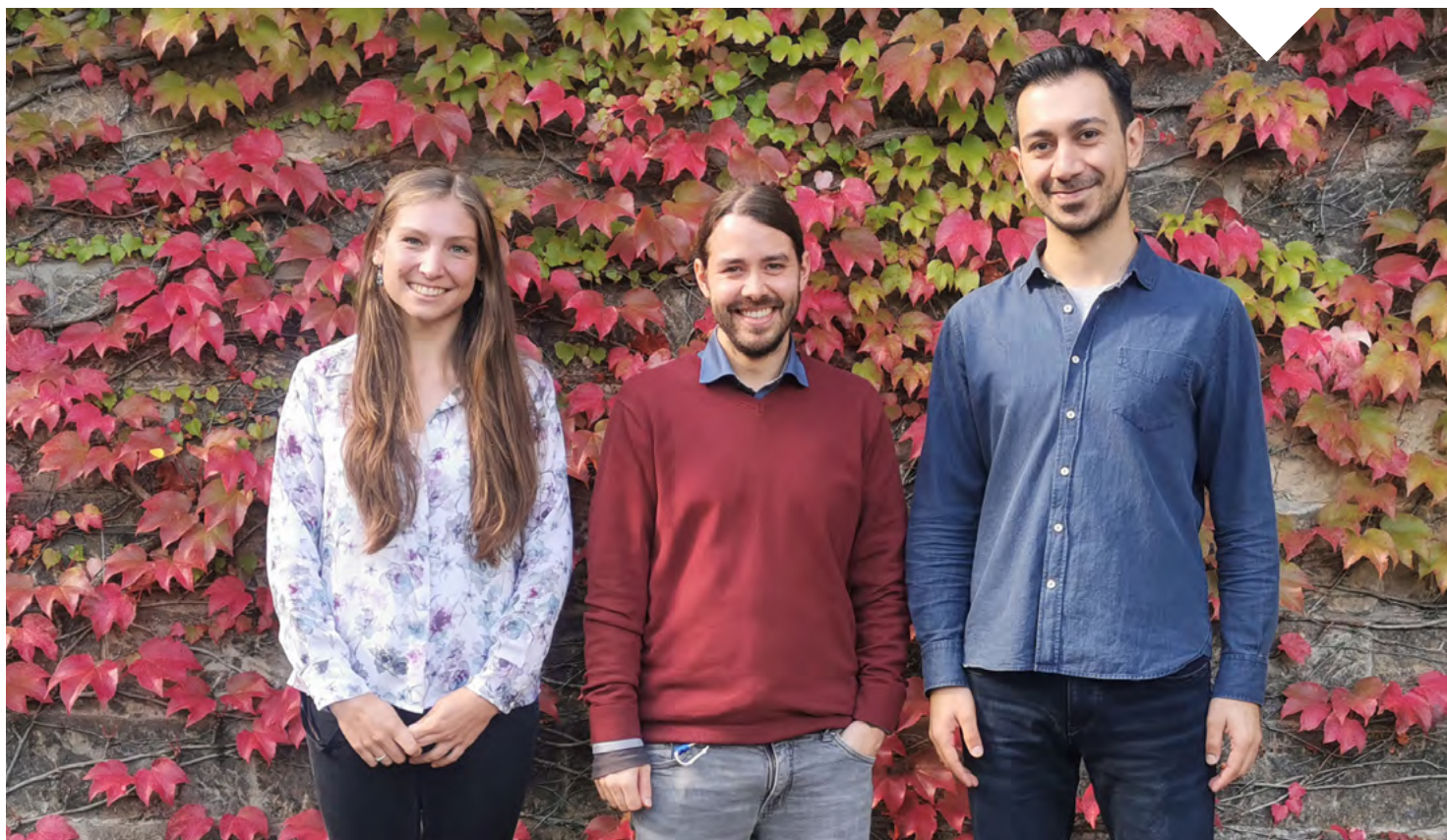
Die Ausbildung von Studierenden und Nachwuchswissenschaftler*innen bleibt ein sehr wichtiges Anliegen unserer Arbeit. An fast allen wissenschaftlichen Projekten und den daraus resultierenden Publikationen sind Promovierende und Studierende beteiligt. Ein Beispiel ist die 2021 gestartete Leibniz Junior Research Group HELICAL zu zweidimensionalen Quantenmaterialien.

2021 wurden 23 Promotionen mit Erfolg abgeschlossen, drei davon mit der bestmöglichen Note summa cum laude. Das IFW würdigt diese herausragenden Leistungen des wissenschaftlichen Nachwuchses mit der Verleihung der Tschirnhaus-Plakette.

Alles in allem sind wir stolz, dass wir auch die besonderen Herausforderungen des zweiten Pandemiejahrs gut gemeistert haben. Wir danken allen Partnern und Förderern, die uns dabei unterstützt haben, sehr herzlich.

Die neue Leibniz Junior Forschungsgruppe HELICAL (2D Heterostructures for Fermionic and Bosonic Topological Phase) beschäftigt sich mit zweidimensionalen Quantenmaterialien. Die Gruppe wird in den kommenden fünf Jahren verschiedene zweidimensionale Materialien zu sogenannten van-der-Waals-Heterostrukturen kombinieren und die entstehenden elektronischen Eigenschaften und topologischen Zustände erforschen.

The new Leibniz Junior Research Group HELICAL (2D Heterostructures for Fermionic and Bosonic Topological Phase) focuses on two-dimensional quantum materials. Over the next five years, the group will work on combining different two-dimensional materials into so-called van-der-Waals heterostructures and researching the resulting electronic properties and topological phases.



The IFW acknowledges these outstanding achievements of young scientist by awarding the Tschirnhaus-Medal.

All in all, we can state that we also mastered the special challenges of the second pandemic year quite well. We would like to express our sincere thanks to all partners and sponsors who supported us in this endeavor.

Unser Forschungsprogramm

Unser Forschungsprogramm bringt die fünf IFW-Institute in einer Matrixstruktur zusammen. In vier Forschungsgebieten verbindet es die Kompetenzen Theorie, experimentelle Physik, Chemie, Charakterisierung und Materialentwicklung der einzelnen Institute. Bei aller Breite und Interdisziplinarität gilt für alle Forschungsaktivitäten des IFW, dass sich die Wissenschaftler*innen mit noch unerforschten Eigenschaften neuer Materialien beschäftigen, mit dem Ziel, neue Funktionalitäten und Anwendungen zu erschließen.

quantum - nano - function

Die Verknüpfung der drei Felder Quantenmaterialien - Nanoskalige Materialien - Funktionsmaterialien ist das Alleinstellungsmerkmal des IFW. Entlang der Verbindungen dieser Felder haben wir drei Forschungsgebiete definiert, die wir strategisch von den Grundlagen bis zu Funktionalitäten bearbeiten. Das vierte Forschungsgebiet in der Mitte des Dreiecks beinhaltet Forschung zu Materialien und Systemen, die bereits Anwendungsreife erreicht haben.

Das IFW-Forschungsdreieck zeigt die Verknüpfung unserer Forschungsfelder Quantenmaterialien - Nanoskalige Materialien - Funktionsmaterialien. Aus den Verbindungen dieser Felder ergeben sich unsere Forschungsgebiete: (1) Functional quantum materials, (2) Function through size und (3) Quantum effects at the nanoscale. Das vierte Forschungsgebiet "Towards Products" (4) in der Mitte des Dreiecks beinhaltet Forschungsthemen mit Bezug zur Anwendung. The IFW-Research triangle illustrates the junction of our research fields Quantum matter - Nanoscale materials - Functional materials. Our Research Areas result from the junctions between these fields: (1) Functional quantum materials, (2) Function through size and (3) Quantum effects at the nanoscale. The fourth Research Area "Towards Products" (4) in the middle of the triangle contains research topics related to application.

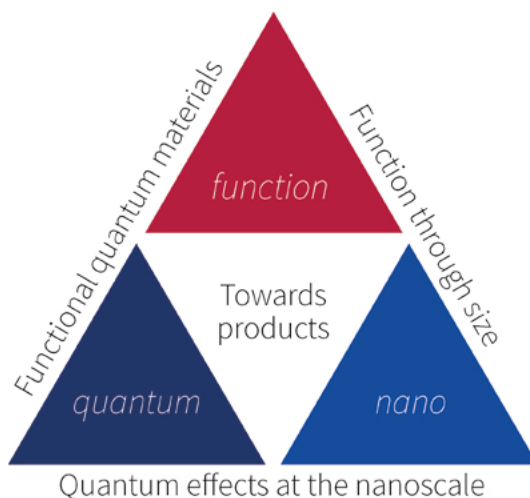
Our Research Program

Our Research Program brings together the five IFW Institutes. It combines theory, experiments, synthesis, characterization and materials and device development in four Research Areas.

Despite its diversity and interdisciplinarity, all IFW research activities have in common that scientists are investigating still unexplored properties of matter with the aim of developing new functionalities and applications.

quantum - nano - function

The junction of the three fields Quantum matter – Nanoscale materials – Functional materials is the unique feature of the IFW. Along the junctions of these fields we have defined three Research Areas where we cover the range from fundamentals to functionalities in a strategic manner. The forth Research Area binds together materials science research that is already at the threshold to prototypes or products.



Fünf Institute des IFWs

Five IFW Institutes

Institut für Festkörperforschung - Institute for Solid State Research (IFF)

Director: Prof. Dr. Bernd Büchner

Das IFF beschäftigt sich mit materialorientierter Festkörperforschung mit den besonderen Schwerpunkten Quantenmaterialien und nanoskalige Substanzen.

The IFF does research in the field of material-oriented experimental solid state physics with a special focus on quantum materials and nanoscale substances.

Institut für Metallische Werkstoffe - Institute for Metallic Materials (IMW)

Director: Prof. Dr. Kornelius Nielsch

Das IMW befasst sich vor allem mit thermoelektrischen, magnetischen und supraleitenden Materialien, funktionellen Dünnschichten sowie mit Metallphysik.

Main research topics of IMW are thermoelectric, magnetic and superconducting materials, functional thin films and metal physics.

Institut für Komplexe Materialien - Institute for Complex Materials (IKM)

Director: Prof. Dr. Bernd Büchner (temp.)

Die Forschungsaktivitäten des IKM fokussieren sich auf Legierungsdesign und Prozesstechnologien, die Chemie funktioneller Materialien sowie Stukturanalytik.

The research activities of the IKM focus on alloy design and processing, chemistry of functional materials and structural analysis.

Institut für Integrative Nanowissenschaften - Institute for Integrative Nanosciences (IIN)

Director: Prof. Dr. Rudolf Schäfer (temp.)

Das IIN beschäftigt sich mit modernen Themen der Nanowissenschaften von Photonik über flexible Elektronik bis hin zu Mikro-/Nano-Robotern.

The IIN deals with a variety of modern nanoscience topics from photonics to flexible electronics to micro/nano-robots.

Institut für Theoretische Festkörperphysik - Institute for Theoretical Solid State Physics (ITF)

Director: Prof. Dr. Jeroen van den Brink

Die Forschung am ITF konzentriert sich auf die theoretischen Aspekte der Physik der kondensierten Materie und der Materialwissenschaften.

The ITF focusses on theoretical aspects of condensed matter physics and materials science.



Schwerpunkt 2021: Nachhaltigkeit

Der aus der Forstwirtschaft stammende Begriff der Nachhaltigkeit ist in aller Munde. Was im Ursprung für eine ressourcenschonende Nutzung des Waldes galt, nämlich nur so viele Bäume für die Holzverarbeitung zu entnehmen wie auch nachwachsen, ist heute auf jedes beliebige Anwendungsfeld übertragbar.

Das IFW orientiert sich in seinem gesamten Wissenschaftsbetrieb an dem Leitbild Nachhaltigkeit der Leibniz-Gemeinschaft. Demnach streben wir an, sowohl den gesamten Forschungsprozess als auch die betrieblichen Abläufe nachhaltig zu gestalten. Das betrifft zum Beispiel die Organisations- und Personalentwicklung, den Betrieb von Gebäuden und Infrastrukturen sowie das Beschaffungswesen und die Mobilität. Zusätzlich zu diesen Anforderungen, die an alle Leibniz-Institute gestellt werden, sind die Themen Nachhaltigkeit und Klimaverträglichkeit auch direkt im Forschungsprogramm des IFW Dresden verankert. Materialforschung spielt eine Schlüsselrolle, wenn es darum geht, neue Technologien zu entwickeln, die nachhaltig sind und zukünftige Klimaneutralität ermöglichen. Auf den folgenden Seiten stellen wir darum einige aktuelle Projekte des IFW Dresden für mehr Nachhaltigkeit vor.

Focus 2021: Sustainability

The concept of sustainability, which originated in forestry, is omnipresent. The term once described that only as many trees should be taken from the forest for wood processing as can grow back. Today, this requirement can be applied to any field of application.

In all its activities, the IFW is guided by the Leibniz Association's guiding principle of sustainability. According to this, we are aiming to shape the entire research process as well as the operational procedures in a sustainable manner. This applies, for example, to organizational and personnel development, the operation of buildings and infrastructures, as well as procurement and mobility. In addition to these requirements, which are imposed on all Leibniz institutes, the topics of sustainability and climate compatibility are also directly anchored in the research program of IFW Dresden. Materials research plays a key role when it comes to developing new technologies that enable sustainability and future climate neutrality. On the following pages we present some current projects running at IFW in this respect.

Akustische Oberflächenwellen-Technologie für Windräder

Auf dem Gebiet der akustischen Oberflächenwellen-Technologie treibt das IFW mit mehreren Projekten Anwendungen im Sektor der erneuerbaren Energien voran. Das Transferprojekt WindSAW widmet sich der Entwicklung von ressourcenschonenden Sensorlösungen für die In-Situ- Rotorblattüberwachung von Windkraftanlagen. Mit Hilfe dieser funkabfragbaren Sensoren auf SAW-Basis lassen sich zuverlässig und in Echtzeit verschiedene, für die Steuerung des optimalen Betriebsregimes wichtige Arten von Oberflächenbelastungen erkennen, ohne dabei die Aerodynamik der Rotorblätter zu stören oder den Blitzschutz zu beeinträchtigen. Des Weiteren sind Wissenschaftler des IFW am EU-Projekt "SOUNDofICE - Sustainable Smart De-Icing by Surface Engineering of Acoustic Waves" beteiligt. Ziel dieses Projekts ist es, kostspielige und umweltschädliche Enteisungsmethoden durch hochfrequente akustische Oberflächen zu ersetzen. Erstmals sollen sowohl die Erkennung als auch die Enteisung nach dem gleichen Prinzip funktionieren. Die neue Enteisungstechnik mit akustischen Oberflächenwellen hat gegenüber herkömmlichen Methoden große Vorteile in Bezug auf Leistung, Multifunktionalität und Ablagerungskapazität und wird insbesondere für Anwendungen in der Luftfahrt- und Windkraftindustrie entwickelt.

Effiziente Wasserstoffspeicherung für den Transport

2021 hat das IFW mit der TU Dresden, der HTW Dresden und der Firma ScIDre das Dresdner HyLiq-Konsortium initiiert und im Rahmen der Nationalen Wasserstoffstrategie ein Verbundprojekt gestartet. Es ist Teil des BMBF-Leitprojekts TransHyDE zum Aufbau einer Wasserstoff-Transportinfrastruktur. Schwerpunkt des HyLiq-Projektes ist die Effizienzsteigerung von Speicherung und Transport Grünen Flüssigwasserstoffs.

Vor dem Hintergrund des nahenden Atom- und Kohleausstiegs werden die bestehenden Erdgas-Pipelines für den Transport von Grünem Wasserstoff für Jahrzehnte nicht in der benötigten Größenordnung verfügbar sein. So besteht für die Beschleunigung der Energiewende die Herausforderung darin, bestehen-

Surface acoustic wave technology for wind turbines

In the field of surface acoustic wave technology, IFW is working on several projects to advance applications in the renewable energy sector. The WindSAW transfer project is dedicated to the development of a battery-free, wireless, resource-efficient sensor system for in-situ and real-time rotor blade monitoring of wind turbines. These wireless SAW-based sensor solutions can instantly and reliably distinguish between different types of surface loads such as ambient air, pollution, and ice cover without disturbing rotor blade aerodynamics or compromising lightning protection. Furthermore, IFW scientists are involved in the EU project "SOUNDofICE - Sustainable Smart De-Icing by Surface Engineering of Acoustic Waves". The aim of this project is to replace costly and environmentally harmful de-icing methods with high-frequency acoustic surface technology. For the first time, both detection and de-icing will share the same operating principle. The new surface acoustic wave deicing technology has significant advantages over conventional methods in terms of performance, multi-functionality and deposition capacity, and is being developed particularly for applications in the aviation and wind power industries.

Logistics solutions for liquid hydrogen

In 2021, IFW initiated the Dresden HyLiq consortium together with TU Dresden, HTW Dresden and the company ScIDre and launched a joint project as part of the National Hydrogen Strategy. It is part of the BMBF lead project TransHyDE for the development of a hydrogen transport infrastructure. The focus of the HyLiq project is on increasing the efficiency of green liquid hydrogen storage and transport.

In view of the upcoming nuclear and coal exit, the existing natural gas pipelines for the transport of green hydrogen will not be available on the required scale for decades. Thus, the challenge for accelerating the energy transition is to make existing transport and distribution networks highly efficient for the renewable energy source LH₂. The HyLiq project therefore specifically addresses the reduction of losses associated with cryogenic LH₂ technology and sees itself as a missing link between H₂ producers and H₂ users.

de Transport- und Verteilnetze hocheffizient für den regenerative Energieträger LH₂ nutzbar zu machen. Das HyLiq-Projekt adressiert daher gezielt die Reduzierung der mit der kryogenen LH₂-Technologie verbundenen Verluste und versteht sich als „missing link“ zwischen H₂-Erzeugern und H₂-Nutzern. Schwerpunkte der IFW-Aktivitäten im HyLiq-Projekt sind Technologien zur innovativen Füllstandsmessung, der Rückkondensation abdampfenden LH₂, des verlustarmen Transfers mittels Kryopumpen und zur Sekundärnutzung der LH₂-Kälte. Neben seinen Erfahrungen im Kryo-Engineering bringt das IFW seine materialwissenschaftlichen Kompetenzen in das Projekt ein. Dabei liegen die Schwerpunkte bei der SAW-Sensorik, Magnetokalorik, Supraleitung und Umformtechnik.

Neue Batterie-Konzepte

Ein wichtiges Forschungsthema am IFW widmet sich der Materialentwicklung für die Energiespeicherung. Ein Schwerpunkt liegt dabei auf der Entwicklung neuartiger Elektrodenmaterialien mit Multielektronen-Redox-Funktionalität für Li-Ionen-Batterien der nächsten Generation. Es werden neuartige Kathodenmaterialien entwickelt, deren Präparation sehr einfach ist und hohe Ausbeuten liefert, was die Energiekosten für die Herstellung um mehr als 50 Prozent reduziert. Außerdem sind die Ausgangsmaterialien frei von Cobalt und damit sehr kostengünstig und vor allem umweltfreundlich. Die Energiekosten und Lieferkosten können um bis zu 90 Prozent gesenkt werden. Des Weiteren werden Batteriekomponenten wie Binder und Elektrolyte für die Anwendung unter extremen Bedingungen, d. h. in einem großen Temperaturintervall und bei sehr schnellen Lade-Entlade-Zyklen, gezielt optimiert. Auch andere Themen, die für eine nachhaltige Kreislaufwirtschaft von großer Bedeutung sind, werden am IFW untersucht, beispielsweise das „sanfte“ Recycling von Kathodenmaterialien oder die Entwicklung wasserbasierter Binder- Systeme, die auf umweltschädliche Lösemittel verzichten.

Im Bereich der Metall-Batterien jenseits von Lithium wie Natrium-, Kalium- oder Zink- Batterien entwickeln wir das strukturelle Design von Elektrodenmaterialien und suchen nach Möglichkeiten, den Ladungstransferwiderstand zu verringern und Diffusionsprozesse in der Zelle zu stabilisieren, insbesondere

IFW's activities in the HyLiq project focus on technologies for innovative level measurement, recondensation of evaporating LH₂, low-loss transfer using cryogenic pumps, and secondary use of LH₂ refrigeration. In addition to its experience in cryoengineering, IFW is contributing its expertise in materials science to the project. The focus here is on SAW sensor technology, magnetocalorics, superconductivity and forming technology.

New materials & concepts for batteries

An important research topic at IFW is dedicated to materials development for energy storage. One focus represents the development of novel electrode materials with multi-electron redox functionality for next generation Li-ion batteries. Novel cathode materials were developed whose preparation with high yields is very simple, which reduces the energy costs for production by more than 50 percent. In addition, the starting materials are free of cobalt, very cost-effective and environmentally friendly. Energy and supply costs can be so reduced up to 90 percent. Furthermore, battery components are specifically optimized for application under extreme conditions, i.e. a large temperature interval and a very fast charge-discharge cycling. Other topics with great importance for sustainable circular economy are also studied at IFW, e.g. “soft” recycling of cathode materials or the development of water-based binder systems avoiding polluting solvents.

In the field of beyond-Lithium metal batteries as Sodium, Potassium or Zink batteries, we develop the structural design of electrode materials and search for ways to decrease the charge transfer resistance and to stabilize diffusion processes in a cell, especially in all-solid-state battery configuration. The greater aim is to fabricate durable batteries suitable for a long-term operation with a performance surpassing the benchmark.

in einer Festkörperbatterien-Konfiguration. Das übergeordnete Ziel dabei ist eine deutliche Verbesserung der Lebensdauer von Batterien.

Permanentmagnete ohne Seltene Erden

In vielen modernen Anwendungen und energiekritischen Technologien werden Dauermagnete eingesetzt, die Seltene Erden - beispielsweise Neodym - als Grundbestandteil enthalten. Die sozialen und Umweltauswirkungen beim Abbau sowie die Exportbeschränkungen der wenigen globalen Anbieter behindern jedoch die langfristige Entwicklung dieser Dauermagnete. Daher besteht ein starkes Interesse an der Suche nach Magnetwerkstoffen, die frei von Seltenen Erden sind und dennoch gute magnetische Eigenschaften aufweisen. Auf der Grundlage des tieferen Verständnisses der physikalischen Zusammenhänge wurde am IFW eine Prozess-Route zur Herstellung von Mangan-Aluminium-Kohlenstoff-Magneten entwickelt, deren magnetische Eigenschaften im internationalen Vergleich mindestens um den Faktor zwei besser sind als die bisher von anderen Gruppen veröffentlichten.

Aufbereitung von Silizium-Abfällen

Die Rückgewinnung von Silizium aus u.a. Abfallprodukten der Solarwaferfertigung sowie End-of-Life Photovoltaic-Modulen stellt eine ökologisch und ökonomisch aussichtsreiche Siliziumquelle für thermoelektrische Werkstoffe dar (Advanced Energy Materials 10, 1904159 (2020)). Verunreinigungen im Abfallmaterial, wie Kupfer, Eisen oder Kohlenstoff hemmen die Steigerung der thermoelektrischen Leistungszahl (zT). Des Weiteren begrenzt die hohe thermischen Leitfähigkeit von Silizium den Einsatz für thermoelektrische Anwendungen. Am IFW werden daher umweltfreundliche, ökonomisch attraktive metallurgische Prozesse angewendet, die eine starke Reduzierung der Verunreinigungen in Siliziumabfällen ermöglichen. Durch die Implementierung von multiskaliger Phononenstreuung konnte die thermische Leitfähigkeit von gereinigtem Silizium um einen Faktor drei (ACS Applied Materials and Interfaces 13, 47912 (2021)) reduziert werden. Durch die dargelegten Strategien gelang es, die durchschnittliche thermoelektrische Leistungszahl zu steigern und thermoelektrische Module für Hochtem-

Permanent magnet without rare earth elements

Many modern applications and energy-critical technologies use permanent magnets that contain rare earths as a basic component, e.g. neodymium. However, the environmental and social impacts of mining and the export restrictions of the few global suppliers hinder the long-term development of these permanent magnets. Therefore, there is a strong interest in finding magnets without rare earths with a sufficiently large energy product. The research on permanent magnets at IFW is focused on developing rare-earth-free materials as a sustainable alternative to Nd-Fe-B. On the base of fundamental understanding of the underlying physics, a processing route has been developed recently at IFW, resulting in the production of Manganese-Aluminum-Carbon magnets with state-of-the-art magnetic properties which are a factor of at least two higher than those for this material produced by any other research groups worldwide.

Processing of silicon waste for the cyclic utilization

The recovery of silicon waste arising, i.a. from wafer production and end-of-life photovoltaic modules, presents a prospective and environmentally friendly Si source in the area of thermoelectric (TE) materials (Advanced Energy Materials 10, 1904159 (2020)). Impurities within the waste like copper, iron and carbon hamper the increase of the thermoelectric figure of merit (zT), besides the high thermal conductivity of Si limiting TE applications. Therefore, at IFW, environmentally friendly, economically attractive metallurgical methods are applied for the reduction of impurities in silicon waste to a very low level. By the implementation of multiscale phonon scattering, the thermal conductivity of purified Si was reduced by a factor of three (ACS Applied Materials and Interfaces 13, 47912 (2021)). These strategies enabled to successfully increase the average zT and the future development of thermoelectric modules for high temperatures (>800 °Celsius) and conversion efficiencies of >5 percent.

In an upcoming IGF joint project, researchers of the Institute for Energy and Environmental Technology e. V. (IUTA) in Duisburg, the Bielefeld University and the IFW Dresden are developing a processing method for the cyclic utilization of silicon by means of gas

peraturanwendungen (>800 °Celsius) zu entwickeln, die zukünftig Umwandlungseffizienzen über 5 Prozent erzielen sollten.

In einem neuen IGF-Gemeinschaftsprojekt des Instituts für Energie- und Umwelttechnik e. V. (IUTA) in Duisburg, der Universität Bielefeld und des IFW Dresden wird ein Aufbereitungsverfahren zur Kreislaufverwertung von Silizium mittels Gasphasensynthese entwickelt. Dabei sollen Siliziumabfälle für den Einsatz in Batterien, Dioden oder thermoelektrischen Bauelementen ertüchtigt werden. Für die Herstellung entsprechender Prototypen wird das selektive Laserschmelzen als additive Fertigungstechnologie validiert, welches eine endkonturnahe Fertigung mit Funktionsintegration ermöglicht.

Ersatz von Tellur in thermoelektrischen Bauteilen

Mehr als 60 Prozent der Energie, die bei der Verbrennung fossiler Brennstoffe entsteht, ist Abwärme. Davon ist mehr als die Hälfte minderwertige Wärme mit Temperaturen unter 300 °Celsius. Die effektive Nutzung dieser minderwertigen Wärme zur Stromerzeugung ist für die Reduzierung der Treibhausgasemissionen von entscheidender Bedeutung. Die thermoelektrische Technologie ist für die Umwandlung von Wärme in Elektrizität besonders attraktiv. Bisher wurden thermoelektrische Module auf Wismut-Tellurid-Basis hergestellt. Die Knappheit von Tellur schränkt die breite Anwendung von Bismut-Tellurid-Modulen aber stark ein. Daher ist es zwingend erforderlich, thermoelektrische Module aus anderen Materialien zu entwickeln, die häufiger vorkommen und vergleichbare Leistung liefern. Forschende des IFW Dresden und der University of Houston haben 2021 einen hocheffizienten Tellur-freien thermoelektrischen Generator auf der Basis von Magnesium-Antimon-Verbindungen vorgestellt. Dieser bietet eine praktikable, nachhaltige Alternative zu Bismut-Tellurid-Modulen und wird die breitere Anwendung der thermoelektrischen Technologie vorantreiben.

phase synthesis. Thereby, silicon waste shall be recovered for the application in batteries, diodes or TE devices. For the manufacturing of respective prototypes, laser powder bed fusion – as additive manufacturing technology – is validated, enabling a near-net-shape production with function integration.

Replacement of Tellurium in thermoelectric components

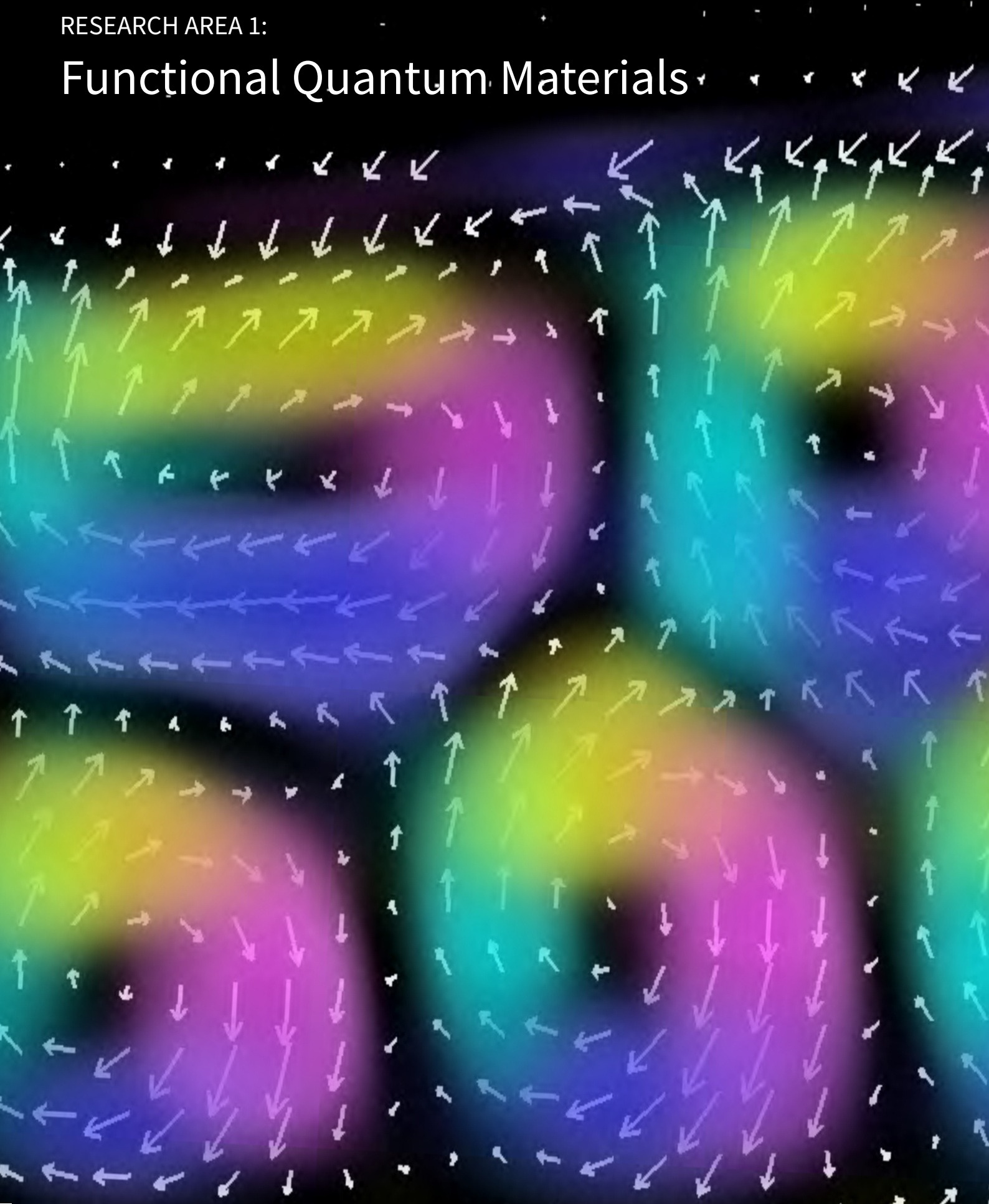
More than 60 percent of the energy generated by burning fossil fuels is dissipated as waste heat, of which more than half is low-grade heat with temperatures below 300 °Celsius. Effective harnessing this low-grade heat to generate electricity is vital for reducing the emission of greenhouse gases. Thermoelectric technology is particularly attractive for heat-to-electricity conversion. Up to now, thermoelectric modules have relied on bismuth-telluride-based compounds because of their unmatched thermoelectric properties. However, the wider applicability of bismuth-telluride modules is severely limited by the scarcity of Tellurium. Therefore, it is essential to develop thermoelectric modules from other, more abundant materials while retaining high performance. Researchers from the IFW Dresden and the University of Houston developed for the first time a highly efficient Tellurium-free thermoelectric generator based on Magnesium-Antimony compounds, by using a simple, versatile, and thus scalable processing routine. This work, published in 2021, marks a feasible, sustainable alternative to Bismuth-telluride-based thermoelectric modules and will spur a wider application of thermoelectric technology in converting low-grade heat to electricity and thermoelectric coolers.

FORSCHUNGSGEBIET 1:

Funktions-Quanten-Materialien

RESEARCH AREA 1:

Functional Quantum Materials



Funktions-Quanten- Materialien

Im Forschungsgebiet 1 erforschen wir Materialien, deren elektronische Eigenschaften zu neuen Funktionalitäten mit interessantem Anwendungspotential führen können. Die physikalischen Eigenschaften manifestieren sich in einer Reihe von Materialklassen: in bestimmten Übergangsmetalloxiden, in molekularen Feststoffen und in intermetallischen Materialien. All diese Systeme weisen ein vielseitiges Zusammenspiel von lokalisierten und delokalisierten elektronischen Freiheitsgraden auf. Das unterscheidet diese Materialien sowohl praktisch als auch konzeptionell sehr deutlich von einfachen Metallen und Halbleitern mit gut verstandener elektronischer Struktur. Häufig führt das quantenmechanische Wechselspiel verschiedener elektronischer Freiheitsgrade zu anormalen Ladungstransporteigenschaften, beispielsweise aufgrund von Metall-Isolator-Übergängen, und zu außergewöhnlichen Ordnungsphänomenen wie unkonventionelle Formen der Supraleitung und Quantenmagnetismus. Hieraus resultierende und nutzbare Funktionalitäten sind zum Beispiel große magnetokalorische Effekte, Hochtemperatursupraleitung, Magnetismus mit sehr starker Anisotropie und der Riesenmagnetowiderstand.

Functional Quantum Materials

Research Area 1 is focused on bulk materials in which a potential for applications emerges from their complex, quantum mechanical electronic properties. These physical material's properties manifest themselves in a number of material classes: in certain families of transition-metal oxides, in molecular solids and in a range of intermetallic materials. What sets these systems apart is that their valence and conduction electrons typically retain to some extent their atomic character, resulting in a rich interplay of localised and delocalised electronic degrees of freedom. This renders these materials both practically and conceptually very different from simple metals and semiconductors with well-understood itinerant quasi-particles. Often the quantum mechanical interplay between the localised and delocalised electronic degrees of freedom leads to anomalous charge transport properties, for instance due to the presence of metal-insulator transitions, and exceptional types of ordering phenomena, such as unconventional forms of superconductivity and quantum magnetism. Functionalities that arise from this are for instance large magneto-caloric effects, high temperature superconductivity, magnetism with very strong anisotropy and giant magnetoresistance.

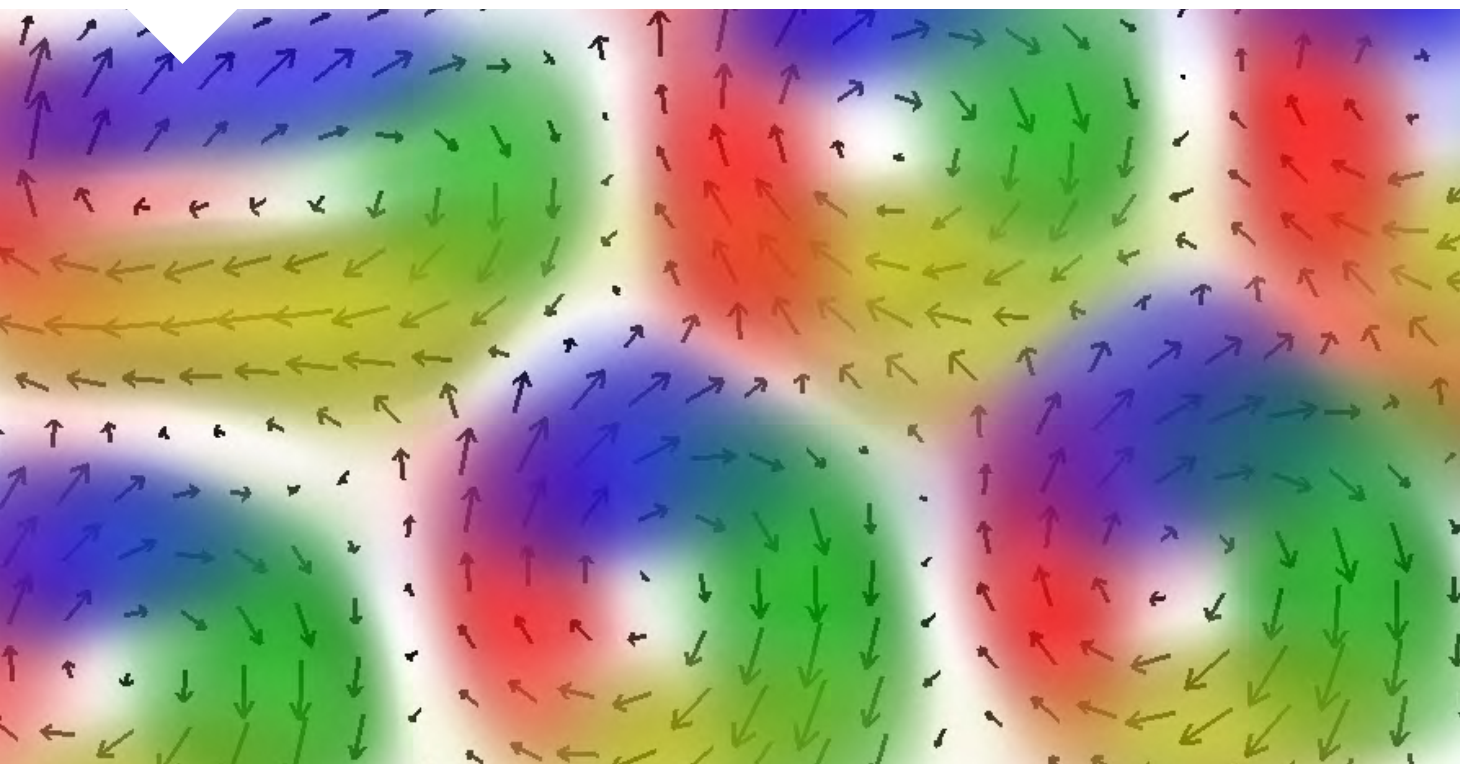
Unveiling the three-dimensional magnetic texture of skyrmion tubes

Daniel Wolf, Sebastian Schneider¹, Ulrich K. Rößler, Andras Kovacs², Marcus Schmidt³, Rafal E. Dunin-Borkowski², Bernd Büchner, Bernd Rellinghaus¹, and Axel Lubk

Skyrmionen sind nanoskopische magnetische Nanowirbel, die in magnetischen Materialien mit chiraler Kristallstruktur entstehen. Theoretische Pionierarbeiten von A. Bogdanov, U. Rößler und Mitarbeitern des IFW haben solche magnetische Texturen bereits vor mehr als 25 Jahren vorhergesagt [1]. Diese Wirbel existieren als isolierte scheibenförmige Gebilde, welche sich in 2D Gittern anordnen können. Deren diskrete Natur alszählbare Objekte eignet sich für vielversprechende Anwendungen in neuartigen energieeffizienten Datenspeichern und Rechnern, woraus sich ein aktives Forschungsfeld, genannt „Skyrmionics“, entwickelt hat. Nun, 25 Jahre später, ist es uns das erste Mal gelungen, sie in drei Dimensionen, als modulierte Skyrmionenschläuche, mittels tomographischer Methoden im Transmissionselektronenmikroskop zu untersuchen und sichtbar zu machen [2].

Skyrmions are nanoscopic magnetic nanoswirls that occur in magnetic materials with chiral crystal structure. Pioneering theoretical studies of A. Bogdanov, U. Rößler and coworkers of the IFW [1] have already postulated such magnetic textures more than 25 years ago. They showed that these swirls may exist as isolated flat entities and can assemble two-dimensional (2D) lattices. Their discrete nature as countable objects makes them promising candidates for novel energy-efficient memory and computing applications. Therefore, a new research field called skyrmionics has been established. Now, 25 years later, we were able to experimentally observe these objects for the first time in three-dimensions, where they appear as modulated Skyrmion tubes, by tomographic methods in the transmission electron microscope [2].

Abb. 1: Nanostruktur magnetischer Wirbel, sogenannter Skyrmionen. Ausschnitt aus Abbildung 2 (siehe Seite 20).
Fig. 1: Nanostructure of magnetic vortices: skyrmions. Detail of figure 2 (see page 20).



Skyrmions are small swirls of magnetic spins that can exist in specific magnetic materials with a chiral lattice structure. In a pioneering theoretical work A. Bogdanov and co-workers at the IFW predicted such structures more than 25 years ago [1]. These swirls have been shown to exist as isolated disk-like entities, which can be organized also in two-dimensional lattices or clusters. Magnetic skyrmions are furthermore characterized by a non-zero winding number, which marks them as topological objects and allows to distinguish skyrmions from antiskyrmions. They have been named after the British physicist Tony H.R. Skyrme, who described elementary particles like neutrons as ball-like knots in a continuum field in a similar manner.

In the meantime, chiral magnetic skyrmions have been found in various materials and elementary skyrmions could be imaged as small circular swirls of the magnetization on the nanometer scale. The research field has become one of the most exciting and active topics in solid-state and nanomagnetism research with deep connections to other fields of science. The digital nature of skyrmions as countable objects promises applications for magnetic data-storage and computing. Moreover, intense research activities showed that the structure of these objects holds many surprising aspects, e.g., concerning the existence of different skyrmion species, their interaction and their arrangement in two and three dimensions.

Notably, in thicker films and in bulk crystals skyrmions are extended in the third dimension and form tubular cylindrical strings. Researchers are currently interested in how these strings may bend and twist as these three dimensional modulations have a large impact on their interaction and mobility in real devices. For instance, in nanomagnetic specimens, surface symmetry breaking and anisotropies, applied fields, and adjacent skyrmions in finite lattice arrays may conspire to distort, bend and pin skyrmions. Experimentally studying these “tertiary structures” of skyrmion strings at the nanoscale, however, is a great challenge for magnetic imaging techniques. Together with scientists from TU Dresden and FZ Jülich, we have therefore developed a tomographic transmission electron microscopy (TEM) method - holographic vector-field electron tomography (VFET) - to dissect these complex three-dimensional

(3D) patterns of bent skyrmions (Fig. 2) and to analyse their internal structure quantitatively [2].

Experimental

In order to carry out high-resolution tomographic TEM investigations of skyrmion strings, we prepared an iron germanium (FeGe) needle-shaped specimen by focused ion beam (FIB) milling. FeGe is a chiral-lattice ferromagnet, in which skyrmions arise from the interplay between the Dzyaloshinskii-Moriya (DM) interaction and conventional ferromagnetic exchange mechanisms. To stabilize the Skyrmion lattice in the FeGe needle, the experiment has to be carried out under cryogenic conditions at -180 °Celsius (provided by a liquid-nitrogen-cooled sample holder) in the presence of an out-of-plane applied magnetic field (provided by a ring magnet of Sm₂Co₁₇ underneath the specimen). The principle setup of the experiment is depicted in Figure 3. Similar to a conventional medical computer tomography (CT) scanner, projections from different directions of the sample are registered in a so-called tilt series. However, in contrast to the CT scanner, where X-rays penetrate through rather thick and large objects, we use electrons, or more precisely, electron waves that propagate through a ca. 200 nm thin specimen of needle shape. In electron tomography, the tilt series is recorded by tilting the specimen, whereas in CT the detector is rotated around the investigated region. In addition, there is only little space of a few millimeters around the sample holder in the TEM rendering tilt series acquisition and cooling challenging. The fundamental interaction of the electron beam with the sample that provides access to the magnetic structure is the well-known Aharonov-Bohm quantum effect [3]. The latter states that an electron wave experiences a phase shift depending on the enclosed magnetic flux between two interfering beam paths. Since phase shifts cannot be measured directly, an interferometric setup, namely off-axis electron holography [4] is established in the electron microscope. For this purpose, an electrostatic Möllenstedt biprism [5], i.e., a positively biased thin metallic wire (~300 nm diameter), acts as wave front splitter slightly above the first image plane to interfere the object-modulated electron wave with an unmodulated reference wave. The resulting interference pattern, the hologram, is then recorded on a

digital camera for each tilt angle and reconstructed in the computer to obtain a tilt series of 2D phase shift distributions. The latter is processed further to compute a tilt series of the projected magnetic induction maps, which are finally fed into tomographic reconstruction algorithms to obtain the tomogram, i.e., the 3D reconstruction of magnetic induction distribution of the skyrmion strings. The entire workflow involves a large amount of data processing, including image acquisition, alignment (e.g., correction of nanometer displacements), holographic-to-magnetic reconstruction and, finally, 3D visualization and analysis [6].

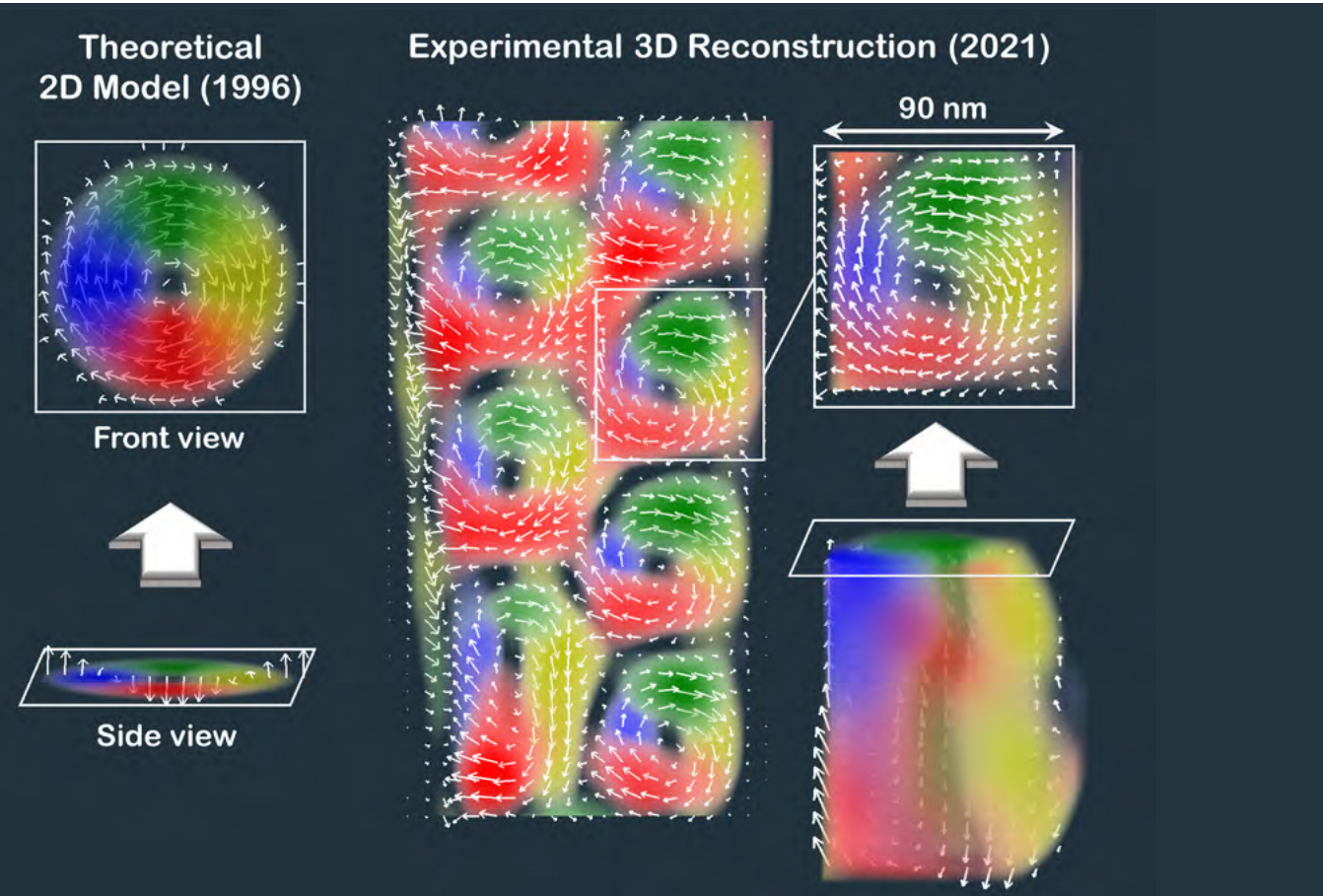
Results

Figure 4 shows the reconstructed 3D vector field of the magnetic induction visualizing the skyrmion lattice in a needle-shaped FeGe sample at a resolution of a few nanometers. These results represent the first direct insight into the 3D skyrmion spin texture, including its extension through the volume

of the sample as so-called Skyrmion tubes (SkTs). In Ref. [2], we discuss in greater detail our findings concerning the various found characteristic modulations of the SkTs. For example, we characterize the complicated breakdown of the skyrmion texture upon approaching surfaces in axial directions and we observe a variety of imperfections in the spatial extension of skyrmion tubes. Among them are axial and planar distortions of the SkTs, local losses of axial symmetry, and the occurrence of unexpected radial (rather than purely tangential) tilts of the magnetic induction in the circumferential Bloch walls. Even indications of in-plane magnetic flux leaking among neighboring SkTs in close-packed regions and abrupt changes of the magnetic induction that may be indicative of the occurrence of Bloch points are found. Also, the 3D course of the SkT axes exhibits a substantial bending and twisting that is locally correlated with the occurrence of pronounced edge states, specifically in directions that are affected by confinements.

Noteworthy, these deformations appear at length

Abb. 2: Nanostruktur magnetischer Wirbel genannt Skyrmionen. Links: Theoretische Vorhersage solcher zwei-dimensionaler (2D) magnetischer Nanotexturen [1]. Rechts: Experimentelle Beobachtung der drei-dimensionalen (3D) Struktur von Skyrmionenschläuchen mittels tomographischer Methoden im Transmissionselektronenmikroskop [2].
 Fig. 2: Nano-structure of magnetic swirls called Skyrmions. Left: Theoretical prediction of such two-dimensional (2D) magnetic nanotextures [1]. Right: Experimental observation of three-dimensional (3D) skyrmion tubes using tomographic methods in the transmission electron microscope [2].



scales, where harmonic modulations are promoted by the magnetic DM interaction. Planar energy density maps across the SkTs were derived from the volume data of the magnetic induction and confirm for the first time experimentally the anticipated formation and stabilization mechanism of skyrmions for a volume sample. The results reveal a substantial energetic gain due to the DM interaction that overcompensates the energetic efforts associated with the conventional magnetic exchange interaction in the core of the SkT thereby stabilizing the SkTs as a whole. We anticipate that this novel experimental approach will pave the way to a better understanding of spin textures in a large variety of complex topologically protected and non-topological magnetization patterns, including other members of the skyrmion family, thereby moving the fields of both nanomagnetism and spintronics significantly forward.

References

- [1] U. K. Rößler et al., *Nature* 442 (2006) 797
- [2] D. Wolf et al., *Nat. Nanotechnol.* (2021).
<https://doi.org/10.1038/s41565-021-01031-x>
- [3] Y. Aharonov and D. Bohm, *Physical Review* 115 (1959) 485
- [4] H. Lichte and M. Lehmann, *Reports on Progress in Physics* 71 (2008) 016102
- [5] G. Möllenstedt and H. Düker, *Naturwissenschaften* 42 (1955) 41
- [6] D. Wolf, et al., *Current Opinion in Solid State and Materials Science* 17 (2013) 126

Funding

Priority Program SPP 2137 Skyrmiomics of the German Research Foundation (DFG)
European Research Council (ERC) starting grant “ATOM” under the Horizon 2020 research and innovation program of the European Union (grant agreement number 715620)

Cooperations

- ¹ Dresden Center for Nanoanalysis, cfaed, Technische Universität Dresden
- ² Ernst Ruska-Centre for Microscopy and Spectroscopy with Electrons and Peter Grünberg Institute, Forschungszentrum Jülich
- ³ Department Chemical Metal Science, Max Planck Institute for Chemical Physics of Solids Dresden

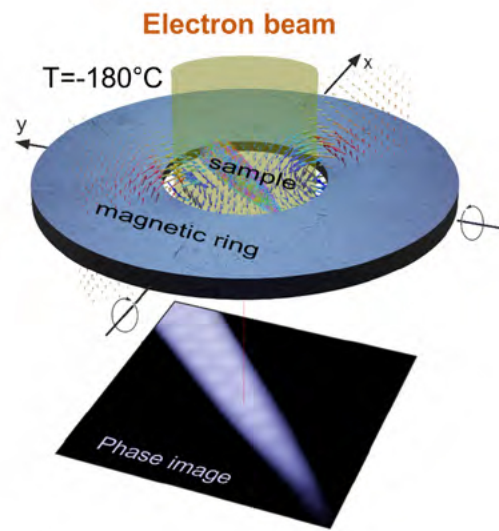


Abb. 3: Prinzip des tomographischen Experimentes im Transmissionselektronenmikroskop. Die Skyrmionen in der Probe werden bei einer Temperatur von -180 °Celsius und einem mittels eines magnetischen Ringes erzeugten äußeren Magnetfeld stabilisiert. Die Probe wird samt Ring um die x- und y-Achse gedreht und die entsprechenden Hologramme aufgezeichnet. Aus den so generierten Daten wird im Computer die magnetische 3D Struktur der Skyrmionenschläuche rekonstruiert.
Fig. 3: Principle of the tomographic experiment in the transmission electron microscope. The skyrmion lattice in the sample is stabilized at a low temperature of -180 °Celsius and by an outer magnetic field generated by a magnetic ring. The sample and the ring are rotated around the x- and y-axis, while the corresponding holograms are acquired. The thereby obtained data are used to reconstruct the magnetic 3D structure of the skyrmion tubes in the computer.

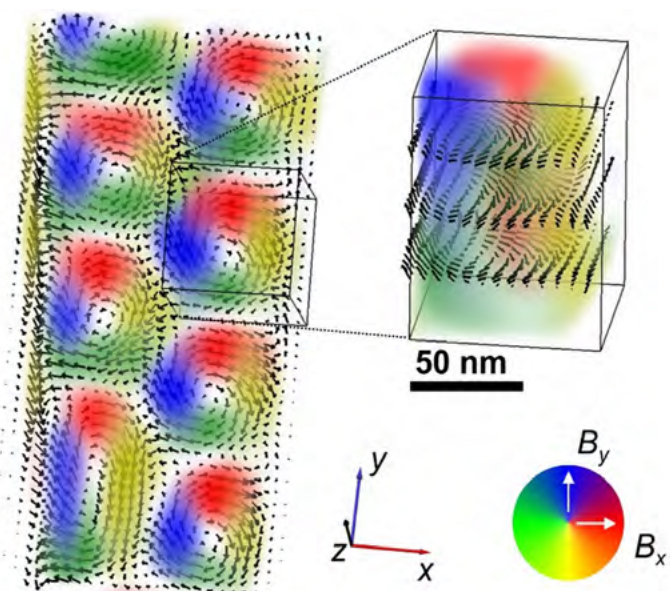


Abb. 4: Rekonstruiertes 3D Vektorfeld der magnetischen Induktion B der Skyrmionen in einer nadelförmigen FeGe Probe. Links: Die farbkodierten Komponenten B_x und B_y sind überlagert mit einer Pfeildarstellung und zeigen Richtung und Stärke des Magnetfeldes mit einer Auflösung von wenigen Nanometern. Rechts: Extrahierter einzelner Skyrmionenschlauch mit Pfeildiagrammen oben, in der Mitte und unten, die erst durch eine tomographische Rekonstruktion zugänglich sind.
Fig. 4: Reconstructed 3D vector field of the magnetic induction B of the skyrmions in a needle-shaped FeGe sample. Left: The color-coded components B_x and B_y overlaid with arrow plots show the direction and magnitude of the magnetic field with a resolution of a few nanometer. Right: Extracted single Skyrmion tube with arrow plots slicing at a top, middle and bottom plane only accessible by tomographic reconstruction.

Saving energy by voltage control of ferrimagnets

Jonas Zehner and Karin Leistner

Die Funktionalisierung magnetischer Eigenschaften mittels elektrischer Felder ermöglicht das Einsparen großer Energiemengen im Informations- und Technologiesektor. Bisher wird die Magnetisierungsumkehr, insbesondere in der magnetischen Datentechnologie, mit elektrischen Strömen bzw. lokalen Magnetfeldern erzielt. Besonders nachteilig erweist sich hierbei der signifikante Energieverlust aufgrund der Joule'schen Erwärmung. Gemeinsam mit den Wissenschaftlern Mantao Huang, Usama Hasan und Geoffrey Beach des Massachusetts Institute of Technology (MIT) konnten wir eine Magnetisierungsumkehr mittels einer geringen elektrischen Spannung in einer ferrimagnetischen Schicht erzielen. Der Ferrimagnet wurde auf einem Antiferromagneten aufgebracht, um eine Verschiebung der Hysteresekurve entlang der Magnetfeldachse zu erreichen.

Voltage control of magnetism is a key concept to dramatically reduce global power consumption in the information and communication sector. So far, in magnetic data technology, the 180° magnetization switching is achieved with electrical currents or local magnetic fields. In both cases, the switching is accompanied with large energy losses by Joule heating. Teaming together with Mantao Huang, Usama Hasan and Geoffrey Beach from Massachusetts Institute of Technology (MIT), we demonstrated 180° magnetization reversal by low voltage-based hydrogen loading into a ferrimagnetic all-solid-state structure. Yielding an adequate sample, the structure was composed of a ferrimagnet sharing an interface with an antiferromagnet yielding a fully shifted hysteresis loop along the magnetic field axis.

Why voltage control of magnetism?

The rapid increase in energy consumption related to digital technologies is a major global challenge. In magnetic data storage media, such as hard disc drives, information is stored through a specific alignment of magnetization in microscopic areas. The direction of magnetization is usually adjusted by electric currents or local magnetic fields –these magnetic fields are also generated by electrical currents in microcoils. In both cases, the electric current leads to energy loss by Joule heating. Therefore, the control of magnetization by electric fields is a promising approach to reduce the energy consumption of magnetic data technologies. [1–3] So far, however, electric field control of magnetization requires high voltages or is restricted to low temperatures. However, a recently discovered approach based on low voltage controlled ionic-migration enables large changes in magnetic properties even at room temperature. [1] The latter approach was generically named magneto-ionics.

What is magneto-ionics?

A typical magneto-ionic device is composed of a ferromagnetic material adjacent to a liquid or solid state electrolyte. The electrolyte serves as a reservoir of ions like oxygen or hydrogen. Upon applying a voltage, the ions in the electrolyte can be moved towards the ferromagnet. The subsequent interaction between the ions and the ferromagnet lead to a change of the magnetic properties, e.g. an ON/OFF switching of the magnetization curve. [1]

What were we aiming for?

In order to profit from the advantages of magneto-ionics and to realize low power magnetic devices, we aimed for a 180° net-magnetization switching in the absence of an external magnetic field.

What sample is suitable for our approach?

As a new approach towards voltage-induced magnetization switching, we took advantage of the specific properties of ferrimagnets. Ferrimagnets offer a multi-sublattice configuration with sublattice magnetizations of different magnitudes opposing each other.

Abb. 1: Dr.-Ing. Jonas Zehner am MOKE-Aufbau zum Messen magnetischer Eigenschaftsänderungen über elektrische Spannungen. Bild: Jonas Zehner/MIT
 Fig. 1: Dr. Jonas Zehner at the MOKE-setup for measuring magnetic property changes triggered by an electrical voltage. Image: Jonas Zehner/MIT

The net magnetization arises from the addition of the sublattice contributions. Ferrimagnets also have technological advantages over conventionally used ferromagnets, as they allow for, for example, fast spin dynamics. [4]

What magneto-ionic effects have been found?

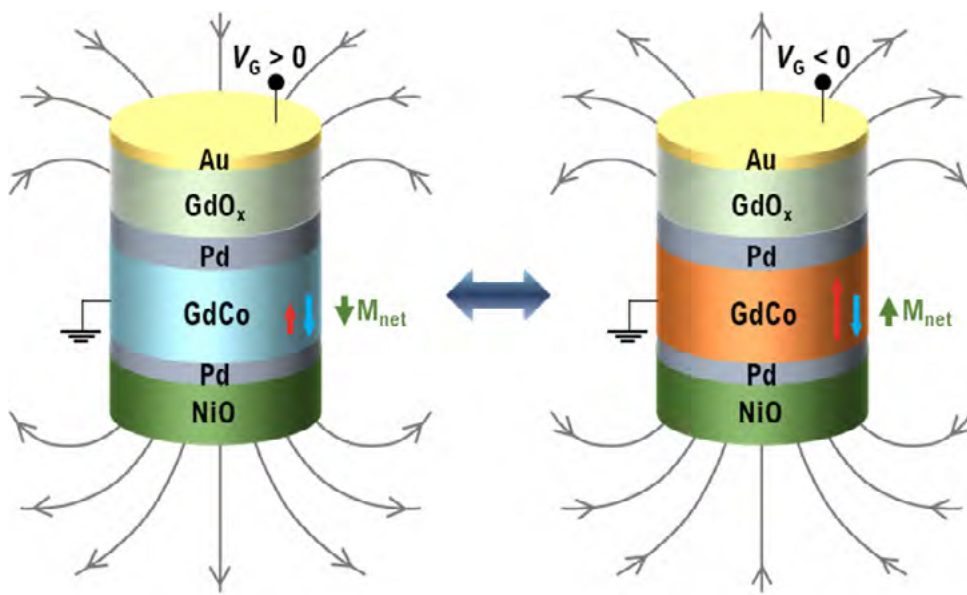
MIT scientists could demonstrate for ferrimagnetic gadolinium-cobalt (GdCo), that the relative sublattice magnetizations can be reversibly toggled by voltage-induced hydrogen loading/unloading. For this, the GdCo was combined with a gadolinium oxide (GdO_x) layer as solid-state electrolyte and a palladium (Pd) interlayer. [5] By applying a gate voltage across the structure, protons are driven to the bottom electrode and lead to hydrogenation of the Pd/GdCo layer. The introduction of hydrogen into the GdCo lattice leads to a stronger reduction of the sublattice magnetization of Gd than that of Co. This so-called magneto-ionic effect is stable over more than 10 000 cycles. It could be evidenced by element-specific X-ray magnetic circular dichroism (XMCD) spectroscopy and is the foundation of the demonstrated magnetization switching.

How can we achieve now a 180° net-magnetization switching?

To achieve 180° magnetization reversal without external magnetic fields, the researchers functionalized the GdCo/Pd/GdO_x-layer structure with an additional antiferromagnetic nickel oxide (NiO) layer. Here, they profit from the so-called “Exchange Bias” effect. This effect occurs when ferri- or ferromagnetic layers are put in contact with an antiferromagnetic layer. It is based on the coupling of the interfacial magnetic spins and leads to the pinning of the magnetization direction of the ferro/ferrimagnet. The exchange bias effect is used, e.g., in magnetic sensors in read heads of hard disc drives to pin the magnetization direction of a reference layer. For ferromagnetic GdCo, the contact to the antiferromagnetic NiO leads to a pinning of the direction of the sublattice magnetizations. In this case, during the magneto-ionic switching, the net magnetization switches by 180°. This signifies, for the first time, a purely electric field controlled magnetization reversal without the assistance of a magnetic field. Prof. Karin Leistner and Dr. Jonas Zehner brought in their expertise on the transfer of magneto-ionic

Abb. 2: Schematische Darstellung der optimierten Exchange bias NiO-GdCo Schicht zur elektrischen Spannungsinduzierten 180° net-Magnetisierungsumkehr.
Bild: Manta Huang

Fig. 2: Scheme of the optimized exchange-biased NiO-GdCo-layers for voltage-induced 180° net magnetization reversal. Image: Manta Huang



180° net magnetization switching sublattices pinned by exchange bias field

control to exchange bias systems. During his PhD time in the research group of Karin Leistner at the IFW Dresden, Jonas Zehner took the opportunity of a six month research stay in the group of Prof. Beach at MIT. During this research stay, together with Prof. Karin Leistner and Prof. Geoffrey Beach, Jonas Zehner initiated and optimized the exchange-bias layer structure required for the 180° magnetization reversal. [5] For this, he first combined the magneto-ionic model system Co/GdO_x with antiferromagnetic NiO. He prepared thin film systems by magnetron sputtering and analyzed the influence of thickness, composition and layer sequence on the resulting exchange bias and magneto-ionic control. The magnetic properties during hydrogen loading were measured with a home-built magneto-optical Kerr Effect setup. With these experiments, he discovered that an ultrathin Pd layer between the GdCo and the NiO is crucial to stabilize the exchange bias effect. [5, 6] With this sample structure, see also Fig. 2, it was possible to demonstrate a voltage induced external-field-free deterministic 180° reversal or the net-magnetization.

Outlook

This result is of outstanding relevance, as 180° magnetization reversal by purely electric fields is inherently difficult from fundamental principles, but it promises a drastic reduction in energy consumption for magnetization switching. For application in data storage and manipulation, 180° magnetization switching is crucial, as the magnetization in the individual bits is usually opposed by 180°. Thus, the result of the study has the potential to open a pathway to dramatically reduced global power consumption of data storage.

Published in

Voltage control of ferrimagnetic order and voltage-assisted writing of ferrimagnetic spin textures
 M. Huang, M. U. Hasan, K. Klyukin, D. Zhang, D. Lyu, P. Gargiani, M. Valvidares, S. Sheffels, A. Churikova, F. Büttner, J. Zehner, L. Caretta, K.-Y. Lee, J. Chang, J.-P. Wang, K. Leistner, B. Yildiz, and G. S. D. Beach Nat. Nanotechnol. 16, 981–988 (2021).
<https://doi.org/10.1038/s41565-021-00940-1>

References

- [1] M. Nichterwitz et al., APL Mater. 9, 030903 (2021).
- [2] J. Puebla et al., Commun. Mater. 1, 24 (2020).
- [3] C. Song et al., Prog. Mater. Sci. 87, 33 (2017).
- [4] L. Caretta et al., Nat. Nanotechnol. 13, 1154 (2018).
- [5] J. Zehner et al., Phys. Rev. Mater. 5, L061401 (2021).
- [6] M. Huang et al., Nat. Nanotechnol. 16, 981 (2021)

Funding

Deutsche Forschungsgemeinschaft (DFG) under project 400178764

Cooperations

Massachusetts Institute of Technology (MIT), Cambridge MA, USA

Kitaev exchange in a geometrically frustrated cobaltate

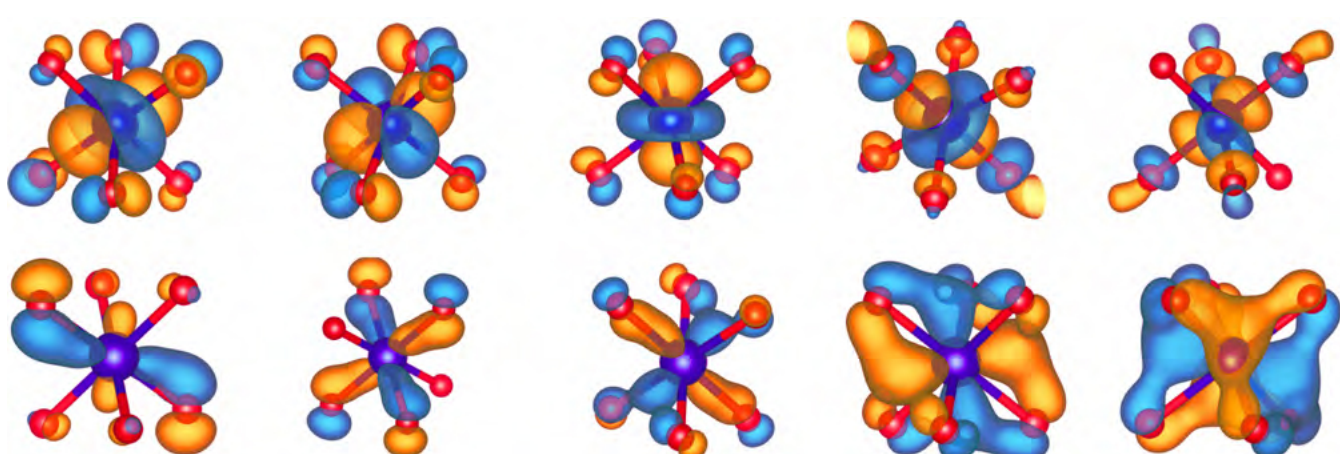
O. Janson, C. Wellm, W. Roscher, J. Zeisner, A. Alfonsov, R. Zhong¹, R. J. Cava¹, A. Savoyant², R. Hayn², S. Nishimoto, J. van den Brink, B. Büchner, and V. Kataev

Das kürzlich synthetisierte Material $\text{Na}_2\text{BaCo}(\text{PO}_4)_2$ hat eine geschichtete Struktur, die aus Dreiecksgittern von Kobaltatomen besteht und weist eine bemerkenswert niedrige kritische Temperatur der magnetischen Ordnung auf. In einer gemeinsamen Studie aus experimentellen und theoretischen Untersuchungen zeigen wir, dass magnetische Korrelationen in diesem Material jedoch erst bei einer viel höheren Temperatur einsetzen. Unsere Berechnungen zeigen, dass das mikroskopische Spinmodell dieses Materials neben dem konventionellen antiferromagnetischen Heisenberg-Austausch auch einen wesentlichen ferromagnetischen Kitaev-Austausch aufweist. Letzteres führt zu Austausch-Frustration, die die vom Dreiecksgitter der Kobaltatome stammende geometrische Frustration verstärkt. Die Kombinationsmöglichkeit der beiden Arten von Frustration macht Kobaltate zu einem vielversprechenden Experimentierfeld für die Entdeckung ungewöhnlicher magnetischer Grundzustände.

The recently synthesized material $\text{Na}_2\text{BaCo}(\text{PO}_4)_2$ has a layered structure shaped by triangular lattices of cobalt atoms and shows a remarkably low long-range magnetic ordering temperature. In this joint experimental and theoretical study, we demonstrate that magnetic correlations in this material, however, set in at a much higher temperature. Using first-principles calculations, we rationalize this puzzling observation and demonstrate that the microscopic spin model of this material features, besides the conventional antiferromagnetic Heisenberg exchange, also a sizable ferromagnetic Kitaev exchange. The latter gives rise to exchange frustration which underpins the geometrical frustration inherent in the triangular lattice formed by cobalt atoms. The possibility of combining the two flavors of frustration renders cobaltates as a promising playground to discover exotic magnetic ground states.

Abb. 1: Wannier-Funktionen, berechnet durch Projektion der vollrelativistischen Bandstruktur auf Kobalt-3D-Orbitalzuständen beider Spins. Sowohl für die Berechnungen als auch für die Visualisierung wurde der am IFW entwickelte Full-Potential-Local-Orbital-Code FPLO verwendet.

Fig. 1: Wannier functions evaluated by projecting the full-relativistic band structure onto cobalt 3D-orbital states of both spins. The full-potential local-orbital code FPLO developed at the IFW was used for calculations as well as visualization.



In the borderland of condensed matter physics and material science, the hunt for unconventional magnetic materials is raging. A renowned hunting ground for exotic magnetism are magnetic Mott insulators with localized magnetic moments. The collective behavior of such moments is captured by the Heisenberg model whose microscopic parameters are magnetic exchange interactions. If these interactions are ferromagnetic, every moment can lower its energy by aligning itself parallel to its neighbors. Conversely, antiparallel arrangement is favored by more ubiquitous antiferromagnetic interactions. Since entropy contributions are dominant at high temperatures, magnetic moments are fluctuating. Cooling down to temperatures comparable to the exchange energy typically promotes long-range magnetic ordering, giving rise to a ferromagnet or to an antiferromagnet, depending on the sign of the magnetic exchange.

Yet, some magnetic insulators order at a much lower temperature or even evade magnetic ordering completely. We know two fundamentally different ways of suppressing the ordering temperature. One possibility is to make antiferromagnetic exchanges compete with each other. This scenario is realized in certain geometries that feature closed loops with an odd number of moments. A prime example of such loops is a triangle, and a lattice comprising triangles - the triangular lattice - is the simplest geometrically frustrated lattice. No ordered state of a triangular lattice can satisfy all antiferromagnetic exchanges simultaneously. This key observation paved the way to the spin liquid, a concept introduced by the Nobel prize winner Philip W. Anderson [1]. Spin liquid is a state that lacks a long-range magnetic order even at zero temperature. Such an exotic state is actively sought for.

Another possible scenario can be realized if exchanges are anisotropic, i.e. they confine the magnetic moments to a certain direction. In most materials, this direction is common for all spins, and it governs the magnetic anisotropy. Yet, competition is reinstated if the preferred directions become bond-dependent. Most prominent example of such frustration is the Kitaev model for which the existence of a spin liquid ground state can be proven rigorously [2]. It remains an open question whether the pure Kitaev

model has any material realizations. However, materials that entail the Heisenberg-Kitaev model, a hybrid of Kitaev and Heisenberg models, that were first predicted theoretically [3], and then found and studied experimentally. An example of such a Heisenberg-Kitaev material is $\alpha\text{-RuCl}_3$ whose physics has been intensively studied in the last five years, with prominent insights contributed by the IFW researchers [4]. More recent theory works put forward honeycomb-lattice materials with divalent cobalt with seven electrons in the 3d-shell as a more promising playground to realize Kitaev physics [5]. Although most cobaltates are high-spin systems with conventional anisotropy, in some materials the spin-orbit coupling stabilizes the effective low-spin behavior at low temperatures, and these systems are particularly interesting. Magnetic frustration here is driven by the exchange anisotropy, because the underlying honeycomb lattice comprises hexagons — closed loops with an even number of spins. Hence, geometrical frustration and exchange frustration are largely two disparate fields.

The status quo seemed to be intact after the successful synthesis of the triangular-lattice cobaltate $\text{Na}_2\text{BaCo}(\text{PO}_4)_2$ (Fig. 2). The behavior of this material conformed to that of a typical geometrically frustrated magnet: the first experimental paper reported a sizable Weiss temperature (this quantity is proportional to the sum of all magnetic exchanges) and failed to see any magnetic ordering down to the lowest temperatures measured [6]. Magnetic ordering has been established in a later study [7] by another group, yet with the ordering temperature of 150 mK which is more than an order of magnitude smaller than the Weiss temperature of 2.5 K, leaving no doubt that this magnet is strongly frustrated. However, the nature of the ground state and even the stability of the low-spin state of cobalt have not been explored.

To get more information on the spin state of cobalt, we measured electron spin resonance (ESR) on powder and single-crystalline samples of $\text{Na}_2\text{BaCo}(\text{PO}_4)_2$. This spectroscopic technique is the method of choice for measuring g-factors, a quantity characteristic for the state of magnetic ions. Even more importantly, ESR is sensitive to spin dynamics and hence can be used as a probe for magnetic

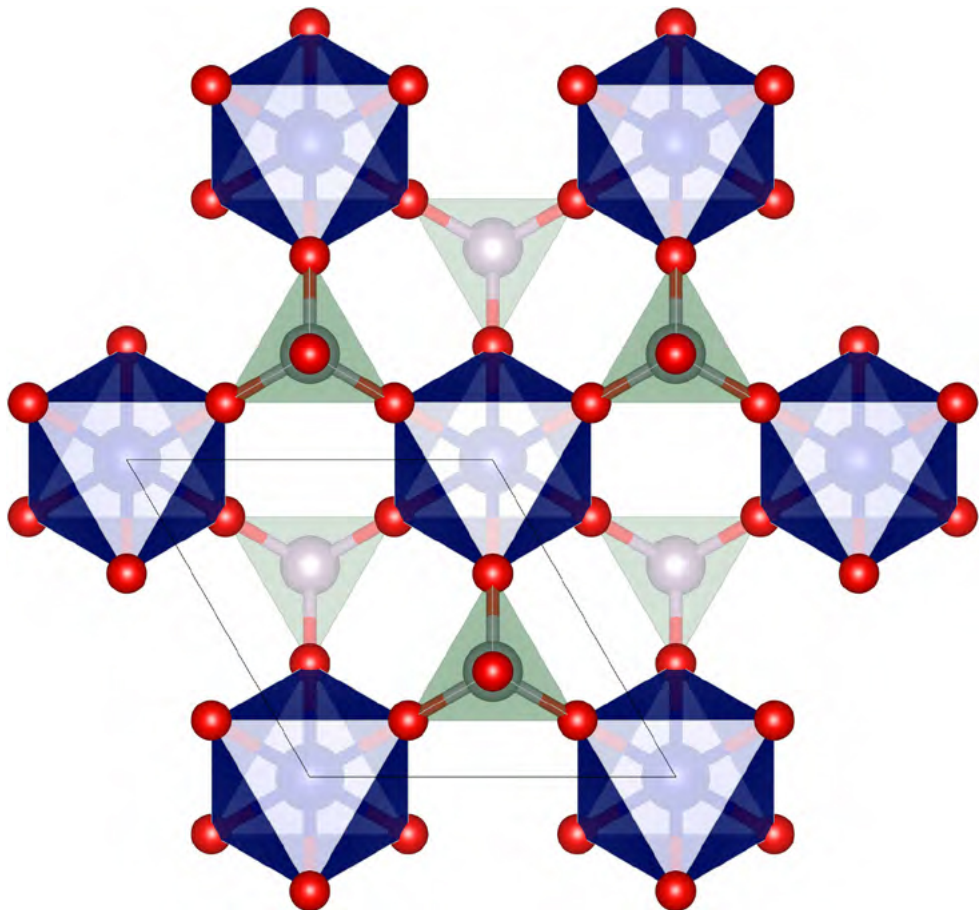


Abb. 2: Kristallstruktur von $\text{Na}_2\text{BaCo}(\text{PO}_4)_2$ mit CoO_6 -Oktaedern, die durch Doppelbrücken von PO_4 -Tetraedern verbunden sind. Diese Überbrückungen ermöglichen neben dem antiferromagnetischen Heisenberg-Austausch auch einen wesentlichen Kitaev-Austausch. Die daraus resultierende Austauschanisotropie unterstützt die geometrische Frustration, die auf das Dreiecksgitter der Kobaltatome zurückzuführen ist.

Fig. 2: Crystal structure of $\text{Na}_2\text{BaCo}(\text{PO}_4)_2$ featuring CoO_6 octahedra connected by double bridges of PO_4 tetrahedra. These connections facilitate besides the antiferromagnetic Heisenberg exchange, also a sizable Kitaev exchange. The resulting exchange anisotropy underpins geometrical frustration stemming from the triangular lattice of cobalt atoms.

correlations: the onset of the latter manifests itself as line broadening. Quite surprisingly, our ESR measurements revealed significant line broadening at temperatures around 20 K, i.e. much higher than the alleged magnetic exchange energy scale estimated from the Weiss temperature.

Puzzled by the unusually high temperature scale of magnetic correlations, we commenced a detailed computational analysis by means of first-principles band-structure calculations. To this end, we employed the density-functional-theory code FPLO [8] developed at the IFW and calculated the full-relativistic band structure of $\text{Na}_2\text{BaCo}(\text{PO}_4)_2$. Using the real-space Wannier representation, we constructed a microscopic model which comprises the cobalt states relevant for the magnetism. This model contains two kinds of terms: local terms that describe electron transfer between different spin-orbitals of the

same atom, and interatomic hopping terms. First, we restricted ourselves to the local picture. By supplementing the model with the Coulomb repulsion terms, we were able to employ multiplet calculations and solve the local problem numerically. In this way, we identified a distinct hierarchy of energy scales (Fig. 3): the cubic crystal-field splitting followed by the spin-orbit coupling and the trigonal crystal field splitting. A quantitative analysis revealed excellent agreement with the experiments and allowed us to confirm the effective low-spin behavior of $\text{Na}_2\text{BaCo}(\text{PO}_4)_2$ at low temperatures. Our calculated g-factors are in good agreement with the experiment, additionally justifying the computational procedure. The analysis of interatomic hopping terms allowed us to exclude the possibility of having additional long-range as well as interplane exchanges, and establish $\text{Na}_2\text{BaCo}(\text{PO}_4)_2$ as an excellent nearest-

neighbor triangular-lattice system. By inspecting the orbital dependence of nearest-neighbor hoppings, we noticed that these processes can be described by an effective model which represents a limiting case of a more elaborate model [9] worked out for honeycomb-lattice cobaltates. In this way, we find that in addition to the antiferromagnetic Heisenberg exchange between the nearest-neighbor cobalt atoms, $\text{Na}_2\text{BaCo}(\text{PO}_4)_2$ features a sizable ferromagnetic Kitaev exchange whose magnitude amounts to 75 percent of its Heisenberg counterpart. Therefore, this geometrically frustrated material also has a sizable exchange anisotropy.

The Kitaev exchange was the missing piece of the puzzle that helped us to reconcile the low Weiss temperature with the onset of magnetic correlations at a much higher temperature. Since the Weiss temperature scales with the sum of all exchanges, the addition of the ferromagnetic Kitaev exchange (a negative number) to the antiferromagnetic Heisenberg exchange (a positive number) drastically suppresses it. At the same time, it enhances the overall magnetic energy scale and propels magnetic correlations to higher temperatures; they manifest themselves in the experimentally observed ESR line broadening.

We additionally found that the microscopic model parameters are very sensitive to internal atomic positions. Hence, the physics of $\text{Na}_2\text{BaCo}(\text{PO}_4)_2$ can be tuned by applying external pressure or by chemical substitutions. Substitutions of phosphorus with arsenic and especially with vanadium may strongly influence the ratio of the Heisenberg and Kitaev exchanges and in this way alter the ground state of the material.

Our joint experimental and theoretical work [10] establishes the triangular-lattice cobaltate $\text{Na}_2\text{BaCo}(\text{PO}_4)_2$ as a very special low-dimensional magnet, where both geometrical and exchange frustration are at play. The latter is facilitated by the sizable ferromagnetic Kitaev exchange.

References

- [1] P. W. Anderson, Mater. Res. Bull. 8, 153 (1973).
- [2] A. Kitaev, Ann. Phys. 321, 2 (2006).
- [3] G. Jackeli et al., Phys. Rev. Lett. 102, 017205 (2009).
- [4] A. Koitzsch et al., Phys. Rev. Lett. 117, 126403 (2016).
- [5] H. Liu et al., Phys. Rev. Lett. 125, 047201 (2020).
- [6] R. Zhong et al., Proc. Natl. Acad. Sci. USA 116, 14505 (2019).
- [7] N. Li et al., Nat. Commun. 11, 4216 (2020).
- [8] K. Koepernik et al., Phys. Rev. B 59, 1743 (1999).
- [9] H. Liu et al., Phys. Rev. B 97, 014407 (2018).
- [10] C. Wellm et al., Phys. Rev. B 104, L100420 (2021).

Funding

This work was supported by the DFG (Project KA 1694/12-1), SFB 1143 (Project No. 247310070), the Cluster of Excellence on *Complexity and Topology in Quantum Matter - ct.qmat* (EXC 2147, Project Id No. 390858490), the Gordon and Betty Moore Foundation (EPiQS Program, Grant No. GBMF-4412), and the Leibniz Association through the Leibniz Competition (Grant No. J50/2018).

Cooperations

- ¹⁾ Princeton University, USA
²⁾ Aix-Marseille Université, France

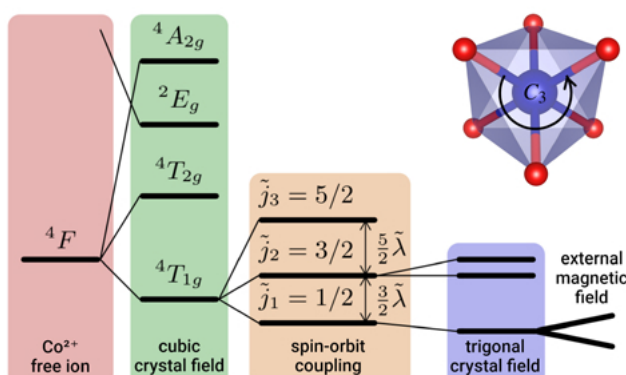


Abb. 3: Energieskalen eines isolierten CoO_6 -Oktaeders in $\text{Na}_2\text{BaCo}(\text{PO}_4)_2$, ausgewertet durch Multiplett-Rechnungen unter Verwendung der durch Ab-Initio-Rechnungen erhaltenen Parameter. Es gibt eine ausgeprägte Hierarchie der Energieskalen: Das kubische Kristalfeld ist viel stärker als die Spin-Bahn-Kopplung, die wiederum viel größer ist als das trigonale Kristalfeld.
 Fig. 3: Energy scales of an isolated CoO_6 octahedron in $\text{Na}_2\text{BaCo}(\text{PO}_4)_2$ evaluated by multiplet calculations using the parameters obtained by first-principles calculations. There is a distinct hierarchy of energy scales: the cubic crystal field is much stronger than the spin-orbit coupling that is in turn much larger than the trigonal crystal field.

Creating ferroic micropatterns through geometrical transformation

Volker Neu, Ivan Soldatov, Rudolf Schäfer, Dmitriy D. Karnaushenko, Alaleh Mirhajivarzaneh, Daniil Karnaushenko, Oliver G. Schmidt

Die Funktionalität eines ferroischen, beispielsweise ferromagnetischen Bauteiles wird entscheidend von der Anordnung der inneren ferroischen Domänen bestimmt. In einem neuen Verfahren wird die Erzeugung solch eines Multidomänenzustandes durch eine geometrische Transformation erreicht. Durch die Deposition einer ferromagnetischen Schicht auf einer strukturierten Polymerunterlage kann durch An- und Abschwellen die funktionale Lage wiederholt auf- und abgerollt werden. Wird die ferromagnetische Schicht nun im aufgerollten 3D-Zustand magnetisiert, entspricht die eingeprägte Magnetisierungsrichtung einem regelmäßigen Mehrdomänenzustand in der abgerollten, ebenen Schicht. Dies bietet einzigartige Möglichkeiten zur Erzeugung neuartiger magnetischer Multidomänenzustände auf der Mikrometerskala.

The functionality of a ferroic such as a ferromagnetic or ferroelectric device is intimately coupled to the configuration of domains and the possibility for tailoring them. We present a novel approach which allows the creation of such ferroic multidomain patterns through a self-assembled geometrical transformation. By preparing a magnetic layer on a polymeric platform including swelling layer, it can repeatedly be transformed into a micron-sized multiwinding tube and back into a flat film. When magnetized in the rolled-up 3D state in a simple homogeneous magnetic field, the imprinted magnetization configuration translates into a regularly arranged multidomain pattern once the tubular structure is unwound. This offers unparalleled possibilities for designing new magnetic or other ferroic micropatterns.

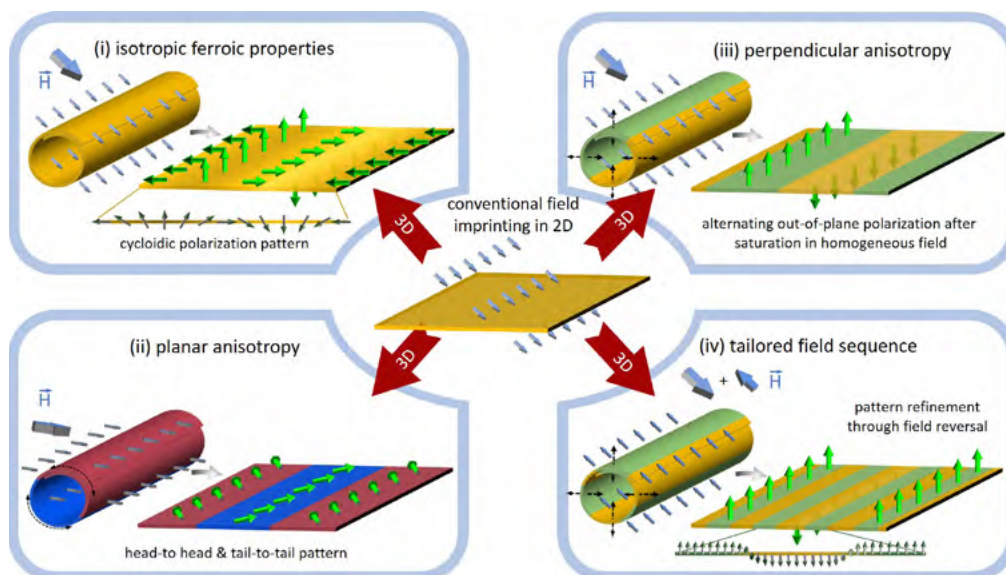


Abb. 1: Beispiele für mögliche ferroische Multidomänenzustände mittels einer geometrischen Transformation: Durch das selbstorganisierte Aufrollen einer Schicht nimmt ein homogenes Feld einen kontinuierlich variierenden Winkel zur lokalen Oberfläche ein. Dies führt, abhängig von der Anisotropie des verwendeten Materials, zu unterschiedlichen regelmäßigen Multidomänenzuständen nach selbstorganisiertem Abrollen.

Fig. 1: Examples of possible ferroic micropatterns created through geometrical transformation: depending on the ferroic anisotropy, a homogeneous physical field applied to a self-assembled tubular structure will create various regular microtextures in the unrolled film.

Designing a microscale multidomain configuration by traditional means requires either a local writing in a serial fashion or the application of a modulated field. The necessity for an increased control of ferroic domain formation and their application in ferroic devices [1, 2] asks for an approach, which is at the same time simple, allows for device integration, resolves limitations of the existing strategies and extends the possibilities to the formation of new, metastable domain and nanoscale domain wall configurations.

We developed such a novel concept for tailoring physical micropatterns in functional ferroic layers by using a geometrical transformation [3]. The central innovation is to bring a 2D layer architecture into an intermediate 3D tube state, in which a simple homogeneous field is applied to polarize the ferroic layer. For a hard-ferroic material, i.e. for non-vanishing coercivity, the polarized state can be maintained in zero field. However, contrary to the polarization of a 2D layer, the locally varying angle between applied field and surface normal enables creating a multitude of regular micropatterns, once the intermediate 3D structure is unwound. Different possibilities arise from various types of ferroic anisotropies and some examples are summarized in Fig. 1. (i) For an isotropic ferroic material, in which the polarization vector locks in the direction of the local field, the unrolling of the tube leads to a cycloidal polarization arrangement along one trajectory (the former rolling direction). (ii) In layers with planar anisotropy, in which polarization can be set along the in-plane projection of the external field, a saturation of the tubular structure leads to regular domains in head-to-head and tail-to-tail configuration. (iii) and (iv) In hard-ferroic films with perpendicular anisotropy, regular domains with alternating polarization in out-of-plane direction are envisaged. The mechanism for this later configuration is detailed in Figure 2a. Once the film is rolled up into a multi-winding tube a saturating field is applied perpendicular to the tube, pulling the polarization in field direction (i). When the field is removed, the polarization will relax locally towards the anisotropy direction with smallest angle to the formerly applied field. Thus, the film will remain polarized in outward direction in the forward bent half of the tube and inwardly polarized in the backward bent half of the tube (ii).

After unrolling, a tailored out-of-plane multi-domain configuration is achieved, naturally imprinting polarization configurations into the ferroic layer, which would otherwise need a much more elaborate process or a serial writing technique.

That the concept indeed leads to the expected result is seen in panel (b, c). A ferromagnetic layer is deposited on a so-called polymeric platform including a swelling layer, which transforms into a multiwinding tube with about 100 µm diameter (Fig. 2b). After saturation and un-rolling of the tubular structure in the remanent magnetic state, Kerr microscopy with polar contrast reveals the regular arrangement of alternating perpendicular domains. The analysis of the domain coordination (Fig. 2d) confirms an average domain period of about 330 µm, which corresponds to the circumferential length according to the model (Fig. 2a (iii)).

In order to realize the experiment, IFW's central interest to comprehend and characterize magnetic microstructures [4 - 6] was combined with the likewise long-standing expertise in transforming thin films into 3-dimensional tubular structures by utilizing strain-driven layer architectures [7, 8]. Here, a ferromagnetic $[Co(0.5)/Pt(1.0)]_5$ multilayer (numbers in parenthesis give layer thicknesses in nanometer) was deposited on a polymeric platform (PP) consisting of sacrificial layer (SL), hydrogel (HG) as a swelling layer and a stiff polyimide (PI) layer. This platform allows a self-assembling of a flat film into a tubular structure by swelling the hydrogel in an appropriate solution, once the sacrificial layer is etched. The technology has already been successfully applied to create miniaturized, 3-dimensional microelectronic devices and magnetic sensors with integrated electrical circuits [9, 10].

The process is easily controlled, self-assembled and works in a parallel fashion on lithographically defined structures on the wafer scale [8]. Contrary to non-organic strain-driven platforms, such as e.g. epitaxially strained InGaAs/GaAs bimorphs [7] or growth-strained SiN_x membranes [11] the PP allows a repeatable geometrical transformation in aqueous solution by simple control of the pH-value [12].

Patterns of SL/HG/PI/ $[Co(0.5)/Pt(1.0)]_5$ /PI are structured by optical lithography, with trenches in the PI layers defining the anchored membrane edge

and rolling direction.

The HG/PI/[Co(0.5)/Pt(1.0)]₅/PI membranes are partially released from the glass substrates by etching the SL in an acidic solution with pH = 1.

After having applied a homogenous magnetic field of $\mu_0 H = 1\text{ T}$ to the rolled-up tube, the 3D structure unrolls upon un-swelling the HG layer in deionized water, and regularly arranged domains are observed which run parallel to the anchored membrane axis (i.e. former tube axis), as already discussed in Fig. 2c.

In the following, a domain refinement process is discussed, which is based on a modified field sequence. Rather than merely saturating the tube, a field opposite to the previous saturation will form new domains in a typical nucleation and growth process. These secondary domains are sketched in Fig. 3b as inwardly oriented magnetization on the right half circle and outwardly oriented magnetization on the left half circle. Nucleation will commence in angular regions with lowest nucleation field, and will not enter angular regions, in which field strength and orientation prohibit nucleation or expansion. Domain boundaries again adopt to the geometry of the rolled tube by running parallel to the tube axis. The back-transformation to 2D now offers an undisgu-

sed look into the magnetization processes occurring in the 3D structure. The initiation and progression of domains is fully apparent, when tubes are unwound after different strengths of the reversal field (Fig. 3a). After simple saturation ($H_{\text{rev}} = 0$) only the primary domains with smooth domain boundaries are observed; for reversal fields of 70 mT and above, secondary domains nucleate in the center of the primary domains, where field orientation is parallel to the local anisotropy axis. With larger H_{rev} these domains grow and fill a larger angular range.

Figure 4b summarizes the corresponding angle dependent reversal field. Qualitatively, it closely follows the $1/\cos \theta$ behavior known for domain wall propagation processes in thin films with uniaxial anisotropy [13]. There, domain wall propagation is driven by the field component parallel to the anisotropy axis, and a tilted orientation requires a correspondingly larger field magnitude. For a quantitative comparison, the angle dependent tilting of magnetization within the domains has to be considered according to the modified Kondorsky law [14]. It describes the experimental data with two fit parameters, the reversal field for normal incidence $H_{\text{rev}}(\mu_0) = 0.065\text{ T}$, and the effective perpendicular anisotropy field

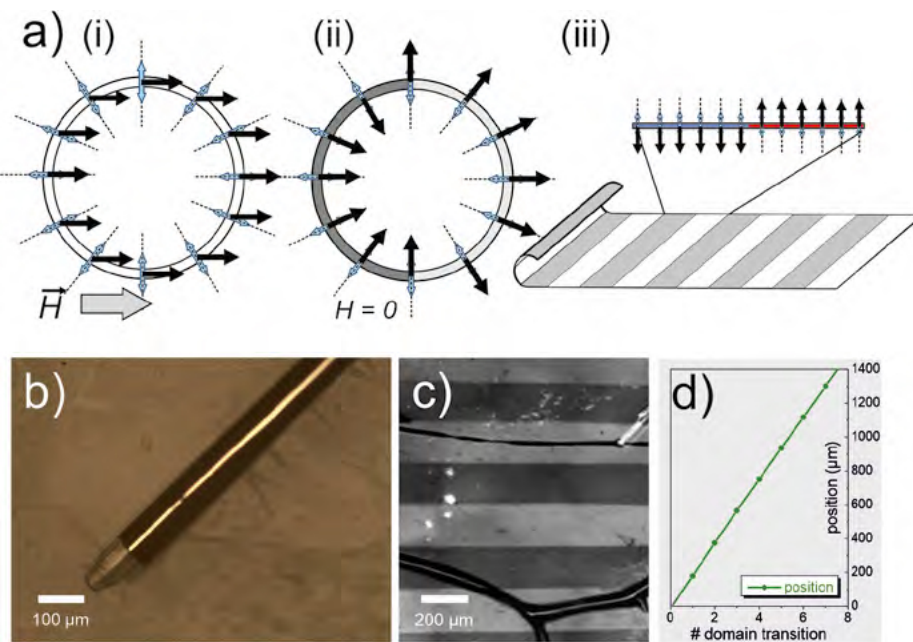


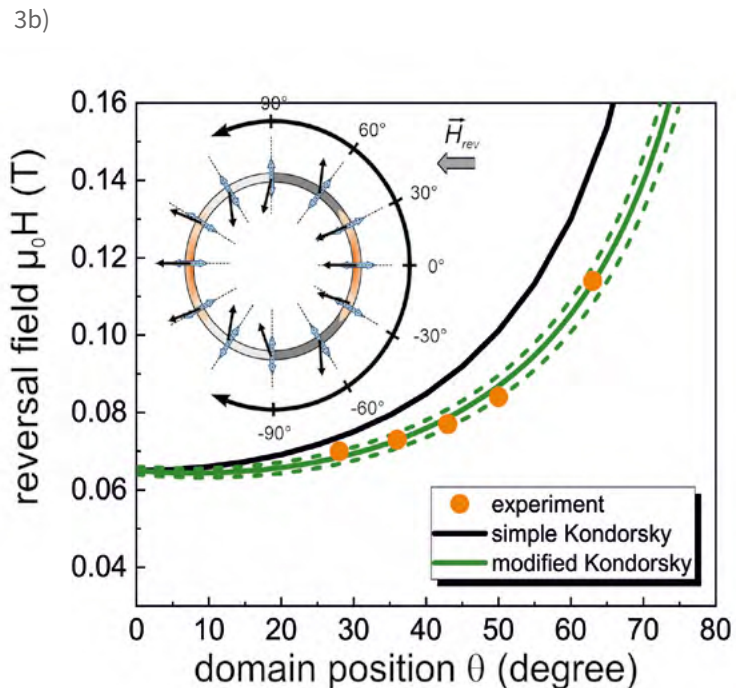
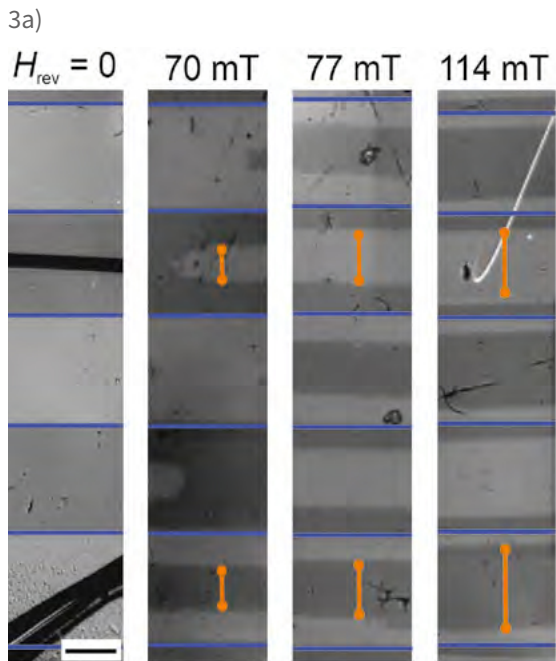
Abb. 2: (a) (i) Aufgerollte Schicht mit senkrechter magnetischer Anisotropie in einem sättigenden Feld senkrecht zur Röhre, und (ii) nach Relaxation in den remanenten Zustand; (iii) nach dem Abrollen ist ein regelmäßiger Zweidomänenzustand eingeprägt. (b) Abbildung einer [Co/Pt] Vielfachschicht auf Polymerunterlage im aufgerollten Zustand. (c) Kerrmikroskopische Aufnahme des regelmäßigen Zweidomänenzustandes nach Abrollen. (d) Analyse der Domänenposition.

Fig. 2: (a) (i) Rolled film with perpendicular magnetic anisotropy exposed to a magnetic field perpendicular to the tube, and (ii) after relaxing into the remanent state; (iii) after unwinding, a bipolar magnetic texture is imprinted. (b) optical image of a [Co/Pt] multilayer prepared on PP in the rolled state. (c) Regular perpendicular magnetic domains after unwinding, observed by Kerr microscopy. (d) Analysis of domain coordination.

$\mu_0 H_{ani} = (700 \pm 50) \text{ mT}$ in good agreement with the values from magnetic hysteresis measurements of the unrolled magnetic layer. In total, the angle dependence resembles the magnetization reversal process expected for a flat film in a tilted field, but with one important difference: the geometrical transformation connects the angular degree of freedom with a lateral degree of freedom, which enables the simple creation of parallel running domains with controlled position of the domain boundaries in a simple homogeneous field.

Abb. 3: Untersuchung der winkelabhängigen Magnetisierungsprozesse im aufgerollten Zustand durch nachträgliches Abrollen der Schicht. (a) Kerrmikroskopische Aufnahme von primären (blaue Linien) und sekundären (orange Pfeile) Domänen als Funktion des Ummagnetisierungsfeldes. Mit größer werdendem Feld wachsen die sekundären Domänen in azimutaler Richtung. (b) Ummagnetisierungsfeld als Funktion der Sekundärdomänenposition (Winkel). Die Daten werden sehr gut mit einem modifizierten Kondorsky-Verhalten beschrieben. Die Modellparameter betragen $\mu_0 H_{rev}(0) = 0.065 \text{ T}$ und $\mu_0 H_{ani} = (0.70 \pm 0.05) \text{ T}$.

Fig. 3: Unveiling the angle dependent magnetization reversals in rolled-up tubes by unwinding the membrane. (a) Primary and secondary domains (polar Kerr contrast) as a function of recoil field. With increasing field, the secondary domains grow in azimuthal direction. The dark features for $H_{rev} = 0$ are topographic contrast from exceptional folds in the unwound membrane. (b) Reversal field as a function of the boundary angle of the secondary domain, deduced from the domain coordination in the unrolled films. Parameters for the modified Kondorsky model are $\mu_0 H_{rev}(0) = 0.065 \text{ T}$ and $\mu_0 H_{ani} = (0.70 \pm 0.05) \text{ T}$. The inset illustrates the domain formation and expansion during the recoil step.



References

- [1] A. Sarella et al., Adv. Mater. 26, 2384 (2014).
- [2] K. Wagner et al., Nat. Nanotechnol. 11, 432 (2016).
- [3] V. Neu et al., Nano Letters 21, 9889 (2021).
- [4] A. Hubert, R. Schäfer, Magnetic Domains; Springer Heidelberg, 1998.
- [5] S. Vock et al., Appl. Phys. Lett. 105, 172409 (2014).
- [6] I. Soldatov, R. Schäfer, Rev. Scient. Instr. 88, 073701 (2017).
- [7] D. Grimm et al., Nano Lett. 13, 213 (2013).
- [8] D. Karnaushenko, T. Kang, and O. G. Schmidt, Adv. Mater. Techn. 4, 1800692 (2019).
- [9] D. Karnaushenko et al., Adv. Matter. 27, 6583 (2015).
- [10] Ch. Becker et al., Self-assembly of highly sensitive 3D magnetic field vector angular encoders. Sci. Adv. 5, eaay7459 (2019).
- [11] W. Huang et al., Nature Electronics 1, 305 (2018).
- [12] D. Karnaushenko et al., Adv. Matter. 27, 6797 (2015).
- [13] E. Kondorsky, J. Phys. (USSR) 2, 161 (1940).
- [14] F. Schumacher, J. Appl. Phys. 70, 3184 (1991).

Funding

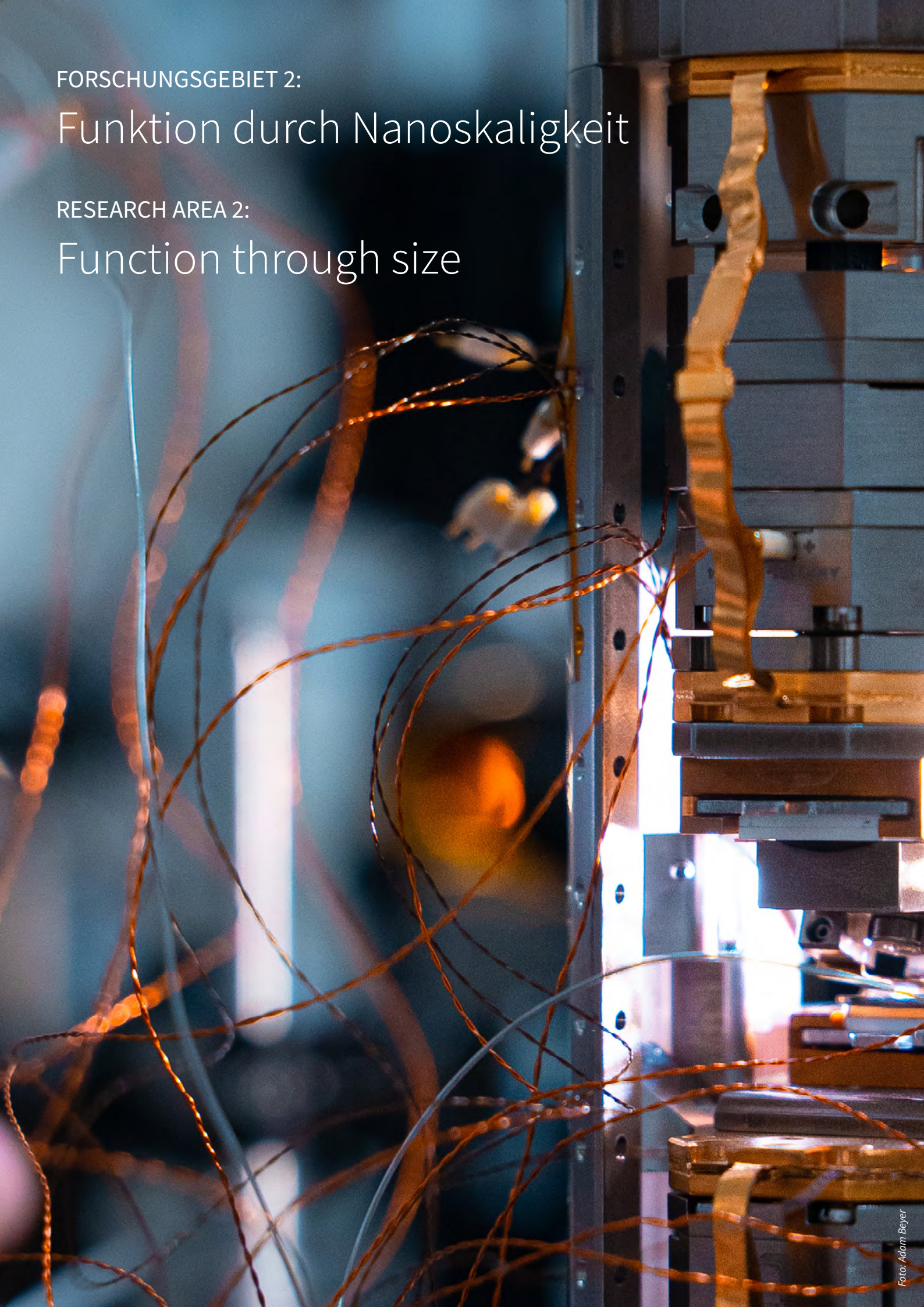
This work was supported by the German Research Foundation DFG (Gottfried Wilhelm Leibniz Prize granted in 2018, SCHM 1298/22-1 and KA5051/1-1), as well as by the Leibniz association (Leibniz Transfer Program 62/2019).

FORSCHUNGSGEBIET 2:

Funktion durch Nanoskaligkeit

RESEARCH AREA 2:

Function through size



Funktion durch Nanoskaligkeit

Dieses Forschungsgebiet befasst sich mit Materialien, deren Eigenschaften aus strukturellen Anordnungen im Nanomaßstab resultieren: Dazu gehören Nichtgleichgewichts- und nanostrukturierte Legierungen, aufgerollte Nanomembranen und Mikromotoren sowie thermoelektrische Materialien. Die Funktionalität dieser Materialien hängt entscheidend von der Größe ihrer Partikel und von Oberflächeneffekten ab. Viele Materialeigenschaften ändern sich beim Übergang vom makroskopischen über den mikroskopischen zum nanoskopischen Maßstab. Das wird in nanostrukturierten Legierungen deutlich, die für Anwendungen als Biomaterialien und als hochfeste Werkzeuge entwickelt werden. Ein weiterer Schwerpunkt sind elastische oder aufgerollte Nanomembranen, die in einer neuen Generation von flexiblen und kompakten On- und Off-Chip-Bauelementen eingesetzt werden. Das Forschungsgebiet 2 umfasst weiterhin die Entwicklung neuer thermoelektrischer Materialien: Durch Nanostrukturierung und den Einsatz spezieller Legierungen soll die Effizienz thermoelektrischer Bauelemente erhöht werden, um das Anwendungspotential zu erweitern. All diese Themen beleuchten die Struktur, die chemische Zusammensetzung und die physikalischen Eigenschaften von Materialien auf unterschiedlichen Längenskalen. Die Forschung wird von der intensiven Vernetzung interdisziplinärer Teams aus den Bereichen Materialwissenschaft, Elektroingenieurwesen, Physik und Chemie getragen.

Function through size

This Research Area comprises research on materials with properties arising from structural arrangements at nanoscale. These are non-equilibrium and nano-structured alloys, rolled-up nanomembranes and micromotors, as well as thermoelectric materials. The functionality of these materials decisively depends on the size of their particles and on interfaces. This is evident in nanostructured alloys that are developed for applications as biomaterials and as high-strength tools. Another focus is on elastic or rolled-up nanomembranes which will be exploited in conceptually new generations of flexible and compact on- and off-chip devices. Shape, size and interfaces also determine the fundamental properties of nanomagnets, which may find use in magnetic probes and data storage elements.

We also address the improvement of new thermoelectric materials, e.g. special alloys, and the various capabilities of nanostructuring show enhanced efficiency and promise new applications. All research efforts are cross-linked by common methodological approaches and interests, which shed light on the structure, chemical composition and physical properties of materials at different length scales. The research area relies on the expertise of an interdisciplinary team of materials and electrical engineers, physicists and chemists and deals with the unique mechanical and functional properties of materials as they or their constituents change from macro-, to micro- and nanoscopic sizes.

Towards tellurium-free thermoelectric modules for power generation from low-grade heat

Pingjun Ying, Ran He, Jun Mao¹, Qihao Zhang, Heiko Reith, Jiehe Sui², Zhifeng Ren¹, Cornelius Nielsch, Gabi Schierning

Mit thermoelektrischen Modulen kann Wärme direkt in sogenannten sauberen Strom umgewandelt werden. Aufgrund der außergewöhnlich günstigen thermoelektrischen Eigenschaften bei Temperaturen unter 300 °Celsius bestehen derartige kommerziell hergestellte Module bisher aus Bismut-Tellurid-Verbindungen. Das Element Tellur kommt jedoch nur in kleinen Mengen in der Erdkruste vor, was die Anwendung im großen Stil stark einschränkt. Wir haben erstmals einen hocheffizienten Tellur-freien thermoelektrischen Generator auf Basis von Magnesium-Antimon-Verbindungen entwickelt. Diese neuen Generatoren übertreffen sogar den Wirkungsgrad vergleichbarer Bauteile auf Bismut-Tellurid-Basis. Diese Arbeit stellt eine nachhaltige Alternative zu bisher bekannten Methoden dar und wird eine breitere Anwendung der thermoelektrischen Technologie ermöglichen. (> Fokus Nachhaltigkeit, Seite 17)

Thermoelectric technology converts heat into electricity directly and is a promising source of clean electricity. Commercial thermoelectric modules have relied on bismuth-telluride-based compounds because of their unparalleled thermoelectric properties below 300 °Celsius. However, the scarcity of elemental tellurium greatly limits the applicability of such modules. Here we developed for the first time a highly efficient tellurium-free thermoelectric generator based on magnesium-antimony compounds. These new thermoelectric generators even exceed the efficiency of commercial bismuth-telluride-based thermoelectric generators. This work marks a feasible, sustainable alternative to bismuth-telluride-based thermoelectric modules and will spur a wider application of thermoelectric technology.

(> Focus Sustainability, page 17)

Abb. 1: Thermoelektrische Generatoren wandelt Temperaturunterschiede direkt in elektrische Energie um.
Fig. 1: A thermoelectric generator converts temperature differences directly into electrical energy.



Thermoelectric low-grade heat harvesting

More than 60 percent of the energy generated by burning fossil fuels is dissipated as waste heat, of which more than half is low-grade heat with temperatures below 300 °Celsius. Effective harnessing this low-grade heat to generate electricity is vital for alleviating the burden on the energy supply and reducing the emission of greenhouse gases. Thermoelectric technology stands out owing to its solid-state nature, which guarantees an ultra-long operational lifetime and is particularly attractive for heat-to-electricity conversion. The broader applicability of thermoelectric technology relies on the availability of high-performance materials and modules that operate efficiently below 300 °Celsius.

Towards tellurium-free thermoelectric module

For more than 50 years, commercial thermoelectric modules have relied on bismuth-telluride-based compounds because of their unmatched thermoelectric properties at temperatures associated with low-grade heat. However, the wider applicability of bismuth-telluride modules is severely limited by the scarcity of Tellurium (Te) with a concentration of <0.001 ppm in the Earth's crust and an annual production of less than 500 metric tons.

Therefore, it is imperative to develop thermoelectric modules from other, more abundant materials while retaining high performance in the low-temperature range (<300 °Celsius).

Mg-based materials, including n-type Mg₃(Sb, Bi)₂ and p-type MgAgSb have attracted great attention from the TE community for replacing Bi₂Te₃ because of the non-toxic nature, the abundance of their constituent elements, and their high *zT* of ~1.0 at temperatures < 300 °Celsius. Moreover, these materials exhibit excellent mechanical robustness and compatible TE properties between the n-type and p-type TE materials. However, scalable synthesis of high-performance Mg-based compounds remains challenging. In addition, device-level issues such as geometry optimization, brazing process, and contact optimization, etc. have not been adequately investigated for Te-free TE modules. Till now, despite their promise, the assembly of Te-free compounds into power-generation modules has not been reported.

Scalable preparation of high-quality TE materials and modules

High-performance TE materials with simple synthesis are favored for module fabrication. However, the synthesis of Mg-based compounds usually involves procedures that are either complicated, expensive, or time-consuming. For example, the synthesis of Mg₃(Sb, Bi)₂ compounds usually involves complicated processing routines including melting (such as arc melting, induction melting, or traditional melting), pre-annealing, powderization, sintering (such as spark plasma sintering, hot pressing, or induction pressing), and post-annealing. In another example, MgAgSb, being in α phase at room temperature, changes to the β phase at ~310 °Celsius, and the γ phase at ~360 °Celsius. Whereas only the α phase has the requisite high *zT*, phase-pure α-MgAgSb is difficult to obtain using traditional melting techniques unless a time-consuming annealing process is followed.

To overcome the limitations of existing approaches, we synthesized n- and p-type legs using only three steps: weighing, mechanical alloying, and rapid sintering (Figures 2(a) - (b)) [1]. We employed mechanical alloying here not only because it is a lower-cost way to realize large-scale production, but also because it allows for accurate stoichiometry that ensures high reproducibility, which is necessary to scale up production. This is especially essential for this work since the compounds studied here are rich in Mg, Bi, and Sb, which would otherwise largely evaporate if traditional melting techniques were used. The phases of the TE materials were characterized by X-ray diffraction (XRD). The XRD patterns indicated high purity for the n-type Mg_{3.3}Bi_{1.498}Sb_{0.5}Te_{0.002} (denoted as n-Sb0.5) and Mg_{3.3}Bi_{1.298}Sb_{0.7}Te_{0.002} (denoted as n-Sb0.7), and the p-type MgAg_{0.97}Sb_{0.99} (abbreviated as "p-MgAgSb"). We then undertook scanning electron microscopy (SEM) and energy-dispersive X-ray spectroscopy (EDX) elemental mapping of n- and p-type legs with contact layers. The elemental distribution was nearly uniform and we could find no obvious interaction between the TE materials and the contact layers. Using the mechanically-alloyed powder samples, we then fabricated the TE legs for module assembly by sintering in one step the TE

powder together with contact-layer powder on both sides. Herein, based on the previous reports, we selected Fe and Ag as the contact layers for the n- and p-type legs, respectively.

Finally, the sintered disks were diced and polished into the desired geometry, placed in the proper positions, and brazed to pre-circuited ceramic plates AlN in a vacuum furnace (Figure 2c). Due to the simplicity, our approach will potentially reduce the assembling time greatly when compared to the traditional routines.

Thermoelectric properties and module optimization

We measured the transport properties of the TE materials including the electrical conductivity, the Seebeck coefficient, and the thermal conductivity. The compounds synthesized in this work, including n-Sb0.5, n-Sb0.7, and p-MgAgSb, possess similar properties when compared to previous reports despite the simplified synthesis procedure. For p-MgAgSb, we obtained a peak zT of ~ 1.0 at 150 °Celsius and an average zT of ~ 0.9 at temperatures ranging from room temperature to 275 °Celsius. For the n-type materials, whereas n-Sb0.5 showed a higher zT up to 150 °Celsius, n-Sb0.7 exhibited better performance at higher temperatures (150 to 275 °C). The peak zT values reach 0.9 (at 150 °C) and 1.2 (at 275 °C) in n-Sb0.5 and n-Sb0.7, respectively.

Based on the zT profiles of n-Sb0.5 and n-Sb0.7, we

postulated that a segmented leg could maximize the average zT of the n-type materials. According to the transport properties of these compounds, we employed finite element simulation to assist in designing the geometrical configuration of the TE modules. With a hot-side temperature (T_{hot}) of 275 °Celsius and a cold-side temperature (T_{cold}) of 20 °Celsius, we evaluated the maximum conversion efficiency as a function of the working current (I), the ratio of the cross-sectional areas between the p- and n-type legs (A_p/A_n), and the height ratio of the two n-type materials ($H_{n-Sb0.7}/H_{n-Sb0.5}$) in a segmented leg.

We found that the ratio of $H_{n-Sb0.7}/H_{n-Sb0.5}$ was optimal over a large range from 0.75 to 1.75.

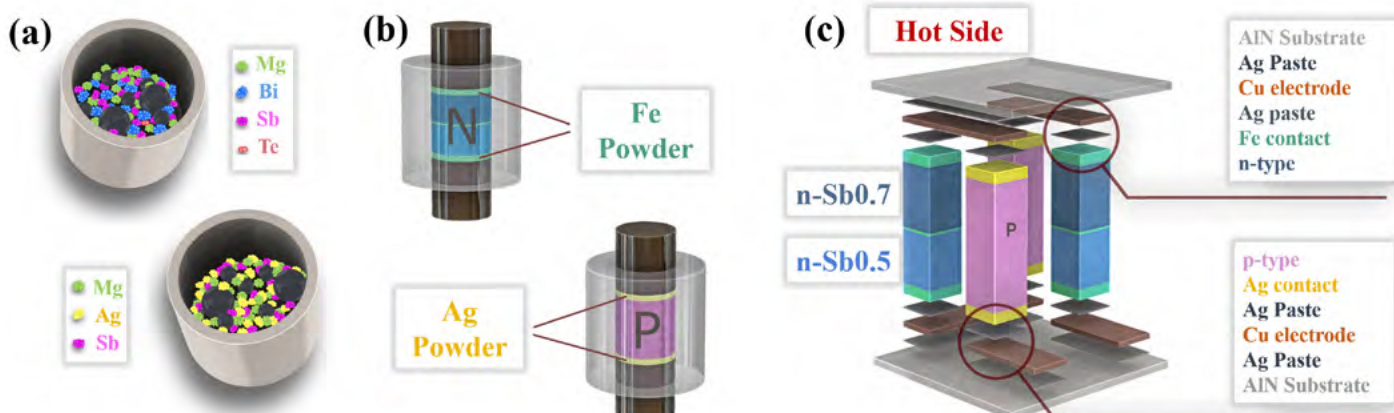
In addition, the ratio of A_p/A_n was found to have a limited impact on efficiency. Accordingly, we fabricated TE modules with segmented n-type legs where the ratio of A_p/A_n is unity to facilitate the device assembling. Note that the segmented n-type legs were prepared by using the same one-step sintering routine that was used for the single-stage module (Figure 2c) where an $H_{n-Sb0.7}/H_{n-Sb0.5}$ ratio of ~ 1.5 was selected. The selected $H_{n-Sb0.7}/H_{n-Sb0.5}$ ratio yielded a temperature profile that fully exploits the zT profiles of the n-type materials.

Based on the simulation results, we assembled single-stage and segmented TE modules, each with 2 p-type and 2 n-type TE legs, with individual leg dimensions of $2 \times 2 \times 6.5$ mm³.

The p-type legs were MgAg_{0.97}Sb_{0.99} for all

Abb. 2: Herstellung von Tellur-freien TE-Materialien und -Modulen. (a) Elementwiegung und mechanisches Legieren, um Pulver der n- und p-Typ-TE-Verbindungen herzustellen. (b) Spark-Plasma-Sintern von Materialien und Kontaktsschichten, um die TE-Schenkel herzustellen. (c) Zusammenbau des Tellur-freien TE-Moduls einschließlich Polieren, Schneiden, Laden, Positionieren und Löten der TE-Schenkel an die tragende AlN-Keramikplatten.

Fig. 2.: Fabrication of tellurium-free TE materials and modules. (a) Element weighing and mechanical alloying to prepare powder of the n- and p-type TE compounds. (b) One-step spark plasma sintering of materials and contact layers to prepare the TE legs. (c) Assembling of the tellurium-free TE module including polishing, cutting, loading, positioning, and brazing the TE legs to the pre-circuited AlN ceramic plates.



modules, but the compositions of the n-type legs were altered in different modules, including single-stage n-Sb0.5 and n-Sb0.7, and segmented n-Sb0.5/Sb0.7. As shown in Figure 3, a high conversion efficiency (η_{\max}) of $\sim 6.5\%$ was realized in the single-stage modules for a temperature difference (ΔT) of 250 °Celsius.

Moreover, the module with segmented legs boosted the η_{\max} to $\sim 7.0\%$ for the same ΔT .

Our modules are comparable to or even outperform the Bi₂Te₃-based ones [2-6], which can potentially extend the applicability of the Te-free TE modules due to their remarkable sustainability.

Conclusion

This work thus realizes, for the first time, high-performance TE modules free from Bi₂Te₃ that are capable of harvesting low-grade (<300 °Celsius) waste heat. The efficiency demonstrated in this work exceeds that of the best Bi₂Te₃-based modules. Subsequent enhancements are possible upon further advance the material properties and optimizing the filling factor of the modules.

The use of abundantly available elements and the ease of fabrication render our Te-free modules a notable substitute for the Bi₂Te₃-based modules in low-grade-heat recovery. This will potentially spur the application of thermoelectric technology for power generation from low-grade heat.

References

- [1] P. Ying et al. Nat. Comm. 12 (2021) 1121
- [2] F. Hao et al. Energy Environ Sci. 9 (2016) 3120-3127
- [3] X. Hu et al. J. Electron. Mater. 44 (2015) 1785-1790
- [4] B. Zhu et al. Energy Environ. Sci. 13 (2020) 2106-2114
- [5] X. Lu et al. Adv. Energy Mater. 10 (2020) 1902986
- [6] R. Deng et al. Energy Environ. Sci. 11 (2018) 1520-1535

Funding

IFW Dresden strategic project
Alexander von Humboldt Foundation

Cooperations

¹ Department of Physics and Texas Center for Superconductivity at the University of Houston (TcSUH), University of Houston, Houston, TX 77204, USA

² National Key Laboratory for Precision Hot Processing of Metals, School of Materials Science and Engineering, Harbin Institute of Technology, 150001 Harbin, China

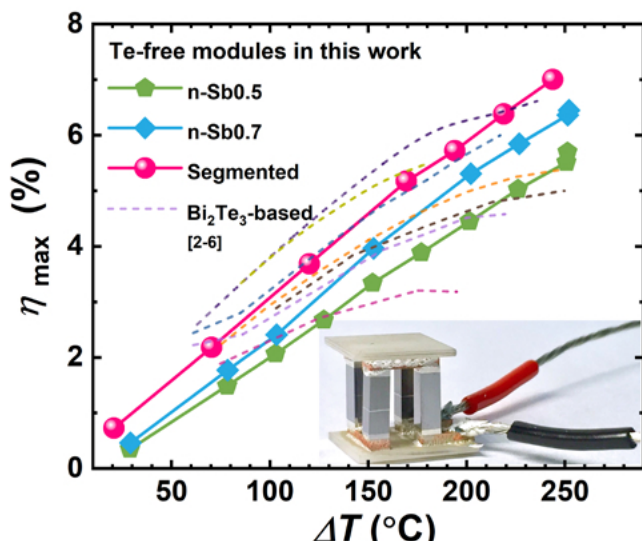


Abb. 3: Leistung der Tellur-freien segmentierten Module. Vergleich der gemessenen Umwandlungseffizienz (η_{\max}) zwischen den Tellur-freien Modulen in dieser Arbeit als Funktion des Temperaturunterschiedes (ΔT). Zum Vergleich wurden auch die η_{\max} der Bi₂Te₃-basierten Module aus der Literatur [2-6] eingetragen. Das Foto zeigt ein segmentiertes Tellur-freies Modul.

Fig. 3: Performance of the tellurium-free segmented modules. Comparison of the measured conversion efficiency (η_{\max}) among the tellurium-free modules in this work under a series of temperature differences (ΔT). The η_{\max} of the Bi₂Te₃-based modules from the literatures were also plotted for comparison [2-6]. The inset shows the photograph of a segmented tellurium-free module.

Miniaturized microcoils for NMR spectroscopy with high resolution and sensitivity

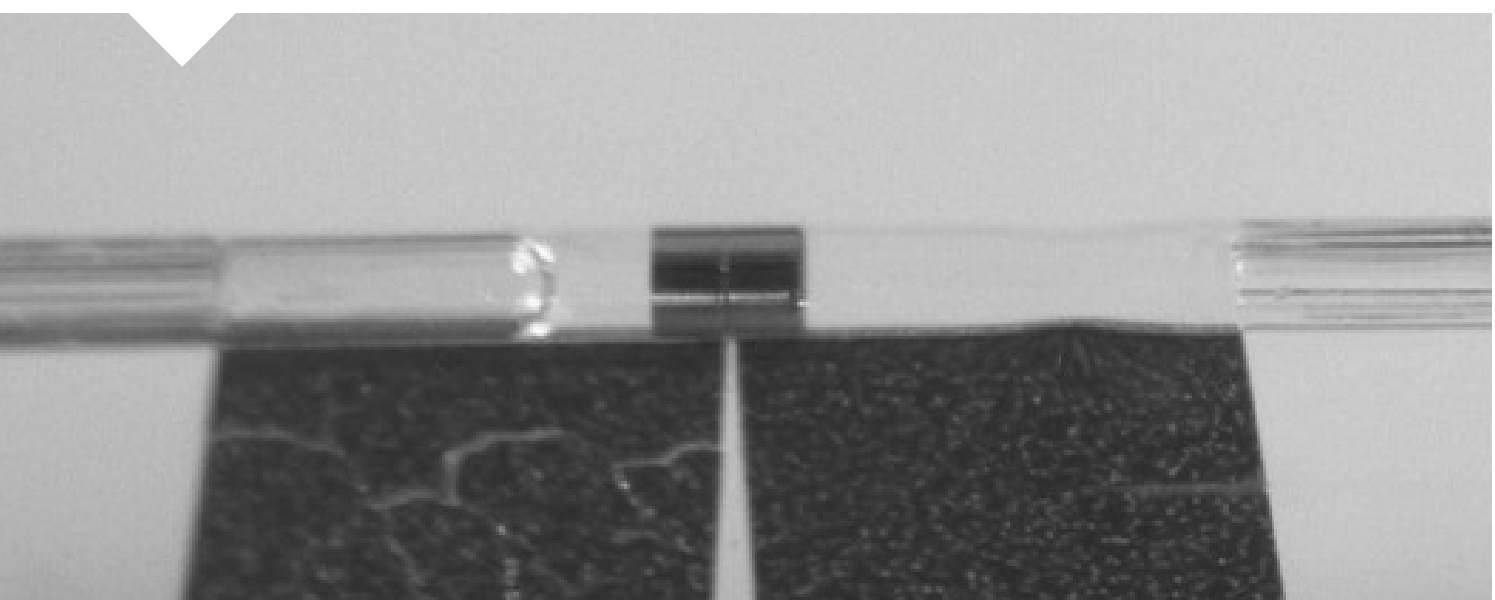
Piotr Lepucki, Alaleh Mirhajivarzaneh, Adam P. Dioguardi, Aleksandr I. Egunov, Marco Rosenkranz, Renato Huber, Daniil Karnaushenko, Dmitry D. Karnaushenko, Oliver G. Schmidt, Bernd Büchner, Hans-Joachim Grafe

Miniaturisierung ist das bestimmende Phänomen unserer Zeit. Ein Smartphone hat heutzutage deutlich mehr Rechenleistung als ein Computer vor 30 Jahren. Auch in der Wissenschaft hilft Miniaturisierung, um kleinste Probenmengen zu untersuchen. Bei der Kernspinresonanzspektroskopie (engl. NMR) werden derzeit für eine ausreichende Sensitivität Proben von etwa 1 Milliliter Volumen benötigt, die in aufwendig „geshimmt“en, d.h. homogenisierten, Magnetfeldern gemessen werden. Am IFW Dresden wurden nun selbstaufrollende NMR-Mikrospulen entwickelt, deren Sensitivität trotz eines Probenvolumens von nur 1,5 Nanolitern vergleichbar mit der von Standard-NMR-Spektrometern ist und die aufgrund des kleineren Volumens mit weniger homogenen Magnetfeldern zureckkommen. Dies soll in Zukunft die Untersuchung kleinstter Probenmengen wie beispielsweise einzelner biologischer Zellen ermöglichen.

Miniaturization is the defining phenomenon of our time. A smartphone today has significantly more power than a computer 30 years ago. Miniaturization also helps in science to investigate the smallest sample quantities. In nuclear magnetic resonance spectroscopy (NMR), samples of about 1 milliliter volume are currently required for sufficient sensitivity, which are measured in elaborately "shimmed", i.e. homogenized, magnetic fields. At IFW Dresden, self-assembled rolled-up microcoils have now been developed whose sensitivity is comparable to that of standard NMR spectrometers despite a sample volume of only 1.5 nanoliters, and which can cope with less homogeneous magnetic fields due to the smaller volume. In the future, this should enable the investigation of the smallest sample volumes, such as single biological cells.

Abb. 1: Eine selbständig aufgerollte NMR-Mikrospule. Die elektrisch leitende Schicht ist dunkel und der Teil in der Mitte ist die eigentliche Spule mit einem Durchmesser von etwa 100 µm. Die flüssige Probe auf der linken Seite der Spule nähert sich dem Inneren der Spule durch einen dünnen Polymerschlauch, der ein Nebenprodukt des Rollvorgangs ist.

Fig. 1: A self-assembled rolled-up NMR microcoil. The conducting layer is dark and the part in the middle is the actual coil with a diameter of about 100 µm. The liquid sample on the left side of the coil is approaching the inner of the coil through a thin polymeric tube, which is a by-product of the rolling process.



Nuclear Magnetic Resonance (NMR) is a powerful tool for investigating chemical or biological samples. It can resolve the chemical structure of a material in a non-destructive way, and can monitor even biological processes in their chronological sequence without disturbance. Videos of a beating human heart or of the inside of a singer at work recorded by magnetic resonance tomography are possibly the most impressive examples of the capability of this technique [1,2].

However, NMR suffers from a low sensitivity, requiring sample volumes on the order of milliliters (ml). This is because of the small magnetic moments of the nuclei, which are the probes for detecting their local, chemical environment. Billions of these nuclei are required to build up a nuclear magnetization that is detectable with a standard NMR coil. These coils are centimeter sized, and the fluctuations of the magnetization of the nuclei inside these coils can be coherently manipulated by a radio frequency pulse. After the pulse, the now coherent nuclear magnetization decays and induces a radio frequency signal in the coil. The frequencies of this signal are obtained by Fourier-transformation, and they reflect the local, chemical environment of the nuclei. In other words: each resonance line corresponds to a certain chemical binding, and the intensity corresponds to the number of atoms that are chemically bound in this way. For small amounts of sample, the interior of the NMR coil cannot be filled anymore, and the signal intensity is reduced by the filling factor, which is the ratio of the sample volume and the coil volume, V_{sample}/V_{coil} . Placing a sample on the order of nanoliter (nl) inside a coil with a volume of ml, reduces the signal intensity by a factor of 10^{-6} , i.e. the signal has disappeared.

Obviously, in order to detect small amounts of sample, one has to reduce the volume of the coil. Winding of a microcoil by hand with an inner diameter of 100 μm is possible, but is not suitable for mass production, and suffers from a low reproducibility [3]. Planar surface coils can be printed on a chip, but it has been shown that this type of resonators have a limited sensitivity and disturb the homogeneity of the external magnetic field [4]. Other types of resonators such as Helmholtz pairs [5], or so-called stripline or microslot resonators can also not outperform

cylindrical coils [6]. Therefore, we made use of the profound knowledge at the IFW Dresden of 3D structural self-assembly from thin films to create a cylindrical rolled-up microcoil, which can be used as the resonator in an NMR circuit [7]. Subsequently, we improved their properties such that they can compete with other NMR coils regarding sensitivity and resolution [8,9]. A picture of such a coil is shown in Figure 1. Two polymeric films are placed on a glass substrate with a flat conductor path on top of this layer stack. By contact with water, one of the layers swells and the whole stack rolls up creating a polymeric microtube with a swiss-roll microcoil formed from the conductor path in the middle of the tube. The microtube can be attached to a microfluidic sampling system for easy sample transfer, and the thin walls of this tube guarantee an almost 100 percent filling factor of the coil for good sensitivity. Another advantage of the small size of the coil is the lower demand on the homogeneity of the external magnetic field, in which the samples need to be placed. These fields are created with large superconducting magnets, which need additional shimming for NMR spectroscopy, i.e. the magnetic field is homogenized. This is an elaborate procedure that increases the size and the cost of these systems, but the variations of an external field obviously depend on volume, so that small samples need less or no shimming. A side effect of the small size is that the coil itself produces field inhomogeneities by its susceptibility, and thereby reduces the resolution. However, this can be counteracted by using both diamagnetic and paramagnetic materials for the conductive layer of the coil, reducing the disturbing susceptibility to almost zero.

We tested the rolled-up microcoils using ethanol, whose NMR spectrum is well known, and which shows a multitude of narrow resonances perfectly suited for demonstrating resolution and sensitivity of our microcoils. The hydrogen (^1H) NMR spectrum of ethanol obtained with a microcoil in an un shimmed superconducting magnet is shown in Figure 2. It contains three separated peaks, one from the OH group (hydroxyl), one from the CH_2 group (methylene), and one from the CH_3 group (methyl). These groups all have different frequencies due to their different chemical environments. The difference in frequency is depicted as a shift

in parts per million (ppm) from an unshifted standard frequency of hydrogen. Furthermore, the CH_2 and CH_3 peaks are split into four and three peaks, respectively. All peaks of the spectrum can be clearly resolved, and fits yield a linewidth of only 22 parts per billion (ppb). A comparable spectrum obtained in the same magnet with a standard coil of 1 mm diameter and 3 mm length gave an order of magnitude larger linewidth due to the increased effect of the field inhomogeneity on the larger sample volume [8].

On the other hand, we measured the spectrum with the microcoil in a chemical-spectroscopy-grade NMR magnet with active shimming, and could further reduce the linewidth to 8 ppb, indicating that the microcoils do not perturb the homogeneity of the external magnetic field substantially and allow for high resolution measurements.

Finally, we measured the limit of detection (LOD) of our microcoils in order to determine the sensitivity of these coils in comparison to other NMR microcoils [9]. A plot of the LOD versus the linewidth is shown in Figure 3. The data from literature was calculated from published measurements, and each data point corresponds to different publications using different resonators. The limit of detection is the minimal amount of sample that can be detected with the used coil and connected NMR setup. It is also

proportional to the linewidth, i.e. to the resolution of the setup, since broad resonance lines are more likely to be lost in the noise than narrow ones. If the used microcoil broadens the resonance line, this will not only have an impact on the resolution, but also on the limit of detection. This is true also for our two measurements in the shimmed and un shimmed magnets, which are represented by red stars in Figure 3. Due to the smaller linewidth in the shimmed magnet compared to the un shimmed (8 ppb versus 22 ppb, respectively), the LOD in the shimmed magnet is lower, even though both measurements have been done with the same microcoil.

During the course of our work we noticed that there is no correct equation for the limit of detection and no standard measurement. Both of which we proposed in our publication [9]. Note that a part of the scattering of the data in Figure 3 is due to the different setups, like NMR spectrometer, pre-amplifier, etc., but mostly it stems from the different performances of the microcoils. For example, there can be setups with a high resolution, i.e. narrow linewidth, which have only a poor sensitivity, i.e. a high limit of detection. For instance, this can be the case if the resistivity of a microcoil is large. In this respect, our data points are on the good side of that figure, in the lower left corner, and they are ready for applications where only small amounts of sample are available.

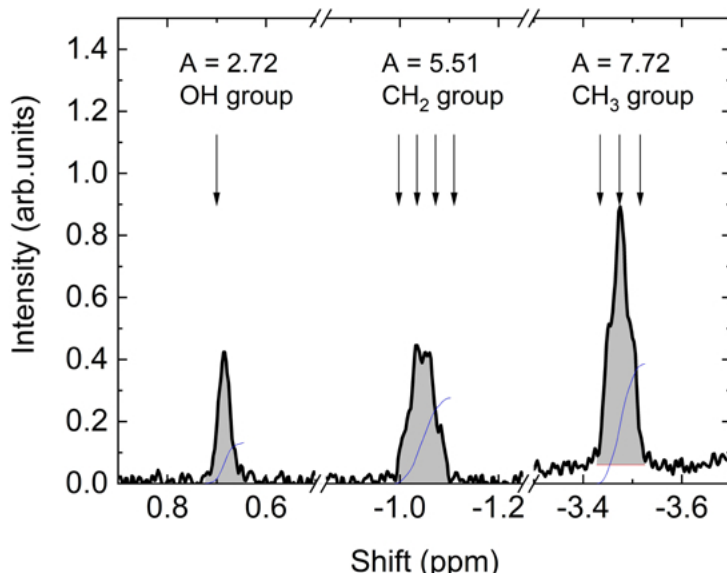


Abb. 2: ^1H NMR Spektrum von Ethanol, aufgenommen mit einer Mikrosäule in einem ungeshimmbten, supraleitenden Magnet mit einer Feldstärke von 7 T. Dies entspricht einer ^1H Resonanzfrequenz von ca. 300 MHz. Um die gute Sensitivität zu belegen, wurde das Spektrum mit nur einem einzelnen Puls aufgenommen. Das Verhältnis der integrierten Intensität A (dünne blaue Linie) der Peaks entspricht dem Verhältnis der Anzahl der Wasserstoffatome in den unterschiedlichen Gruppen, nämlich 1:2:3. Nachbildung aus [8].

Fig. 2: ^1H NMR spectrum of ethanol obtained with a microcoil in an un shimmed superconducting magnet with a field strength of 7 T, corresponding to a resonance frequency of ^1H of about 300 MHz. In order to demonstrate the high sensitivity, the spectrum has been obtained with a single radio frequency pulse. The ratio of the integrated intensity A (thin blue lines) of the peaks corresponds to the ratio of the number of hydrogen atoms in the different groups, which is 1:2:3. Reproduced from [8].

References

- [1] <https://www.youtube.com/watch?v=G4dFVeP9Vdo>
- [2] <https://www.youtube.com/watch?v=519LLxaqi8E>
- [3] D. A. Seeber et al., Rev. Sci. Instru. 72 (2001) 2171
- [4] C. Massin et al., J. Magn. Reson. 164 (2003) 242
- [5] N. Sprengler et al., J. Micromech. Microeng. 24 (2014) 034004
- [6] J. Bart et al., J. Magn. Reson. 201 (2009) 175
- [7] D. D. Karnaushenko et al., Adv. Electron. Mater. 4 (2018) 1800298
- [8] P. Lepucki et al., Adv. Mater. Technol. 6 (2021) 2000679
- [9] P. Lepucki et al., J. Magn. Reson. 332 (2021) 107077

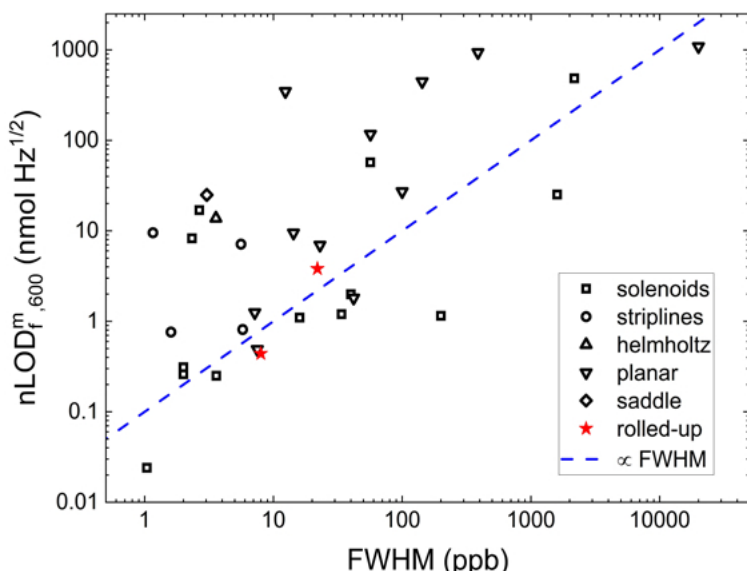
Funding

Leibniz Transfer Project 2020:
Micro-scale resonators for nuclear and electron spin resonance spectroscopies

Abb. 3: Das normierte Detektionslimit (nLOD) aufgetragen gegen die Linienbreite. Die Daten wurden aus mehreren Veröffentlichungen mit ganz unterschiedlichen Spulen und Resonatoren berechnet.

Die roten Sterne stammen aus unseren Messungen mit den aufgerollten Mikrospulen im ungeshimmerten ($\text{FWHM} = 22 \text{ ppb}$) und im geshimmerten ($\text{FWHM} = 8 \text{ ppb}$) Magnet. Je niedriger das nLOD und je kleiner die Linienbreite, um so besser ist der verwendete Resonator. Nachbildung aus [9].

Fig. 3: The normalized limit of detection (nLOD) versus the linewidth. The data was derived from several publications, with all different kinds of resonators. The red stars represent our data obtained with the rolled-up microcoils in the unshimmed ($\text{FWHM} = 22 \text{ ppb}$) and shimmed ($\text{FWHM} = 8 \text{ ppb}$) magnet. The lower the nLOD and the smaller the FWHM, the better the resonator. Reproduced from [9]



Medical imaging of microrobots: From in vitro to in vivo

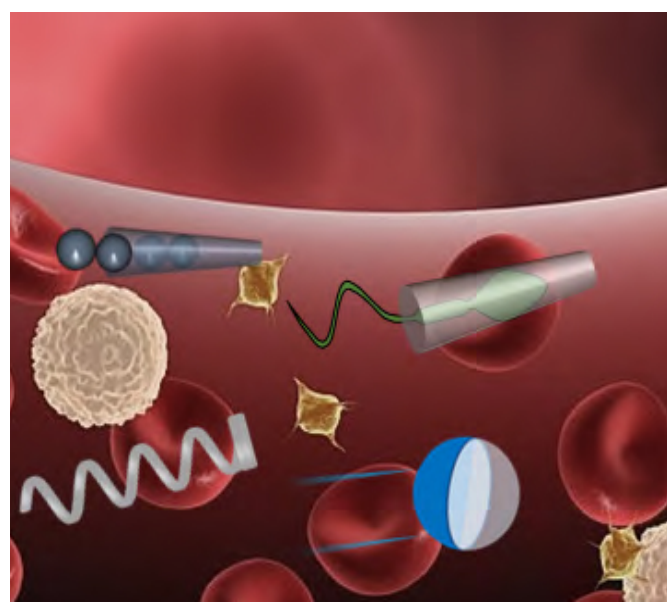
Azaam Aziz, Joost Holthof, Sandra Meyer, Oliver G. Schmidt, and Mariana Medina-Sánchez

Mikromotoren sind miniaturisierte Geräte, die im menschlichen Körper gesteuert werden können, um Krankheiten besser erkennen und behandeln zu können. Es existiert eine Vielzahl an Geräten für verschiedene biomedizinische Anwendungen wie beispielsweise zur Herstellung von künstlichem Gewebe (Tissue Engineering), zur Arzneimittelabgabe und für assistierte Befruchtungen. Die meisten dieser Anwendungen erfolgten jedoch in sogenannten In-vitro-Umgebungen, das bedeutet: sie finden außerhalb des Körpers statt. Die Übertragung solcher Ansätze auf eine Anwendung im lebenden Körper - auf eine In-vivo-Umgebung - ist eine Herausforderung [1]. Hier berichten wir über die Verwendung von Hochfrequenz-Ultraschall (US) und photoakustischer (PA) Bildgebung, um anatomische und molekulare Informationen der magnetisch angetriebenen Mikromotoren in vitro und unter ex vivo-Geweben zu erhalten. Darüber hinaus zeigen wir die Steuerbarkeit der Mikromotoren durch die Einwirkung eines externen Magnetfeldes in die Gebärmutter und die Blase von lebenden Mäusen in Echtzeit.

Micromotors are miniaturized devices that can be controlled inside the human body to aid doctors in identifying and treating diseases. Such devices have been demonstrated for a variety of non-invasive biomedical applications, such as tissue engineering, drug delivery, and assisted fertilization, among others. However, most of these demonstrations have been carried out in in vitro settings, and translating such approaches to an in vivo environment is challenging [1]. Here, we report the use of high-frequency ultrasound (US) and photoacoustic (PA) imaging to obtain anatomical and molecular information of the magnetically-driven micromotors in vitro and under ex vivo tissues. Furthermore, we demonstrate the steerability of the micromotors by the action of an external magnetic field into the uterus and bladder of living mice in real-time.

Abb. 1: Durchführung von magnetischen Kontrollexperimenten an medizinischen Mikrorobotern mit dem Magnebotix-Controller (links) und Schema solcher Mikroroboter, die sich im Mausmodell bewegen (rechts).

Fig. 1: Performing magnetic control experiments of medical microrobots using magnebotix controller (left) and schematic of such microrobots moving in a mouse model (right).



Medical imaging of microrobots

To translate this technology to the living body and despite all the ethical discussions around the employment of medical micro and nanorobots (MNRs) which will arise in the next years, some technical limitations need to be solved such as spatiotemporal resolution and the penetration depth with micro-metric resolution [2]. Biodegradability is another prerequisite and eventually, the micromotors should clear the body after performing an assigned task without any diverse effects. A preliminary study of micromotors using the dual US and PA system and an envisioned application in the field of supervised cargo delivery is presented.

Despite various challenges, deep tissue imaging remains a major challenge that must be addressed to achieve precise localization and tracking of such tiny therapeutic machines when used in medical-relevant applications. So far, different imaging techniques have been explored, but they are still too coarse for deep tissue single-microrobot imaging. For example, in nuclear medicine and X-rays, hazardous radiation which in some applications would be a limiting factor. MRI can resolve structures with submillimeter resolution and in some cases offering temporal resolutions in the millisecond range but demands expensive infrastructure and continuous presence of strong magnetic fields. Besides, CT provides deep tissue penetration but lacks temporal resolution and long-term exposures might harm the organism. PET and SPECT provide high sensitivity and molecular information, but the radiation dose remains the foremost concern when an extended use is required to monitor MNRs. Additionally, the optical methods including fluorescence [3] or reflection-based IR imaging [4] have been used to track MNRs below scattering tissues with excellent spatiotemporal resolution but have been limited to sub-skin level or superficial medical applications (typically ~1-2 mm in thick biological tissues) [5].

To preserve the spatial resolution and molecular specificity of optical techniques while enhancing the temporal resolution and penetration depth, PA imaging provides a unique absorption signal to image micromotor. The use of stand-alone PA imaging for the visualization of moving medical micromotors was first suggested by us in 2017 where we visualized single magnetic conical micromotors (up to 100 µm

long) in 3D, underneath ca. 1 cm in ex vivo chicken tissue [6].

Dual ultrasound and photoacoustic tracking of magnetically-driven micromotors: From *in vitro* to *in vivo*

Here, we present dual US and PA imaging for real-time tracking of a single moving micromotor *in vivo* which is a prerequisite for various biomedical applications. A multi-modal US and PA system equipped with a linear array ultrasound transducer and fiber optic bundles on either side of the transducer for illumination (680 to 970 nm) was used for the static imaging of single micromotors (Fig. 2a). This technique provided both functional and structural imaging of swimming micromotors deep in the bladder and uterus of a mice model, envisioning their application for targeted drug delivery (Fig. 2b). To actuate the magnetic micromotors in a controlled manner, a setup consisting of an integrated coil setup and the imaging system was implemented (Fig. 2c). The set of coils produces fields up to 50 mT in a frequency range from 0 to 200 Hz, and gradients of up to 2T/m at 10 Hz. In this experiment, we applied field strength of 5 mT at a frequency range between 1 and 5 Hz, to steer a single micromotor in a narrow channel. SiO₂ particles with a diameter of 100 µm were drop-casted onto a substrate, followed by the evaporation of subsequent thin metal layers (Ti=10 nm, Fe=50 nm, and Ti=10 nm). The particles were half-coated with metal layers by electron beam, resulting in what we call magnetic Janus micromotors (Fig. 2d) and such micromotors were actuated using an external magnetic field. The micromotors were inserted into the tube and immersed in the phantom chamber containing DI water for better acoustic coupling (Fig. 2e-i). After the PA acquisition, the spectral characteristics of the samples were recorded as shown in US and PA images (Fig. 2e, ii-iii).

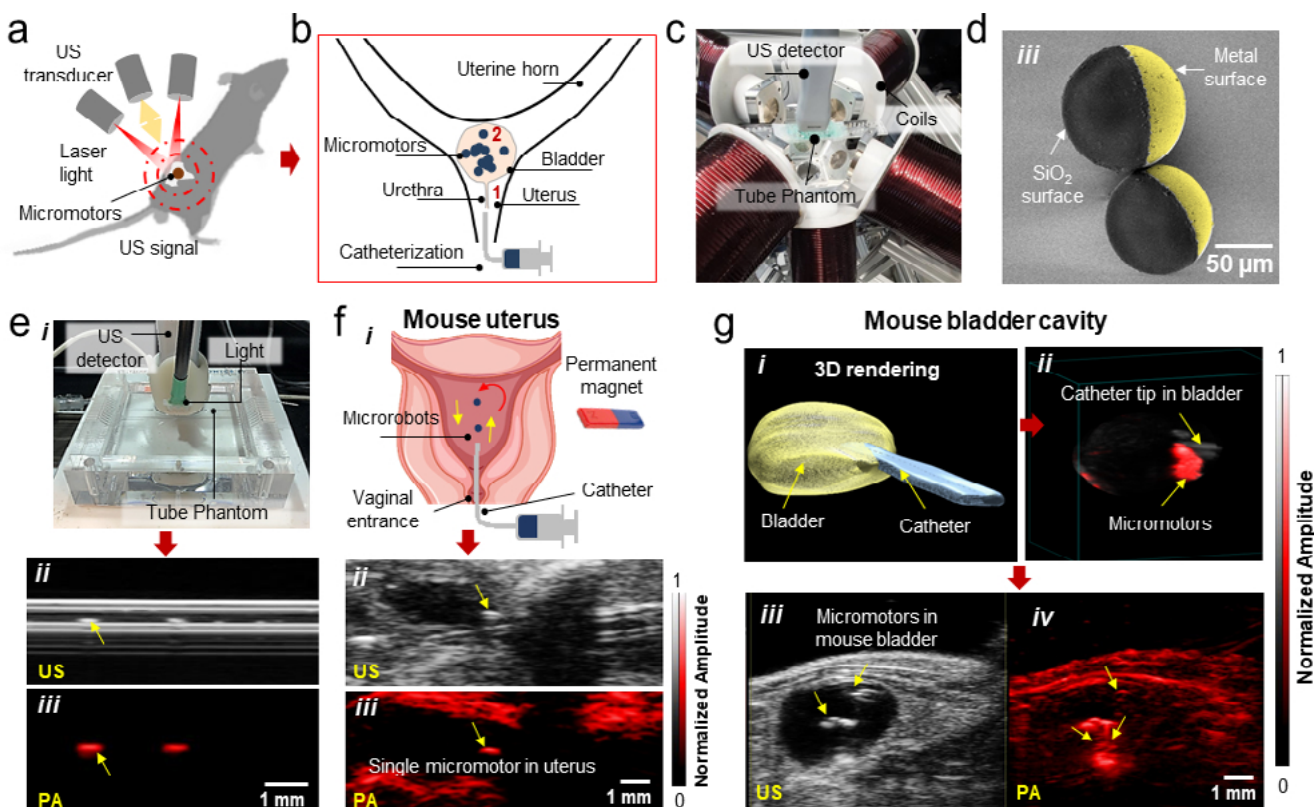
After *in vitro* study, we performed *in vivo* tracking of micromotors in the bladder and uterus of 12-week old mice and the experiments were performed under the animal handling license No. DVS06, hold by the co-authors of FUJIFILM VisualSonics, The Netherlands. We selected the bladder and uterus cavity as sites of injection to allow enough room for the free-swimming of the micromotors. First, the micromotors were inserted into the mouse uterus as depicted in

a schematic (Fig. 2f-i). Under anesthesia, the mouse bladder was catheterized by following standard safety guidelines and protocols [7]. The catheter was inserted via the vagina and cervix into the mouse uterus cavity. We investigated the smallest detectable feature size of the micromotors in the uterus by injecting a controlled number of micromotors. By employing US imaging, it was possible to precisely locate the catheter tip at the opening of the uterus cavity before micromotors insertion. Ultimately, it was possible to deliver ca. 2-3 micromotors in the mouse uterus from the catheter needle. One of the micromotors was steered in real-time in the uterus channel as shown in US and PA images (Fig. 2f, ii-iii). Apart from the uterus, we also evaluated the micromotors imaging in the mouse bladder. The bladder is a hollow soft organ that serves as a reservoir for the storage and periodic release of

urine. Before starting the experiment, the physiological parameters of the mouse were monitored. The micromotors were collected (15-25 in $\sim 20 \mu\text{l}$ PBS) in a catheter and then inserted into the bladder. The catheter was inserted through the urethra of an anesthetized mouse while being monitored in vivo as shown in the 3D US reconstructed image (Fig. 2g-i). After reaching the entrance of the bladder, the micromotors were released gradually into the bladder cavity. The overlaid US and PA image shows the micromotors near the catheter edge after release (Fig. 2g-ii). PA signal (red spot) highlights the presence of a swarm of micromotors being ejected from the catheter, while US image shows the anatomy of the organ of operation. After release, the micromotors started to move down in the urinal cavity, and it was possible to visualize the micromotors from few to

Abb. 2: a) Schematische Darstellung des Arbeitsprinzips der verwendeten dualen US- und PA-Bildgebungstechnik. b) Schwarm von Mikromotoren, die in der Blase und der Gebärmutter einer Maus schwimmen. c) Integrierte Bildgebung und magnetische Betätigungsanordnung. d) Herstellung von Janus-Mikromotoren ($\varnothing = 100 \mu\text{m}$), die mit Metallschichten (10 nm Ti, 50 nm Fe und 10 nm Ti) halbbeschichtet sind, unter Verwendung von Elektronenstrahlverdampfung. e) Phantomkammer mit in ein Wasserbad getauchten Schläuchen mit US-PA-Detektor (i). Die Bilder eines sich bewegenden Mikromotors in den Modi US (ii) und PA (iii). Gelbe Pfeile zeigen den sich einzeln bewegenden Mikromotor. f) Schematische Darstellung des Einführens des Katheters in den Uteruskörper durch die Vagina (i). Die Bilder einzelner sich bewegender Mikromotoren in der Gebärmutter (gelbe Pfeile zeigen die Position des sich bewegenden Mikromotors) in den Modi US (ii) und PA (iii). g) 3D-Rekonstruktion der Blase mit eingeführtem Katheter (i). US- und PA-Überlagerungsbild, das die Position der Katheterspitze mit Mikromotoren zeigt (ii). Der Schwarm schwimmender Mikromotoren unter der Betätigung eines Magnetfelds in den Modus US (iii) und PA (iv).

Fig. 2: a) Schematic showing the working principle of the employed dual US and PA imaging technique. b) Swarm of micromotors swimming inside a mouse bladder and uterus. c) Integrated imaging and magnetic actuation setup. d) Fabrication of Janus micromotors ($\varnothing = 100 \mu\text{m}$) half-coated with metal layers (10 nm Ti, 50 nm Fe and 10 nm Ti) using electron beam evaporation. e) Phantom chamber with tubing immersed in a water bath with US-PA detector (i). The images of a moving micromotor in US (ii), and PA (iii) modes. Yellow arrows show the single-moving micromotor. f) Schematic showing the insertion of the catheter into the uterus body through the vagina (i). The images of single moving micromotors inside the uterus (yellow arrows show the position of moving micromotor) in US (ii) and PA (iii) modes. g) 3D reconstruction of the bladder with the inserted catheter (i). US and PA overlaid image showing the location of the catheter tip with micromotors (ii). The swarm of swimming micromotors under the actuation of a magnetic field in US (iii) and PA (iv) modes.



swarm of them (Fig. 2g, iii-iv). The US and PA images show the swimming behavior of micromotors in urinal fluid from top to bottom surface of the bladder and the falling velocity of a cluster of micromotors in the bladder was estimated to be ca. 1250 $\mu\text{m/s}$ (in the current experiment). Finally, the whole swarm of micromotors at the bottom of the bladder was manipulated by using an external magnet. The speed of a single or swarm of micromotors also depends on the strength of the applied field at the evaluated distance from the micromotor position. In this experiment, an estimated magnetic field gradient of $\sim 220 \text{ mT/cm}$ was applied.

Conclusion

We implemented a dual high-frequency US and PA imaging system to carry out functional and structural imaging of swimming micromotors deep in the bladder and uterus of a mice model, envisioning their application for targeted drug delivery. Single or few micromotors were successfully visualized in phantoms, ex vivo, and in vivo environments. Furthermore, we also explored the use of multiwavelength excitation to spectrally distinguish the employed micromotors from the surrounding tissues. US imaging showed clear boundaries among different types of organs and precisely identified the position of the catheter (with micromotors) in the body with real-time feedback, improving the accuracy of the procedure and avoiding tissue-damaging during catheterization. In US images, internal structures like a bladder and uterus were visible to inject the micromotors while the PA images displayed the optical absorption characteristics of tissues and microstructures in mice.

This dual system is a powerful tool in addressing various imaging challenges of micromotors that require correlation with molecular and biological data, opening up a possibility for imaging of medical micro-robots in living organisms and performing a medical task while being externally controlled and monitored in hard-to-reach target sites, which could significantly improve the accuracy and effectiveness of current diagnosis and therapeutics in the future.

The summarized version of the already published manuscript: *Dual Ultrasound and Photoacoustic Tracking of Magnetically Driven Micromotors: From In Vitro to In Vivo* A. Aziz, J. Holthof, S. Meyer, O. G. Schmidt and M. Medina-Sánchez, *Adv. Healthcare Mater.*, vol. 10, no. 22, Nov. 2021, doi: <https://doi.org/10.1002/adhm.202101077>.

References

- [1] M. Medina-Sánchez and O. G. Schmidt, "Medical microbots need better imaging and control," *Nature*, vol. 545, no. 7655, pp. 406–408, May 2017, doi: 10.1038/545406a.
- [2] A. Aziz, S. Pane V. Iacovacci, N. Koukourakis, J. W. Czarske, A. Menciassi, M. Medina-Sánchez and O. G. Schmidt, *ACS Nano*, vol. 14, no. 9, pp. 10865–10893, Sep. 2020, doi: 10.1021/acsnano.0c05530.
- [3] A. Servant, F. Qiu, M. Mazza, K. Kostarelos, and B. J. Nelson, "Controlled in vivo swimming of a swarm of bacteria-like microrobotic flagella," *Adv. Mater.*, vol. 27, no. 19, pp. 2981–2988, 2015, doi: 10.1002/adma.201404444.
- [4] A. Aziz, M. Medina-Sánchez, N. Koukourakis, J. Wang, R. Kuschmierz, H. Radner, J. W. Czarske and O. G. Schmidt, "Real-time IR tracking of single reflective micromotors through scattering tissues" *Adv. Funct. Mater.*, vol. 29, no. 51, Dec. 2019, doi: 10.1002/adfm.201905272.
- [5] V. Ntziachristos, "Going deeper than microscopy: the optical imaging frontier in biology," *Nat. Methods*, vol. 7, no. 8, pp. 603–614, 2010, doi: 10.1038/nmeth.1483.
- [6] A. Aziz, M. Medina-Sánchez, J. Claussen, and O. G. Schmidt, "Real-Time Optoacoustic Tracking of Single Moving Micro-objects in Deep Phantom and Ex Vivo Tissues," *Nano Lett.*, vol. 19, no. 9, pp. 6612–6620, Aug. 2019, doi: 10.1021/acs.nanolett.9b02869.
- [7] P. A. Oliveira et al., "Technical report: Technique of bladder catheterization in female mice and rats for intravesical instillation in models of bladder cancer," *Scand. J. Lab. Anim. Sci.*, vol. 36, no. 1, pp. 5–9, 2009.

Cooperation

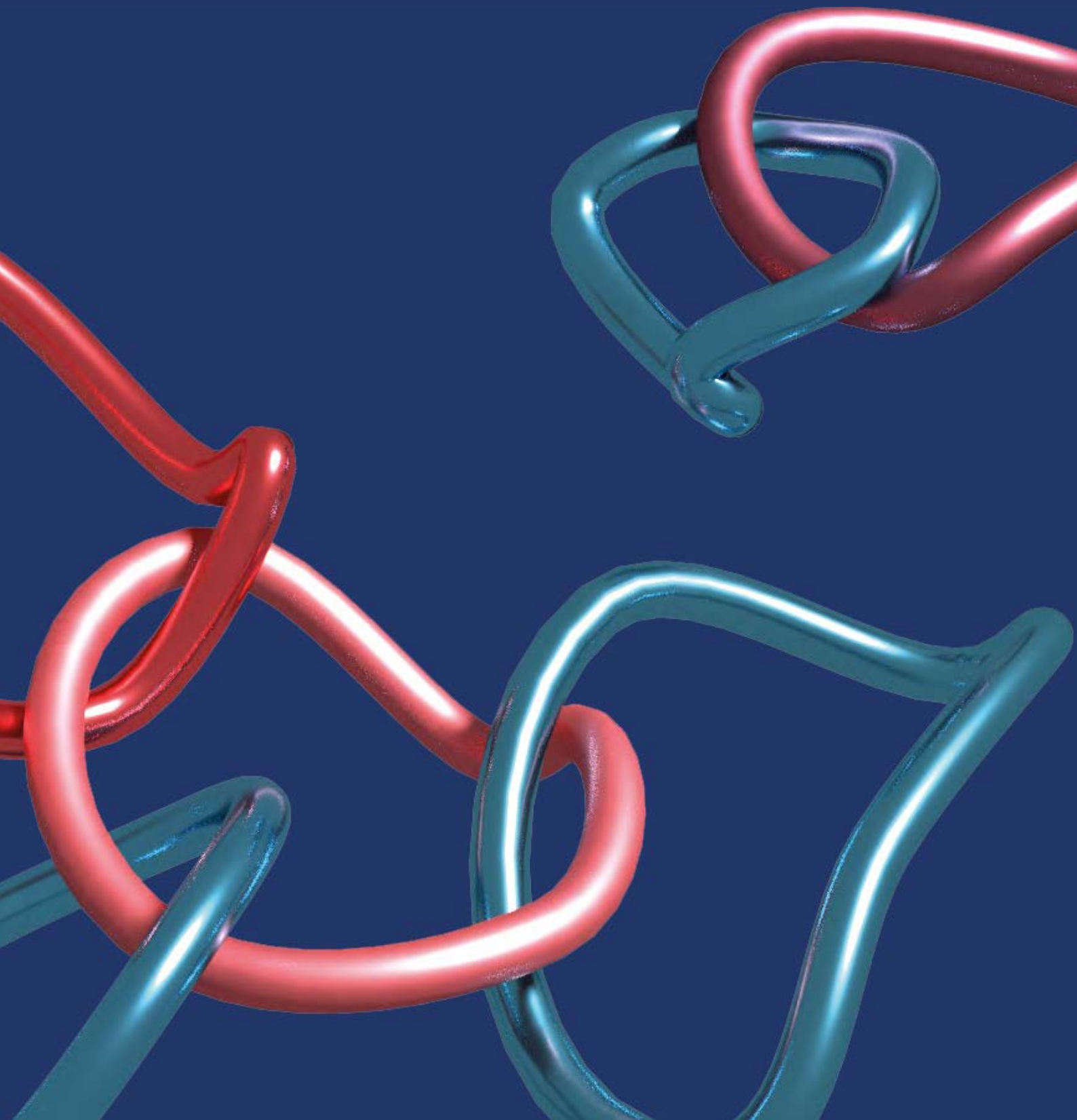
VisualSonics, Amsterdam

FORSCHUNGSGEBIET 3:

Quantenphänomene im Nanomaßstab

RESEARCH AREA 3:

Quantum Effects at the Nanoscale



Quantenphänomene im Nanomaßstab

In diesem Forschungsbereich beschäftigen wir uns mit Materialien und Strukturen, deren quantenmechanische Effekte auf ihre Nanoskaligkeit zurückzuführen sind. Dies sind sehr dünne Filme, Oberflächen und Grenzflächen, Quantenpunkte, photonische Kristalle und molekulare Nanostrukturen wie Fullerene, leitende Polymere und organische Halbleiter.

Im Bereich der Nanophotonik bearbeiten wir grundlegende Themen wie die Erzeugung von Einzelphotonen und verschränkten Photonenpaaren mit Halbleiter-Nanomaterialien sowie starke Licht-Materie-Wechselwirkungen im Quantenbereich. Anwendungsorientierte Fragestellungen betreffen die Herstellung moderner photischer Bauelemente wie Quanten-Leuchtdioden, aufgerollte optische Mikrokavitäten und 3D-Photonische Kristalle. Das Ziel dieser Forschung ist die Realisierung einer integrierten opto-elektronischen Plattform zur Erzeugung komplexer photischer Funktionalitäten.

Auf der Nanoskala können auch völlig neue physikalische Eigenschaften entstehen, etwa an Oberflächen und Grenzflächen topologischer Isolatoren. Dort ist der Spin von Oberflächenelektronen an ihren Impuls gebunden - eine Eigenschaft, die im Kontext der Spintronik interessant ist. Die Arbeit in diesem Bereich ist ein weiteres Beispiel für die Interdisziplinarität unserer Forschung. In enger Kooperation wirken experimentelles Knowhow und theoretische Expertise zusammen, um neue topologische Isolatoren zu erforschen und ihre Oberflächenzustände und Transporteigenschaften zu verstehen.

Quantum Effects at the Nanoscale

In this Research Area we address materials and structures with quantum mechanical effects that are due to their nanoscale. These are very thin films, surfaces and interfaces, so called heterostructures formed by thin films of different composition, quantum dots, photonic crystals and molecular nanostructures like fullerenes, conducting polymers and organic semiconductors.

In the field of nanophotonic the research work at IFW aims to explore several long-standing questions and challenges. Our work approaches fundamental topics: such as the generation of single photons and entangled photon pairs with semiconductor nanomaterials, the strong light-matter interactions in the quantum regime. More applied questions concern the fabrication of advanced photonic devices such as quantum light emitting diodes, rolled-up optical microcavities and 3D photonic crystals. When combined together, this multifaceted research could enable the realization of complex photonic functionalities with an integrated opto-electronic platform.

At the nanoscale also entirely new physical properties may emerge, for instance at surfaces and interfaces of topological insulators where the spin of surface electrons is locked to their momentum, a property that is interesting in the context of spintronics. Work at the IFW Dresden in this area is a nice example of a very interdisciplinary research effort, combining the available experimental and theoretical expertise to investigate topologically protected surface states and transport properties, again combining synthesis, theory and experiment.

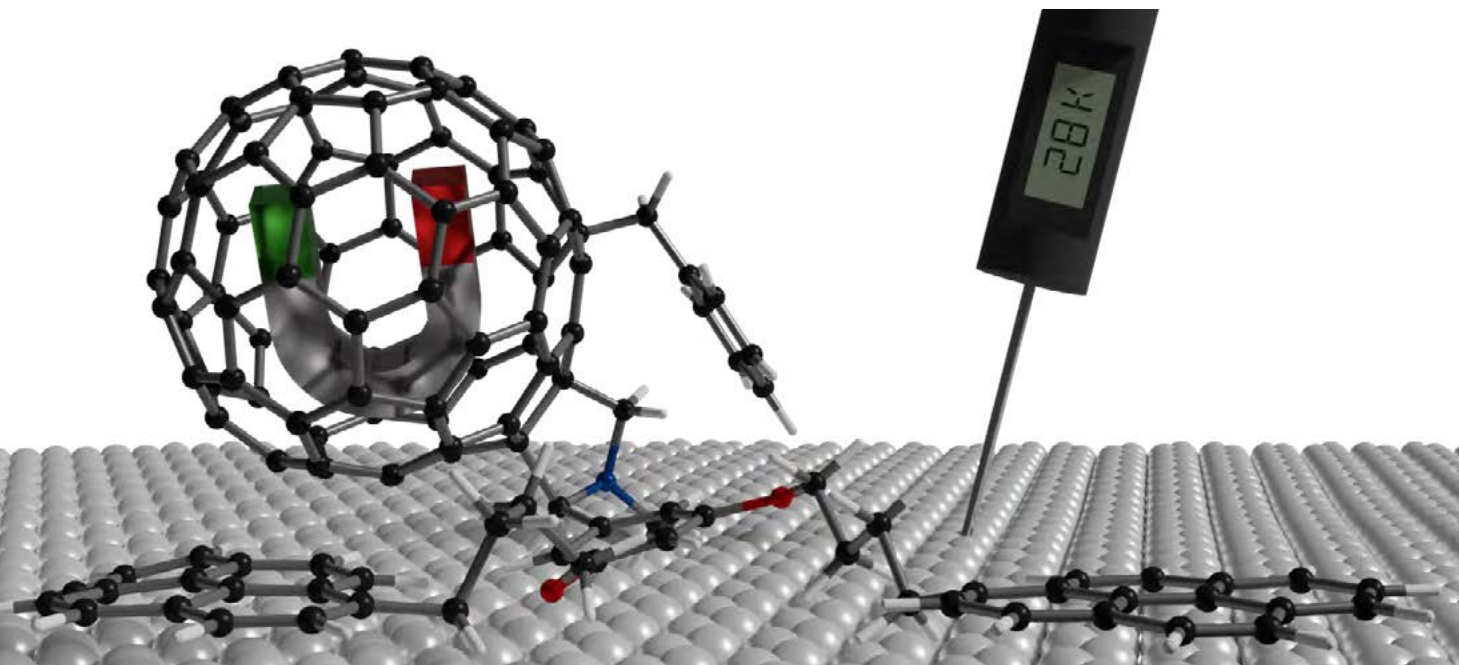
Self-assembled monolayers of fullerene-based single-molecule magnets on graphite and graphene

Lukas Spree, Fupin Liu, Volker Neu, Marco Rosenkranz, Georgios Velkos, Yaofeng Wang, Sandra Schiemenz, Chia-Hsiang Chen, Bernd Büchner, Stanislav M. Avdoshenko, Alexey A. Popov

Für die Anwendung von Einzelspin-Bauelementen in der (Quanten-)Informationsverarbeitung ist eine Funktionalisierung magnetischer Einheiten auf geeigneten Substraten erforderlich. Eine der Materialgruppen, die den Ansprüchen solcher Anwendungen gerecht werden können, sind Einzelmolekülmagnete. Wir zeigen, dass die Funktionalisierung des Materials $Tb_2@C_{80}(CH_2Ph)$ mit einem Pyren-Endgruppen-Verbindungs molekül die Bildung von selbstorganisierenden Monoschichten auf Substraten wie beispielsweise Graphen erleichtert. Die Schichten dieser Moleküle weisen eine weite magnetische Hysterese bis zu 28 K auf und zeigen keine negativen Auswirkungen der Funktionalisierung oder des Abscheidungsprozesses auf die magnetischen Eigenschaften. Die hier beschriebene, außergewöhnlich einfache Methode zur Herstellung von 2D-Fulleren-Graphen-Hybridmaterialien ebnet den Weg für die Integration von spintragenden endohedralem Fullerenen in Bauelemente, seien es Einzelmolekülmagnete oder Qubit-Kandidaten.

The application of single-spin devices in (quantum) information computing requires functionalization of magnetic units on suitable substrates. One of the groups of materials that can meet the requirements of such applications are single-molecule magnets. We show that functionalization of the material $Tb_2@C_{80}(CH_2Ph)$ with a pyrene end-group linking molecule facilitates the formation of self-assembling monolayers on substrates such as graphene. The layers of these molecules exhibit wide magnetic hysteresis up to 28 K and show no negative effects of functionalization or deposition process on magnetic properties. The exceptionally simple method described here for the preparation of 2D fullerene-graphene hybrid materials paves the way for the integration of spin-bearing endohedral fullerenes into devices, be they single-molecule magnets or qubit candidates.

Abb. 1: Pyren-funktionalisierte $Tb_2@C_{80}(CH_2Ph)$ -Einzmolekülmagneten auf einem Graphensubstrat mit magnetischer Bistabilität bis 28 K.
Fig. 1: Pyrene-functionalized $Tb_2@C_{80}(CH_2Ph)$ single molecule magnet on graphene substrate showing magnetic bistability up to 28 K.



The realization of single-spin devices for magnetic memory or quantum information processing relies on the possibility to create arrays of discrete magnetic units on suitable substrates, which can function as device electrodes. Useful properties of these units, such as the long lifetime of magnetic states, should be sustained on contact. At the same time, the magnetic units should possess a certain thermal and chemical stability to facilitate their processing. One of the material platforms, in which such properties can be potentially realized is single-molecule magnets (SMMs). In SMMs, stability of spin states is achieved by via long relaxation of magnetization, which can be verified experimentally through appearance of magnetic hysteresis. In the first SMMs discovered in 1993 [1], the effect was realized at 2–3 K, but the continuous development of lanthanide-based SMMs boosted their temperature range up to 80 K. [2, 3] However, the transfer of these properties from the bulk to nanoscale assemblies is lagging behind. Over a decade after the first observation of magnetic hysteresis in a monolayer of transition-metal complex {Fe₄}, [4, 5] the temperature range in which this phenomenon could be observed for SMM monolayers expanded from sub-K regime to only 10 Kelvin. [6–8]

Encapsulation of lanthanide ions inside the carbon offers an opportunity to stabilize unusual magnetic species. Particular interesting is the family of lanthanide dimetallofullerenes, such as Tb₂@C₈₀(CH₂Ph) ({Tb₂} hereafter). [9–12] The metal dimer in {Tb₂} features a single-electron Tb–Tb bond, which is responsible for the unique magnetic structure of the molecule. Each of the local Tb-4f moments is coupled ferromagnetically to the spin of the unpaired electron residing on the Tb–Tb bonding molecular orbital with *spd*-hybrid character. As a result, {Tb₂} demonstrates SMM behavior with a high blocking temperature of 29 K and very broad magnetic hysteresis. [9] Despite the unconventional lanthanide oxidation state of +2.5, {Tb₂} is air-stable. This combination of outstanding SMM properties and stability makes {Tb₂} a prime candidate for integration into spintronic devices.

In this work we concentrated on the deposition of {Tb₂} onto graphene and graphite (HOPG) as carbon-based conducting materials. [13] Dipolar cycloaddition reaction was utilized to functionalize

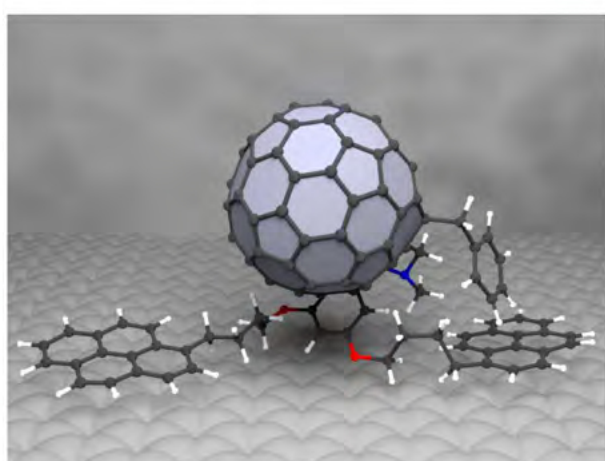
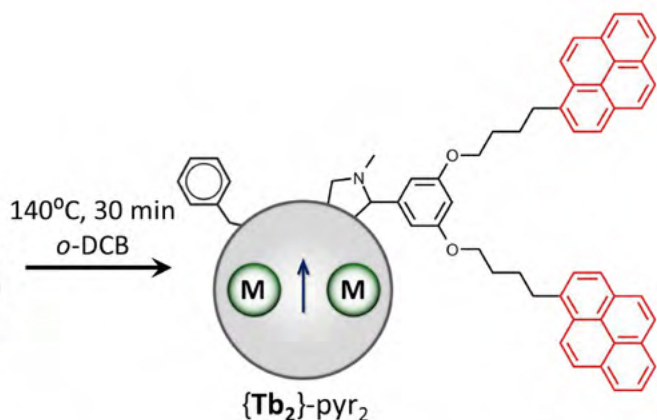
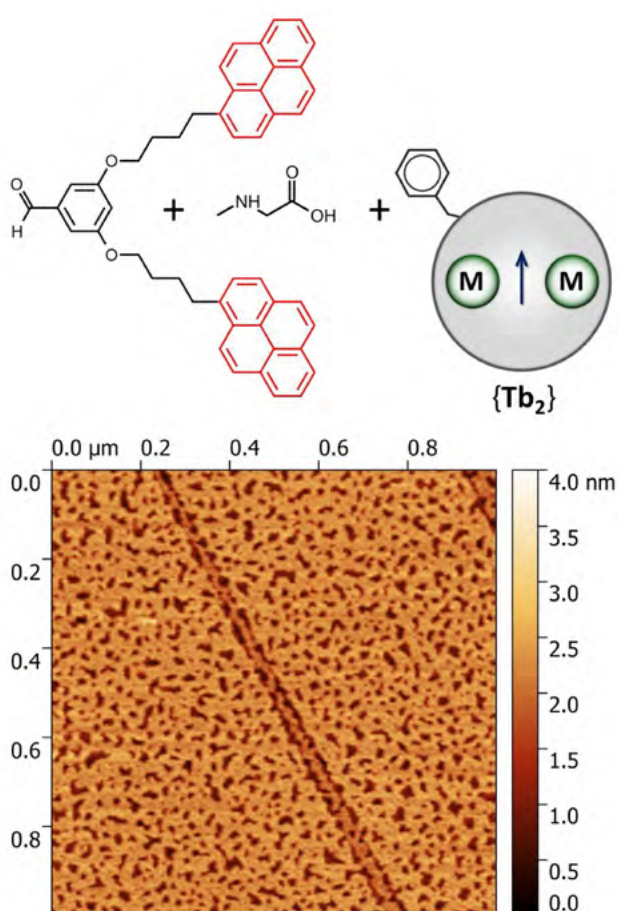
{Tb₂} with a linker moiety, terminated by pyrene anchor groups (Fig. 2). Pyrene shows high affinity to graphitic substrates and hence facilitates formation of self-assembled monolayers. Diluted solutions of the synthesized derivative ({Tb₂}-pyr₂) were then used for self-assembly of the fullerene derivative on freshly cleaved HOPG and graphene on SiO₂/Si. The binding of {Tb₂}-pyr₂ to either substrate was achieved by depositing a droplet of the solution for some time, before washing said droplet and excess fullerene molecules from the substrate with clean solvent. Characterization of the resulting {Tb₂}-pyr₂ films by atomic force microscopy revealed the formation of a layer with uniform single-molecule thickness of 1.8–2 nm in the whole area exposed to the solution (Fig. 2), and similar results were obtained by scanning tunneling microscopy. Molecular dynamics simulations showed that single {Tb₂}-pyr₂ molecule on graphene would adopt a laying-down conformation. However, when surrounded by other molecules, the fullerene core tends to elevate above the substrate, giving the height of 1.5–1.6 nm for a still rather sparse arrangement of molecules in the island (Fig. 2).

Facile preparation of self-assembled monolayers of {Tb₂}-pyr₂ demonstrated that they might be well suited for design of molecular spintronic devices based on integration with graphene electronics, unless magnetic properties of {Tb₂} are negatively affected by derivatization and deposition. To evaluate the effect of derivatization, we first characterized magnetic properties of a powder {Tb₂}-pyr₂ sample by SQUID magnetometry. The measurements demonstrated the cycloaddition even slightly improved the SMM properties of the fullerene in comparison to pristine {Tb₂}. Broad magnetic hysteresis of {Tb₂}-pyr₂ with a large coercive field of 5.0–5.4 T was found below 20 K, and the hysteresis remained open up to 28 K.

The sensitivity of SQUID magnetometry is not sufficient for the measurement of very thin films, and surface magnetism of {Tb₂}-pyr₂ monolayers on HOPG and graphene was studied by X-ray magnetic circular dichroism (XMCD) with synchrotron radiation at the Swiss Light Source, Paul Scherrer Institute and at ALBA synchrotron. X-ray absorption spectra of a {Tb₂}-pyr₂ monolayer at the Tb-M4,5 edge (corresponding to 3d→4f excitations) measured

with clockwise and counter-clockwise polarizations of incoming X-ray beam develop a dichroism in the presence of a net magnetization along the beam direction (Fig. 3). A magnetic field collinear with the X-ray beam was employed in the measurements, and therefore the size of the XMCD signal is proportional to the magnetization in the direction of the X-ray beam. The maximum of the XMCD signal at 1235 eV was used to monitor the changes of the SAM magnetization during magnetic field sweeps. At 2 K, $\{\text{Tb}_2\}\text{-pyr}_2$ monolayers exhibit open magnetic hysteresis on both HOPG and graphene substrates (Fig. 3). Measurements with different X-ray fluxes revealed that the increase of the X-ray intensity leads to a narrowing of the hysteresis, which indicates that the hysteresis width is limited by the demagnetization effect of the X-rays. Thus, the intrinsic hysteresis of the $\{\text{Tb}_2\}\text{-pyr}_2$ monolayer is probably even broader. The hysteresis of $\{\text{Tb}_2\}\text{-pyr}_2$ monolayers remains open up to 28 K and is closed at 30 K.

Our work shows that $\{\text{Tb}_2\}\text{-pyr}_2$ retains slow relaxation of magnetization in monolayer form on conducting graphitic substrates and exhibits measurable magnetic bistability. The solution-based preparation procedure of the $\{\text{Tb}_2\}\text{-pyr}_2$ monolayers on graphitic substrates is exceptionally simple and fast, consumes tiny amounts of material, can be run on air, and does not require UHV conditions or special temperature regimes. The method should lend itself well to larger scale manufacturing techniques, like ink-jet printing and the use of nanospotters, and is compatible with graphene electronics and spintronics, opening the way towards patterned devices with hybrid graphene-SMM interfaces. Furthermore, while $\{\text{Tb}_2\}$ is an excellent SMM, its non-4f analogs $\{\text{Y}_2\}$ and especially $\{\text{Sc}_2\}$ have recently been shown to be promising qubit candidates, [14] and the functionalization and deposition methods presented here might be a way of addressing them on a single molecule level.



References

- [1] R. Sessoli et al., *Nature* 365 (1993) 141-143.
- [2] F.-S. Guo et al., *Science* 362 (2018) 1400-1403.
- [3] C. A. P. Goodwin et al., *Nature* 548 (2017) 439-442.
- [4] M. Mannini et al., *Nature* 468 (2010) 417-421.
- [5] M. Mannini et al., *Nat. Mater.* 8 (2009) 194-197.
- [6] C.-H. Chen et al., *Adv. Sci.* 8 (2021) 2000777.
- [7] D. S. Krylov et al., *Angew. Chem. Int. Ed.* 59 (2020) 5756-5764.
- [8] C. Wäckerlin et al., *Adv. Mater.* 28 (2016) 5195-5199.
- [9] F. Liu et al., *Nat. Commun.* 10 (2019) 571.
- [10] F. Liu et al., *Acc. Chem. Res.* 52 (2019) 2981-2993.
- [11] Y. Wang et al., *J. Am. Chem. Soc.* 143 (2021) 18139-18149.
- [12] F. Paschke et al., *Adv. Mater.* 33 (2021) 2102844.
- [13] L. Spree et al., *Adv. Funct. Mater.* 31 (2021) 2105516.
- [14] R. B. Zaripov et al., *Nanoscale* 12 (2020) 20513-20521.

Funding

ERC Consolidator Grant *Gram3*
 German Research Foundation (DFG)

Cooperations

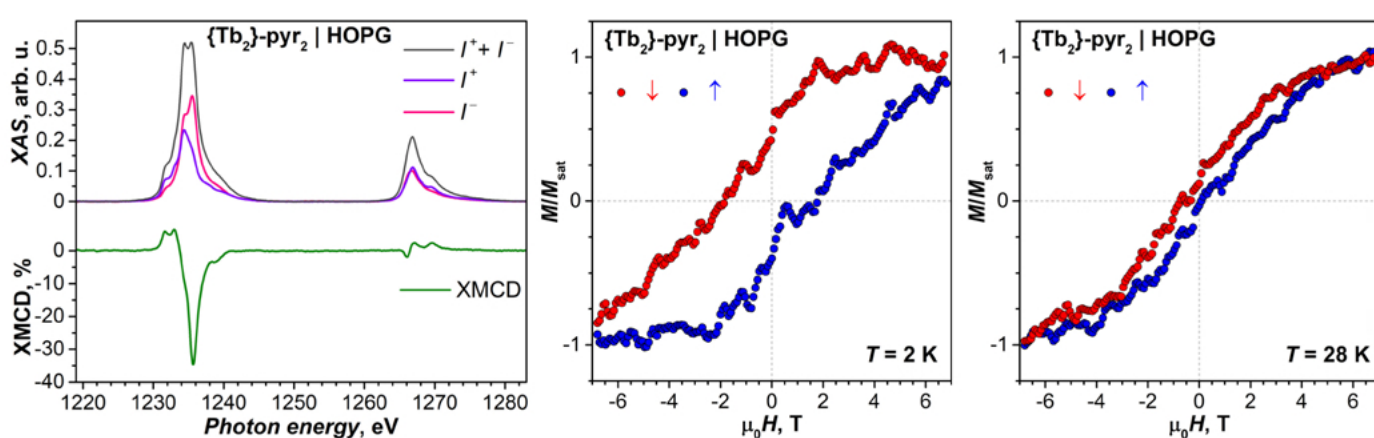
Paul Scherrer Institute, Switzerland
 ALBA Synchrotron, Spain

linke Seite: Abb. 2: Obere Reihe: Derivatisierung von $\text{Tb}_2@\text{C}_{80}(\text{CH}_2\text{Ph})$ mit Pyrengruppen durch dipolare Cycloaddition (Pyrengruppen sind rot dargestellt, ungepaartes Elektron, das zwischen zwei Tb-Ionen delokalisiert ist, ist als Pfeil gekennzeichnet). Untere Reihe: Rasterkraftmikroskopie-Topographie der selbstorganisierten $\{\text{Tb}_2\}\text{-pyr}_2$ -Monoschicht auf Graphit (links) und molekulare Struktur von $\{\text{Tb}_2\}\text{-pyr}_2$ in einer Monoschicht gemäß Molekulardynamiksimulations (rechts).

Page left: Fig. 2: Top row: Scheme of derivatization of $\text{Tb}_2@\text{C}_{80}(\text{CH}_2\text{Ph})$ with pyrene groups by dipolar cycloaddition (pyrene groups are shown in red, unpaired electron delocalized between two Tb ions is denoted as an arrow). Bottom row: atomic force microscopy topography of the $\{\text{Tb}_2\}\text{-pyr}_2$ self-assembled monolayer on graphite (left) and molecular structure of $\{\text{Tb}_2\}\text{-pyr}_2$ in a monolayer according to molecular dynamics simulations (right).

unten: Abb. 3: Röntgenabsorptions- (XAS) und magnetischer zirkularer Dichroismus (XMCD)-Spektren der selbstorganisierten $\{\text{Tb}_2\}\text{-pyr}_2$ -Monoschicht auf Graphit (links) und magnetische Hysteresekurven gemessen mit XMCD bei 2 K und 28 K (Mitte und rechts).

Fig. 3: X-ray absorption (XAS) and X-ray magnetic circular dichroism (XMCD) spectra of the $\{\text{Tb}_2\}\text{-pyr}_2$ self-assembled monolayer on graphite (left) and magnetic hysteresis curves measured with XMCD at 2 K and 28 K (middle and right).



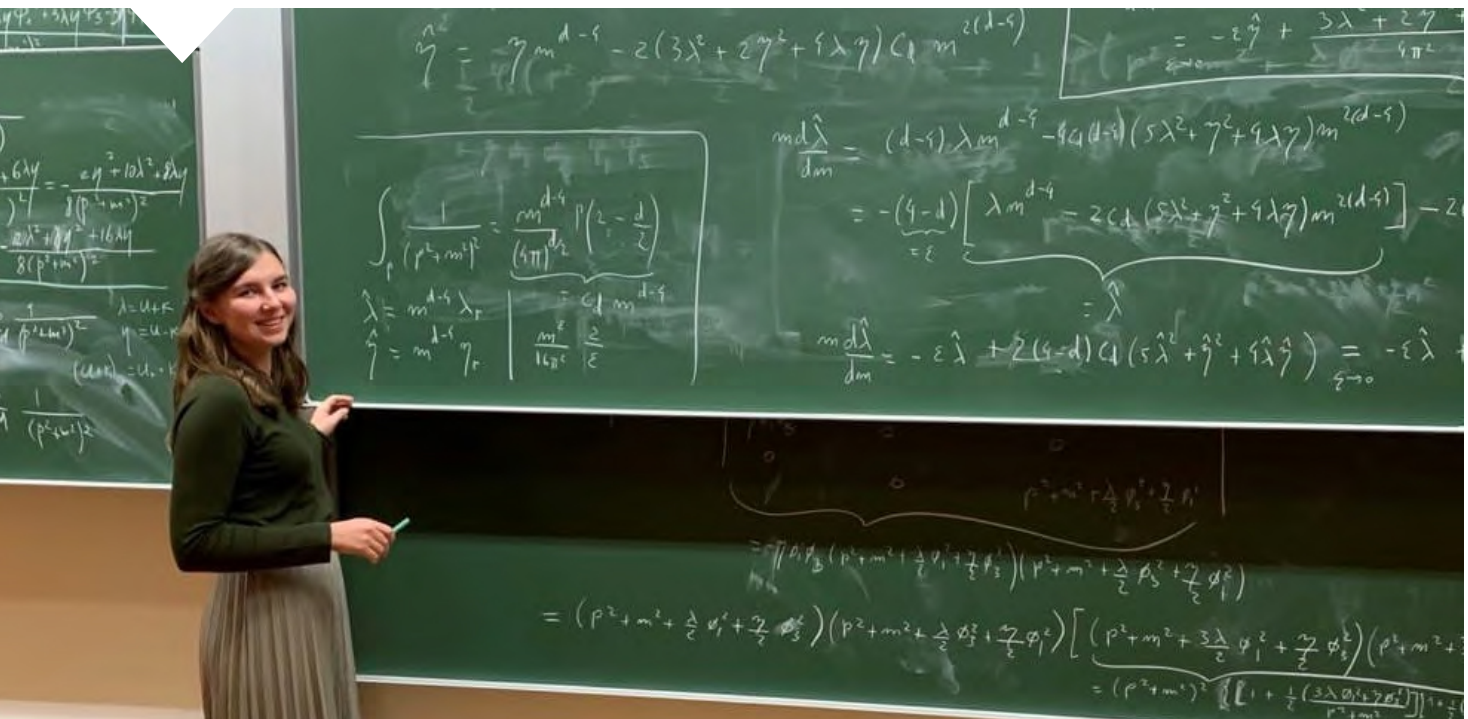
2D topological quantum magnets and bosonization duality for massless Dirac fermions

Vira Shyta

Einige zweidimensionale Quantensysteme weisen eine spezifische Art des kontinuierlichen Phasenübergangs auf, die sich im Rahmen traditioneller Ansätze nicht erklären lässt. Vor diesem Hintergrund wurde die Phasenstruktur von planaren anisotropen Antiferromagneten untersucht, in denen sich elektromagnetische Wirbel bilden können. Durch exakte analytische Methoden wurde gezeigt, dass das Modell tatsächlich einen kritischen Punkt mit einzigartigem kritischem Verhalten hat. Darüber hinaus liefert die Theorie in der Nähe des kritischen Punktes eine Abbildung zwischen der ursprünglichen Bosonentheorie und der der masselosen Dirac-Fermionen. Da eine solche Transmutation der Statistik bisher nur für niedrigere Dimensionen etabliert wurde, ebnen wir mit dieser Arbeit einen Weg, die Bosonisierungsdualität experimentell in Doppelschicht-Quanten-Hall-Magneten zu untersuchen.

Some two-dimensional quantum systems feature a specific type of the continuous phase transition that cannot be explained in the scope of traditional approaches. Considering that, the phase structure of planar anisotropic antiferromagnets, in which electromagnetic vortices can be formed, was examined. By exact analytical means, it was demonstrated that the model indeed has a critical point with unique near-critical behavior. Moreover, the theory at criticality provides a mapping between the original bosonic theory and the one of massless Dirac fermions. This is of interest because such a transmutation of statistics had only been established before for lower dimensions. With this work we pave a way to probe the bosonization duality experimentally in bilayer quantum Hall magnets.

Abb. 1: Doktorandin Vira Shyta äußert ihre Ideen während einer Tafeldiskussion.
 Fig. 1: PhD student Vira Shyta expressing her ideas during a blackboard discussion.



Deconfined quantum criticality

In our everyday life, we usually deal with phase transitions caused by a change in temperature - we boil water to make tea or we freeze juice to make ice pop. The changes of state that we can observe in these processes happen rapidly and not gradually. In physics, we distinguish two types of phase transitions — discontinuous and continuous. The latter do not occur in our everyday experiences, but are the subject of research in the physics laboratory. For instance, phase transitions in magnetic materials are typically of the continuous kind.

Continuous phase transitions are characterized by a critical point separating the different phases. The behavior of the system near such a critical point can be analyzed more extensively than in a discontinuous phase transition. This is why continuous phase transitions are of particular interest to the scientific community. In this way, they allow detailed predictions about the material behavior under specific conditions.

In quantum materials research, one is particularly interested in phase transitions that occur at zero temperature. These transitions are induced by changes in external influences, such as pressure or an external magnetic field, or by variations in parameters of the theory.

In our article [1] we examine the behavior of a specific type of two-dimensional quantum antiferromagnets. These materials possess a magnetic order in which their spins are aligned in a regular pattern, where neighboring spins point in opposite directions. To consider a more nuanced case, we forced the spins to lie in one plane instead of pointing in all three directions. The “adjusting screw” corresponds to the magnetic anisotropy and describes the directionality in the material.

The motivation to explore this particular system stems from the fact that there is no consensus among physicists about the type of the phase transition that occurs when quantum fluctuations can become so strong that they destroy magnetic ordering. We have additionally modified our theory by accounting for a non-trivial topology of the electromagnetic fields, which can form magnetic vortices. This change eventually led to even more fascinating results than anticipated.

The main result of our work is that two-dimensional topological anisotropic antiferromagnets undergo a continuous phase transition, which goes beyond the traditional theory of quantum phase transitions. The mechanism underlying such behavior is dubbed “deconfined quantum criticality” and refers to the fact that while antiferromagnetic and paramagnetic phases are described by two different parameters, like magnetization in the case of antiferromagnets, both of those descriptions do not persist at the critical point but rather fall apart (deconfine) into more elementary fields.

The existence of the deconfined critical point in the theory was shown through the renormalization group analysis, which found two non-trivial fixed points in the renormalization group flow of the couplings (Fig. 2). The fixed points correspond to regimes with divergent correlation lengths that one observes at critical points of continuous phase transitions. Besides demonstrating and explaining the existence of a continuous transition, we were able to make a few very precise predictions about the near-critical behavior of the theory. The results can actually be tested experimentally in so-called chiral spin liquid systems and bilayer quantum Hall systems.

Bosonization duality for massless fermions

The topological aspects of our theory were instrumental in obtaining the continuous transition and helped produce another beautiful result — an exact bosonization duality for massless Dirac fermions in two spatial dimensions. In both high-energy and condensed matter theory, physicists are interested in the notion of duality between theories. The duality manifests in two different descriptions of the same theory that provide new perspectives and can connect seemingly unrelated physical properties. In one spatial dimension, there is an established duality between fermions and bosons — two basic flavors of quantum particles. Yet everything becomes much more complicated once we move one dimension higher. Dualities in two spatial dimensions were only available for massive fermions, while the bosonization duality involving massless fermions had remained a conjecture.

We showed that the theory of topological anisotropic antiferromagnets at criticality is defined strictly

by the configuration of the electromagnetic vortex loops (in Fig. 3) that appear in the system. The way two vortex loops curl around each other is described by their linking number that can only take integer values as this is a topological property. Additionally, a single vortex loop can coil around itself even without being connected to other loops. This is a geometric property of the loop, it is described by the writhe, which can take any real values. After taking into account these properties of the vortex loops, we noticed that the critical theory at its final form is reminiscent of the theory of a Dirac fermion in two dimensions in terms of loops [2]. Nevertheless, the crucial difference with other related works lies in the fact that our case contains a parity anomaly implying that the fermions are massless. It is remarkable that even though our original model of topological anisotropic antiferromagnets is bosonic and does not explicitly employ fermionic fields, still a result that can only follow from massless fermions is obtained. Hence, we arrive at the bosonization duality for massless Dirac fermions.

These results are also quite important in the experimental context. The theory we considered relates the so-called (1,1,1) quantum Hall (QH) state associated to a bilayer QH system [3] and a two-component topological superconductor. Therefore, our analysis

naturally connects the observed resonant tunneling in bilayer QH ferromagnets [4] to a Josephson-like effect in a system that is not superconducting [5]. Such an experimental setup represents the dual physical system to the actual topological easy-plane antiferromagnet, and so the bilayer QH ferromagnet offers a controllable experimental system for a deconfined critical point that we predict. Moreover, in view of the connection to massless Dirac fermions, bilayer QH ferromagnets offer a platform to experimentally explore the bosonization duality in two spatial dimensions.

In conclusion, we have demonstrated that two-dimensional quantum antiferromagnets with additional anisotropy and nontrivial topology undergo a second-order phase transition. The near-critical behavior of this system has a unique signature and can be explored in real condensed matter systems. Furthermore, the theory at criticality allowed us to make a connection to massless Dirac fermions, thereby establishing an exact bosonization duality. These findings are significant from a theoretical point of view, because they provide a theoretical derivation of a result that up to now had remained a conjecture. From an experimental perspective, the results predict a specific critical behavior in two-dimensional quantum systems as well as suggest prospective candidate systems to achieve the bosonization duality.

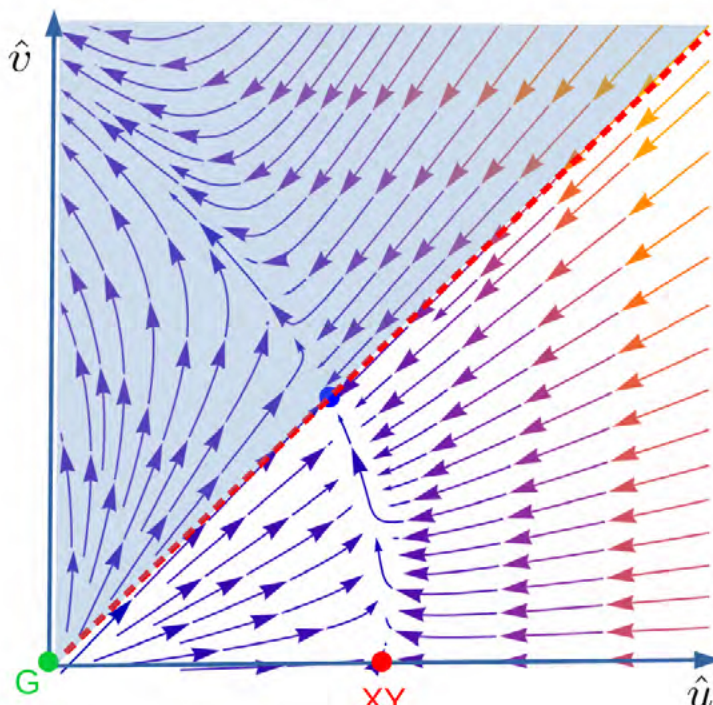


Abb. 2: Renormierungsgruppenfluss der dimensionslosen Kopplungen der Theorie. Es gibt zwei nichttriviale Fixpunkte: den XY-Fixpunkt (roter Punkt) entsprechend dem anisotropen Regime und den O(4)-symmetrischen Fixpunkt (blauer Punkt) entsprechend der höheren Symmetrie. Regime, die zum schattierten Bereich gehören, weisen Phasenübergänge erster Ordnung auf.
 Fig. 2: The renormalization group flow of dimensionless couplings of the theory. There are two nontrivial fixed points: the XY fixed point (red dot) corresponding to the anisotropic regime and the O(4)-symmetric fixed point (blue dot) corresponding to higher symmetry. Regimes belonging to the shaded area feature first-order phase transitions.

References

- [1] V. Shyta, J. van den Brink, and F. S. Nogueira, Phys. Rev. Lett. 127, 045701 (2021).
- [2] H. Goldman and E. Fradkin, Phys. Rev. B 97, 195112 (2018).
- [3] X.-G. Wen and A. Zee., Phys. Rev. Lett. 69, 1811–1814 (1992).
- [4] I. B. Spielman, J. P. Eisenstein, L. N. Pfeiffer et al., Phys. Rev. Lett. 84, 5808–5811 (2000).
- [5] M. M. Fogleret and F. Wilczek, Phys. Rev. Lett. 86, 1833–1836 (2001).

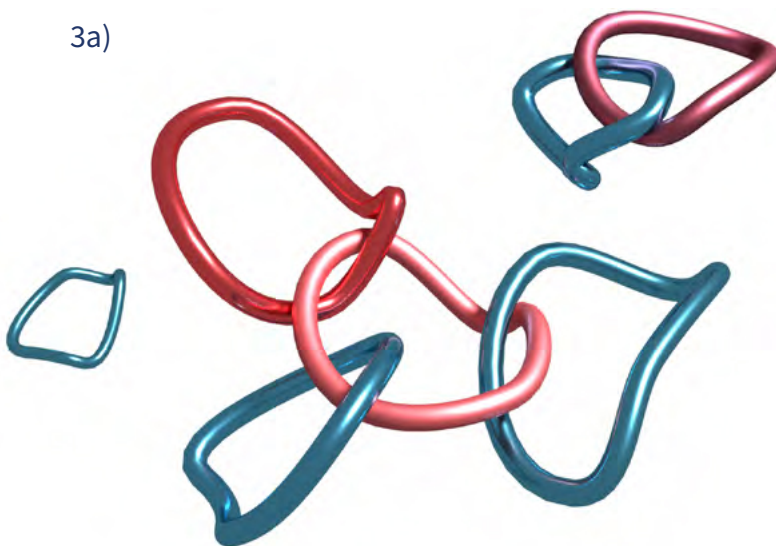
Funding

Deutsche Forschungsgemeinschaft (DFG) through the Würzburg-Dresden Cluster of Excellence on *Complexity and Topology in Quantum Matter – ct.qmat* (EXC 2147, project-id 39085490) and through SFB 1143 (project-id 247310070) Ukrainian-German Excellence Center UKRATOP, funded by BMBF under reference 01DK18002).

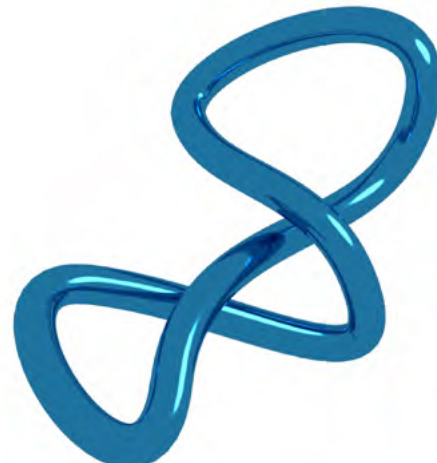
Abb. 3: Schematische Darstellung der Wirbelschleifen. Die Theorie topologischer Chern-Simons-Antiferromagneten, deren Anisotropie zum Typ der leichten Ebene gehören, wird bei Kritikalität ausschließlich durch die Eigenschaften der Wirbelschleifenkonfiguration definiert. Abbildung 3a zeigt, wie sich Schleifen umeinanderwinden können. Dies ist eine topologische Eigenschaft, die durch die sogenannte Verschlingungszahl charakterisiert wird. Zwei verschiedene Farben der Schleifen verdeutlichen, dass es in unserer Theorie zwei Arten von Schleifen gibt. Abbildung 3b zeigt eine sich um sich selbst windende Schleife. Dies ist eine geometrische Eigenschaft der Schleifen, die von der sogenannten Verwringung beschrieben wird, die jeden reellen Wert annehmen kann.

Fig. 3: A schematic representation of the vortex loops. The theory of topological Chern-Simons easy-plane antiferromagnets at criticality is defined purely by properties of the vortex loops configuration. Panel 3a illustrates how loops can curl around each other. This is their topological property characterized by the linking number. Two different colors of the loops highlight the fact that there are two types of loops in our theory. Panel 3b depicts a loop coiling around itself. This is a geometric property of the loop described by the writhe, which can take any real value.

3a)



3b)



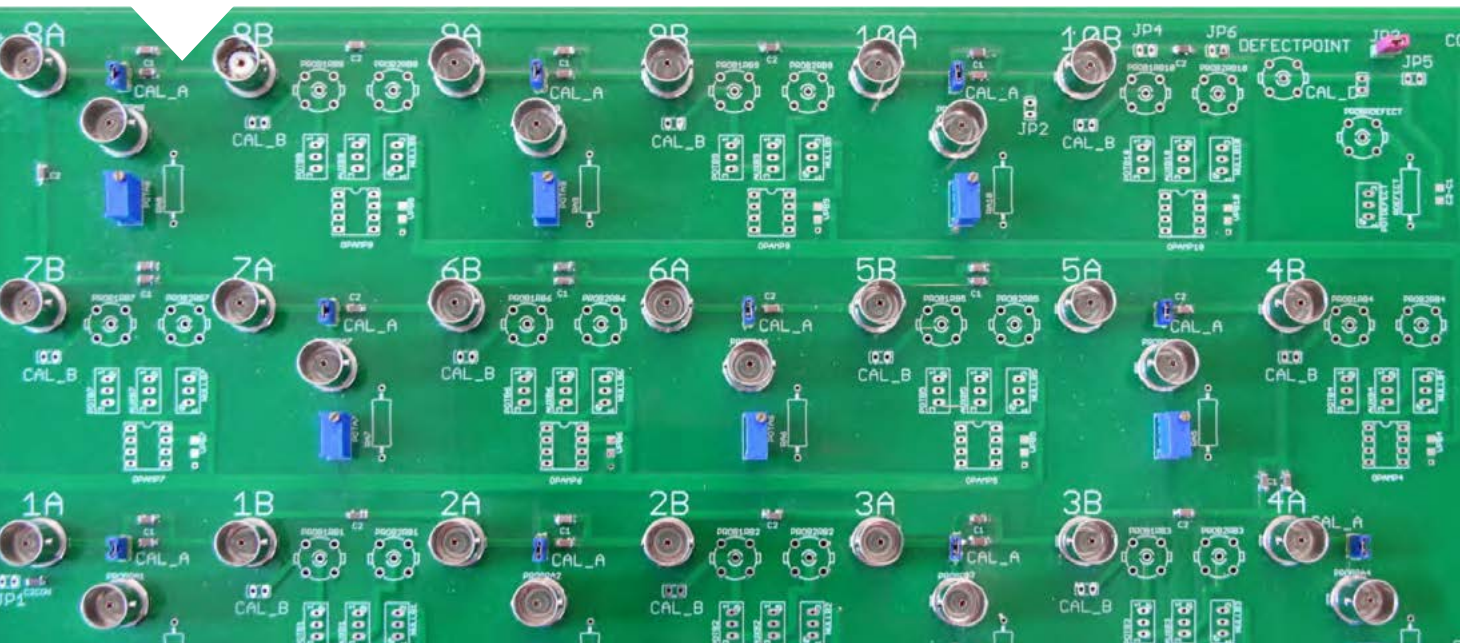
Electric circuits access a new regime of topology

Alexander Stegmaier¹, Stefan Imhof², Tobias Helbig¹, Tobias Hofmann¹, Ching Hua Lee³, Mark Kremer⁴, Alexander Fritzsche^{1,4}, Thorsten Feichtner², Sebastian Klembt⁵, Sven Höfling², Igor Boettcher⁶, Ion Cosma Fulga, Oliver G. Schmidt, Martin Greiter¹, Tobias Kiessling², Alexander Szameit⁴, Ronny Thomale¹

Elektronische Schaltkreise erlauben eine detaillierte Untersuchung äußerer Einflüsse auf die Stabilität topologischen Zustände, da sie eine gesteuerte Zu- und Abnahme der äußeren Widerstände ermöglichen. Das ist ein entscheidender Vorteil gegenüber Untersuchungen an kondensierter Materie, bei denen beispielsweise Kristall-Verunreinigungen spontane Defekte in der Messung hervorrufen. Durch die Konstruktion einer einfachen Schaltung, die aus Widerständen, Induktoren und Kondensatoren besteht, wurde in dieser Arbeit die Stabilität topologischer Zustände analysiert. Das System weist eine stabile, topologisch geschützte Resonanz auf, die an einen Defekt in der Systemmitte geknüpft ist. Ist das System unzureichend von der Außenwelt abgeschirmt, wird die Eigenresonanz zerstört. Bei noch stärkerer Kopplung taucht die Resonanz jedoch wieder auf, was zeigt, dass große Verluste für die topologischen Eigenschaften sogar von Vorteil sein können.

Electronic circuits allow a detailed analysis of external influences on the stability of topological states, since they enable a controlled increase and decrease of the external resistances. This is a key advantage over condensed matter studies where, for example, crystal impurities cause spontaneous defects in the measurement. By constructing a simple circuit consisting of resistors, inductors, and capacitors, the stability of topological states was analyzed in this work. The system exhibits a stable, topologically protected resonance that is tied to a defect in the center of the system. If the system is insufficiently shielded from the outside world, the self-resonance is destroyed. However, with even stronger coupling, the resonance reappears, showing that large losses can actually be beneficial for the topological properties.

Abb. 1: Foto einer der im Experiment verwendeten elektrischen Schaltplatten. Die zur Messung der topologischen Eigenschaften verwendeten Anschlüsse sind mit 1A, 1B, 2A, 2B usw. gekennzeichnet. Das gesamte System besteht aus vier in Reihe geschalteten Platten dieser Art.
 Fig. 1: Photo of one of the electric circuit boards used in the experiment. The ports used to measure topological properties are marked as 1A, 1B, 2A, 2B, etc. The full system consists of four such boards, connected in series.



The study of topological properties of materials is one of the more actively researched areas in physics. One of the well-known examples of topological matter is the quantum Hall effect, a system in which electrical current can flow only on the boundaries, and only in one direction. The unidirectional current flow, which is ensured by topology, leads to robust properties. The resistance of quantum Hall devices is quantized to such a high degree that it is today a standard of metrology [1].

In recent years, a growing body of work has focused on the topological properties of systems beyond the crystals that condensed-matter physicists typically work with. These are so-called meta-materials, such as photonic crystals [2], electric circuit boards [3], or even coupled mechanical pendulums [4]. Similar to their quantum counterparts, these classical systems can show robust topological features, such as unidirectional light propagation in photonic crystals [2], or robust electrical resonances pinned to the ends of a circuit made up of resistors and capacitors.

Unfortunately, both classical and quantum manifestations of topology often suffer from the same drawbacks. For example, when a device is not properly shielded, or isolated from the outside world, its topological signatures may lose their robustness, or even disappear altogether. This is because when systems are not isolated, energy can flow into or out of them. These phenomena are referred to as gain and loss, and they are now actively studied at the IFW as part of the emerging field of non-Hermitian topology [5].

In a collaboration between the IFW Dresden, our ct.qmat partners in Würzburg, as well as researchers from Rostock, Italy, Singapore, and the United States, we set out to investigate how gain and loss affect topological properties. We theoretically and experimentally studied a simple electric circuit composed of capacitors, resistors, and inductors. The circuit diagram is shown in Figure 2, and an actual circuit board used in the measurement is shown in the photo (Fig. 1). The circuit is grounded, meaning that it is coupled to the outside world, but we can control the strength of this coupling by varying the resistances R_A and R_B . Our aim was to test which of its topological properties will remain robust as losses

gradually become greater, meaning the resistances connecting the circuit to the ground become smaller.

Unlike typical condensed-matter systems, where crystals may have impurities or defects at random positions, electric circuits are highly tunable, since each capacitor and resistor can be individually adjusted to achieve the desired effect. We used this fact to our advantage and designed the circuit so that it hosts topological resonances at its ends, as well as a topological resonance pinned to a defect in the middle of the circuit, which we have purposely introduced. When the circuit is relatively well isolated, meaning that it is connected to ground using a relatively large resistance, both the ends and the defect show robust topological features. This known as the "PT symmetric phase" (see Figure 3a).

As losses gradually become stronger, the defect mode disappears completely, even though the edge modes remain robust, as shown in Figure 3b. This change marks the transition between the PT symmetric phase from before, and a new, so-called "PT broken phase." As expected, a stronger coupling to the outside world is detrimental to some topological properties. This fact was known from before, and was recently demonstrated experimentally, in a photonic crystal realizing the same topology as our circuit [6].

In photonic crystals, however, greater losses make the measurement more difficult. This is because the stronger the losses, the less light remains inside the photonic crystal, so at some point there is no light left to measure. In contrast, in electric circuits our measurement technique can reach regimes where the coupling to the outside world is very large (the resistance R_B is very small) while keeping a good quality of the measured signal. We have taken advantage of this fact by going to a regime which is beyond those possible in current photonic crystals, where the coupling between the system and the outside world is stronger than any other coupling term in the circuit.

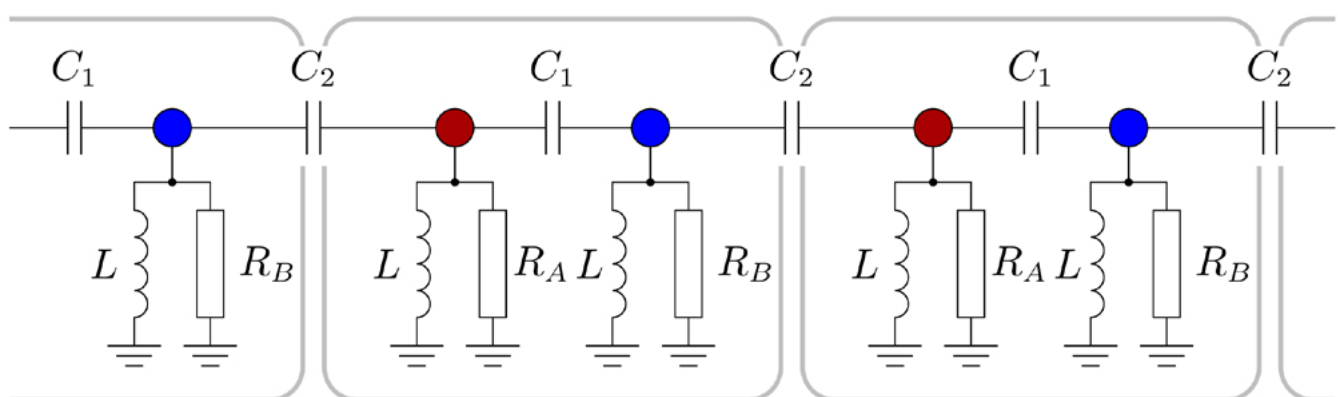
Remarkably, in this newly accessed "APT symmetric phase," all of the circuit's topological properties are restored (see Figure 3c). Even though it suffers from large losses, the topological resonance at its central

defect is restored, and even becomes sharper and more well-defined than in the well-shielded, PT symmetric phase. Contrary to intuition, a larger coupling between a system and the outside world can in fact be beneficial, and helps to stabilize topological properties.

We have focused on a very specific circuit, which was specially tailored to show a particular type of topology. However, our measurement techniques are applicable to electric circuits in general, meaning that they may be used for other systems as well. Thus, it should be possible to perform similar experiments for two and three-dimensional circuits, as well as in circuits showing varied types of topological resonances. Electric circuits offer the possibility of experimentally investigating regimes that go beyond those possible in many other meta-material platforms, allowing to study the features of the newly seen, APT symmetric phase.

More generally, our work is one of the many results which are currently filling the gap between the study of topological phases, a young and emerging field, and electronics, which is by now very well-known and mature. We each have, in our pockets and on our desks, highly complex electronic circuits whose basic building blocks were first discovered many decades ago. In contrast, new types of topological phases are being discovered almost every year. Many well-known electronic devices such as circulators, resonators, and amplifiers, are just beginning to be understood using the language of topological physics, even though they were first invented before this field existed. In the future, we hope that an increased understanding of topological phases will lead to new types of electronic circuits which will be useful in our daily lives.

Abb. 2: Schaltplan bestehend aus Kondensatoren (C_1, C_2), Widerständen (R_A, R_B) und Induktoren (L). Jede "Einheit" der Schaltung ist durch einen grauen Kasten gekennzeichnet und besteht aus zwei Schaltknoten (farbige Kreise). Insgesamt besteht die vollständige Schaltung aus einer Kette von 20 Einheiten.
 Fig. 2: Circuit diagram consisting of capacitors (C_1, C_2), resistors (R_A, R_B), and inductors (L). Each "unit" of the circuit is marked by a gray box, and consists of two circuit nodes (colored circles). In total, the full circuit is a chain consisting of 20 units.



References

- [1] K. v. Klitzing and G. Ebert, Metrologia 21, 1118 (1985)
- [2] M. C. Rechtsman et al., Nature 496, 196 (2013).
- [3] C. H. Lee et al., Commun. Phys. 1, 39 (2018)
- [4] R. Süssstrunk et al., Science, 349, 47 (2015)
- [5] H. Liu et al., Phys. Rev. B 104, 155412 (2021)
- [6] S. Weimann et al., Nat. Mater. 16, 433 (2016).

Funding

This work is funded by the Deutsche Forschungsgemeinschaft (DFG, German Research Foundation) through Project-ID 258499086 - SFB 1170 and through the Würzburg-Dresden Cluster of Excellence on *Complexity and Topology in Quantum Matter-ct.qmat* Project-ID 390858490 - EXC 2147. T.He. was supported by a Ph.D. scholarship of the Studienstiftung des deutschen Volkes.

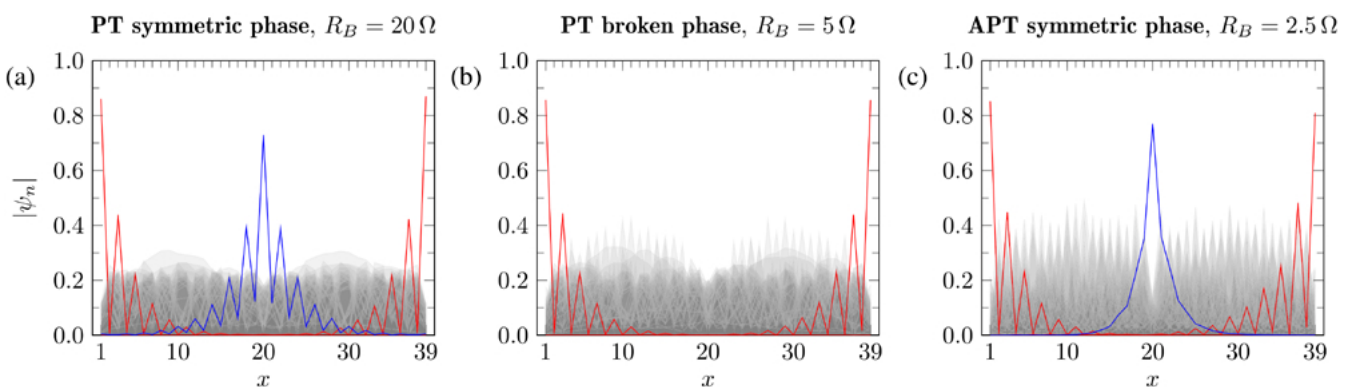
IB is funded by the DoE BES Materials and Chemical Sciences Research for Quantum Information Science program (award No. DE-SC0019449), NSF PFCQC program, DoE ASCR (award No. DE-SC0020312 and DE-SC0019040), AFOSR, ARO MURI, ARL CDQI, AFOSR MURI, and NSF PFC at JQI.

Cooperations

- ¹ Institute for Theoretical Physics and Astrophysics, University of Würzburg, Am Hubland, D-97074 Würzburg, Germany
- ² Physikalisches Institut and Röntgen Research Center for Complex Material Systems, Universität Würzburg, D-97074 Würzburg, Germany
- ³ Department of Physics, National University of Singapore, Singapore 117542
- ⁴ Institut für Physik, Universität Rostock, Albert-Einstein-Straße 23, 18059 Rostock
- ⁵ Technische Physik and Wilhelm-Conrad-Röntgen-Research Center for Complex Material Systems, Universität Würzburg, Am Hubland, D-97074 Würzburg, Germany
- ⁶ Joint Quantum Institute, University of Maryland, College Park, MD 20742, USA

Abb. 3: Gemessene Eigenvektoren des Stromkreises, die die Positionen der Resonanzen (grau, rot und blau gefärbt) in drei verschiedenen Zuständen zeigen: die PT symmetrische Phase (a), die PT gebrochene Phase (b) und die APT symmetrische Phase (c). An den Enden des Kreises (rot) treten stark lokalisierte Schwingungen auf. Die ausgeprägte Resonanz in der Mitte der Kette (blau, Schaubild a und c) ist an einen Defekt gebunden, der dort absichtlich eingeführt wurde.

Fig. 3: Measured eigenvectors of the electric circuit, showing the positions of resonances (colored gray, red, and blue) in three different regimes: the PT symmetric phase (a), the PT broken phase (b), and the APT symmetric phase (c). Sharply localized resonances appear at the ends of the circuit (red). The sharp resonance in the middle of the chain (blue, panels a and c) is bound to a defect which has been purposely introduced there.



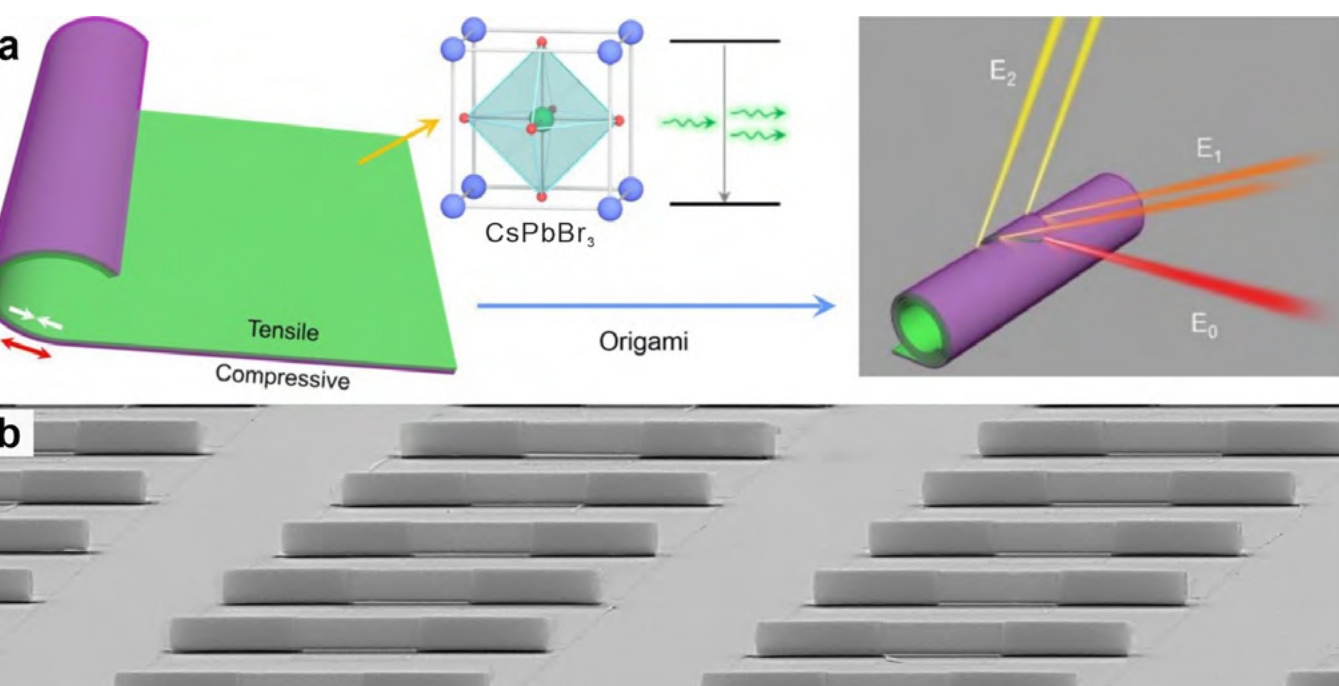
Origami perovskite microtube cavity for programmable three-dimensional lasing

Haiyun Dong, Christian N. Saggau, Minshen Zhu, Jie Liang¹, Shengkai Duan, Xiaoyu Wang, Hongmei Tang, Yin Yin², Xiaoxia Wang, Jiawei Wang³, Chunhuan Zhang¹, Yong Sheng Zhao¹, Libo Ma, Oliver G. Schmidt⁴

Das Design von Mikro-Kavitäten ist entscheidend für die Erforschung neuartiger Mikrolaser und deren weiteren Anwendungsmöglichkeiten. Obwohl hochdimensionale Mikro-Kavitäten mehr Freiheitsgrade für die Laserkontrolle bieten, sind aktuelle Verfahren auf niedrigdimensionale Konfigurationen beschränkt, die sich einem Leistungsengpass nähern. Aus diesem Grund entwickeln wir eine Mikro-Origami-Technik zur Herstellung von Perowskit-Mikroröhren-Hohlräumen für dreidimensionales (3D) Lasern. Mit ihren einzigartigen 3D-Eigenschaften ermöglichen diese Perowskit-Mikroröhrenresonatoren sowohl herausragende Laserleistungen (z. B. niedriger Schwellenwert, gerichtete Emission, abstimmbare Leistung und hohe Stabilität) als auch neuartige Laserfunktionen (z. B. Laser-Array in Array-Emission und 3D-Mode-Lasing). Solche 3D-Mikro-Kavitäts-laser versprechen, die Praxis der 3D-Photonenintegration zu revolutionieren.

Microcavity design is crucial for exploring novel type of micro-lasers with extended applications. Although high-dimensional microcavities provide higher degrees of freedom for laser control, current laser microcavities are constrained to low-dimensional configurations approaching a performance bottleneck. Here we develop a micro-origami technique to fabricate perovskite microtube cavities for three-dimensional (3D) lasing. With unique 3D characteristics, the perovskite microtube resonators allow for both outstanding laser performance (e.g. low threshold, directional emission, tunable output, and high stability) and novel laser functionalities (e.g. laser array in array emission and 3D mode lasing). Such 3D microcavity lasers promise to change the practice of 3D photonic integration.

Abb. 1: a) Design of Perowskit-Origami for 3D-Mikroröhrchenlaser. b) REM-Aufnahme eines großflächigen Perowskit-Mikroröhrchen-Laserarrays.



Microcavity lasers go three-dimensional

The invention and continued development of laser devices have revolutionized science, technology, and industry.[1] A laser is a strong coherent light source consisting of a gain medium, a pump source, and an optical cavity. The optical cavity provides optical feedback for laser oscillation and controls laser output characteristics. New types of optical cavities have always been pursued with the expectation to enhance laser performance and explore new applications. With an unprecedented ability to deliver intense coherent light signals at the microscale, microcavity lasers have found many important applications including chemical sensing, biological labeling, and on-chip photonic integration.[2, 3] So far, typical microlasers rely on one-dimensional (1D) Fabry-Pérot and two-dimensional (2D) whispering-gallery-mode microcavities. Constrained to simple low-dimensional microcavity structures, the current microlasers suffer from limited design freedom, holding up laser performance improvement and functionality upgrades. It is anticipated that extending the microcavity geometry to a 3D configuration will lead to higher tiers of microlaser design and application potential.

Microscale origami is an art of folding 2D nanomembranes into 3D microarchitectures, offering a versatile route to 3D microdevices with new characteristics and functionalities.[4, 5] The origami microtubes with circular cross-sections constitute 3D microcavities supporting optical resonances along a ring trajectory. By intruding an optical potential well along the tube axis, unique 3D optical confinement and resonance can be realized along both azimuthal and axial dimensions of the microtube cavity.[6] With 3D characteristics, the microtube cavities have been generating intriguing photonic phenomena and applications.[7-9] Hence, incorporating optical gain media into the microtube cavities promises to produce unique 3D microlasers with improved performance and novel functionalities. Although several attempts have been made to incorporate semiconductor quantum dots/wells into the microtube to achieve lasing,[10, 11] great concerns have been raised that sufficient evidence to support a claim of lasing in the microtube was not always provided. Besides, the microtube laser is still in its infancy with

difficult challenges on many fronts, such as limited materials choice, costly fabrication, cryogenic operation, and therefore limited application.

Here, we design a versatile micro-origami approach to programmatically assemble perovskite thin films into customized microtubes for the construction of a new generation of 3D microcavity lasers.[12] The functional bilayer composed of tensilely strained perovskite and compressively strained silicon nitride provides the driving force for origami. The origami perovskite microtube cavities support room-temperature laser operation. With unique 3D characteristics, the perovskite microtube cavities not only show superior laser performance, such as low threshold, directional emission, tunable output, and high stability, but also produce novel laser features, such as laser array-in-array emission and 3D mode lasing. This investigation establishes a platform for extending the functionality and application of microcavity lasers to the third dimension.

Origami perovskite microtube lasers with superior performance and novel functionalities

The key to micro-origami design lies in the clever construction of differentially strained bilayers that provide the driving force for the self-assembly of thin solid films into 3D microarchitectures. Here tensilely strained perovskite and compressively strained silicon nitride constitute the functional bilayers where the differential strain drives the top and bottom layers to contract and expand, respectively, causing the whole film to roll up into a Swiss-roll tubular microstructure (Figure 1). The perovskite microtubes can function as lasers by simultaneously providing high optical gain and effective optical feedback. All fabrication processes involved in the origami approach are silicon-compatible and enable wafer-scale fabrication of microtube lasers.

The perovskite microtube cavities support room-temperature laser oscillations along the tube cross-section. The lasing threshold of $1.86 \mu\text{J}/\text{cm}^2$ is among the lowest values for inorganic perovskite lasers, which is attributed to the smooth and free-standing microtube structure with minimized scattering loss and suppressed optical leakage into the substrate. Because the perovskite layer is well protected by aluminum oxide and silicon nitride films, the micro-

tube laser exhibits excellent operation stability under ambient conditions. With an intrinsic spiral structure breaking the cavity rotational symmetry, the perovskite microtube laser experiences directional emission behavior, which is essential for almost all practical laser applications. More interestingly, each perovskite microtube constitutes a 1D laser array by itself because each circular cross-section of the microtube supports a set of optical ring resonances (Figure 2).

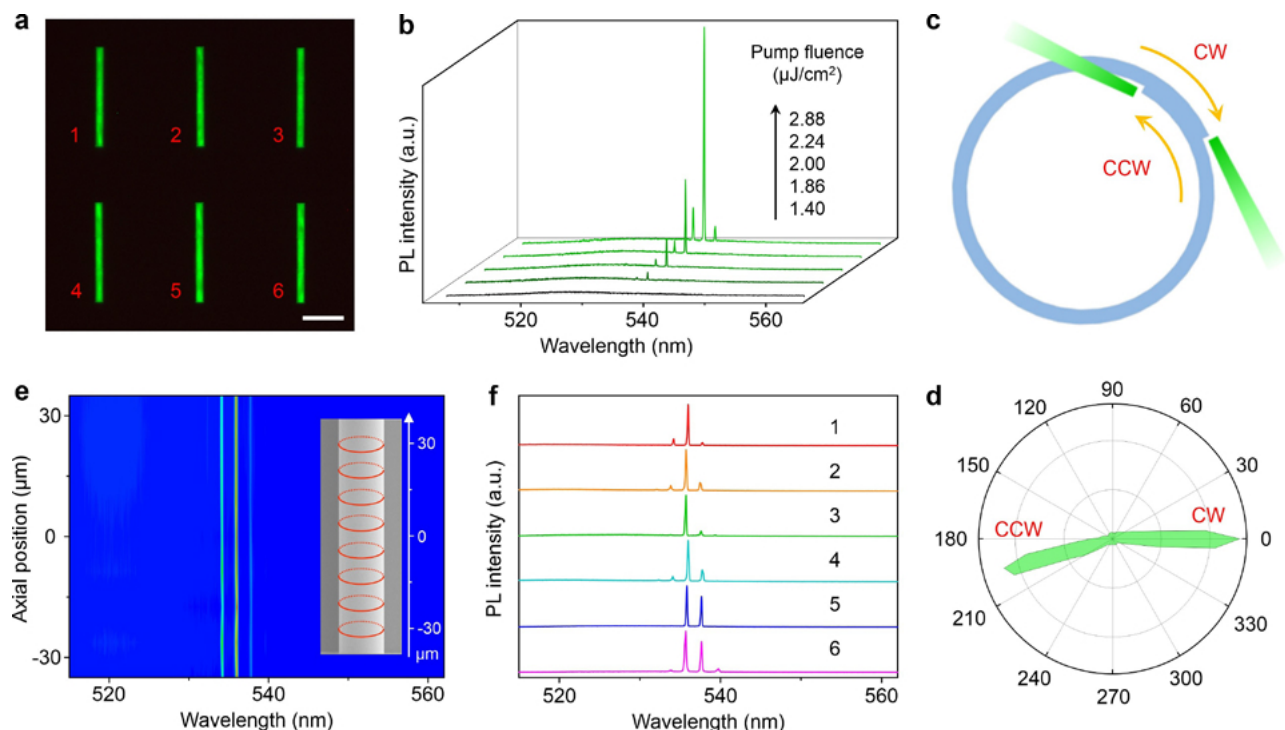
A large number of perovskite microtubes further form a 2D array exhibiting almost the same laser output characteristics. Such a laser “array-in-array” facilitates the construction of high-density on-chip photonic integrated systems and circuits.

The origami method offers high design flexibility in both device geometry and materials composition toward programmed laser emission properties.

The laser mode and color can be well tuned by controlling the diameter and composition of the perovskite microtube cavities. Another unique feature of the microtube cavity for lasing is the realization of 3D optical confinement along both azimuthal and axial dimensions by introducing a lobe structure onto the microtube (Figure 3). Strong 3D optical confinement further increases the cavity quality factors and lowers the lasing thresholds. Besides, an axial optical potential well defined by the lobe structure splits the azimuthal mode into fundamental and higher-order axial modes, which exhibits directional emission along different azimuths. Such a 3D directional laser output behavior is expected to find applications in 3D photonic integration, for instance, simultaneously delivering coherent light signals for different photonic components distributed in 3D space.

Abb. 2: a) PL-Aufnahme eines CsPbBr_3 -Perowskit-Mikroröhrchenarrays. b) Emissionsspektren eines einzelnen Perowskit-Mikroröhrchens unter verschiedenen Pumpflüssen, welche die Entwicklung von spontaner Emission zur Laseremission zeigen. c) Schematische Darstellung der gerichteten Laseremission an der inneren und äußeren Rollkante. d) Fernfeld-Laseremissionsmuster des Perowskit-Mikroröhrchens. e) Örtlich aufgelöste Laserspektren entlang der Perowskit-Mikroröhrenachse. f) Laserspektren des Perowskit-Mikroröhrchenarrays.

Fig. 2: a) PL image of a CsPbBr_3 perovskite microtube array. b) Emission spectra of an individual perovskite microtube under different pump fluences, showing the evolution from spontaneous emission to lasing. c) Schematic diagram of the directional laser emission at the internal and external rolling edges. d) Far-field laser emission pattern of the perovskite microtube. e) Mapping of lasing spectra along the perovskite microtube axis. f) Lasing spectra of the perovskite microtube array.



References

- [1] N. R. Council, Optics and Photonics: Essential Technologies for Our Nation, The National Academies Press, Washington, DC 2013.
- [2] M. T. Hill et al., Nat. Photonics 2014, 8, 908.
- [3] W. Zhang et al., Acc. Chem. Res. 2016, 49, 1691.
- [4] D. Karnaushenko et al., Adv. Mater. 2020, 32, 1902994.
- [5] Y. Zhang et al., Nat. Rev. Mater. 2017, 2, 17019.
- [6] C. Strelow et al., Phys. Rev. Lett. 2008, 101, 127403.
- [7] L. B. Ma et al., Nat. Commun. 2016, 7, 10983.
- [8] Y. Yin et al., Phys. Rev. Lett. 2016, 116, 253904.
- [9] Y. Yin et al., Sci. Adv. 2019, 5, eaax6973.
- [10] F. Li et al., Opt. Express 2009, 17, 19933.
- [11] Y. Li et al., Opt. Express 2017, 25, 18072.
- [12] H. Dong et al., Adv. Funct. Mater. 2021, 31, 2109080.

Funding

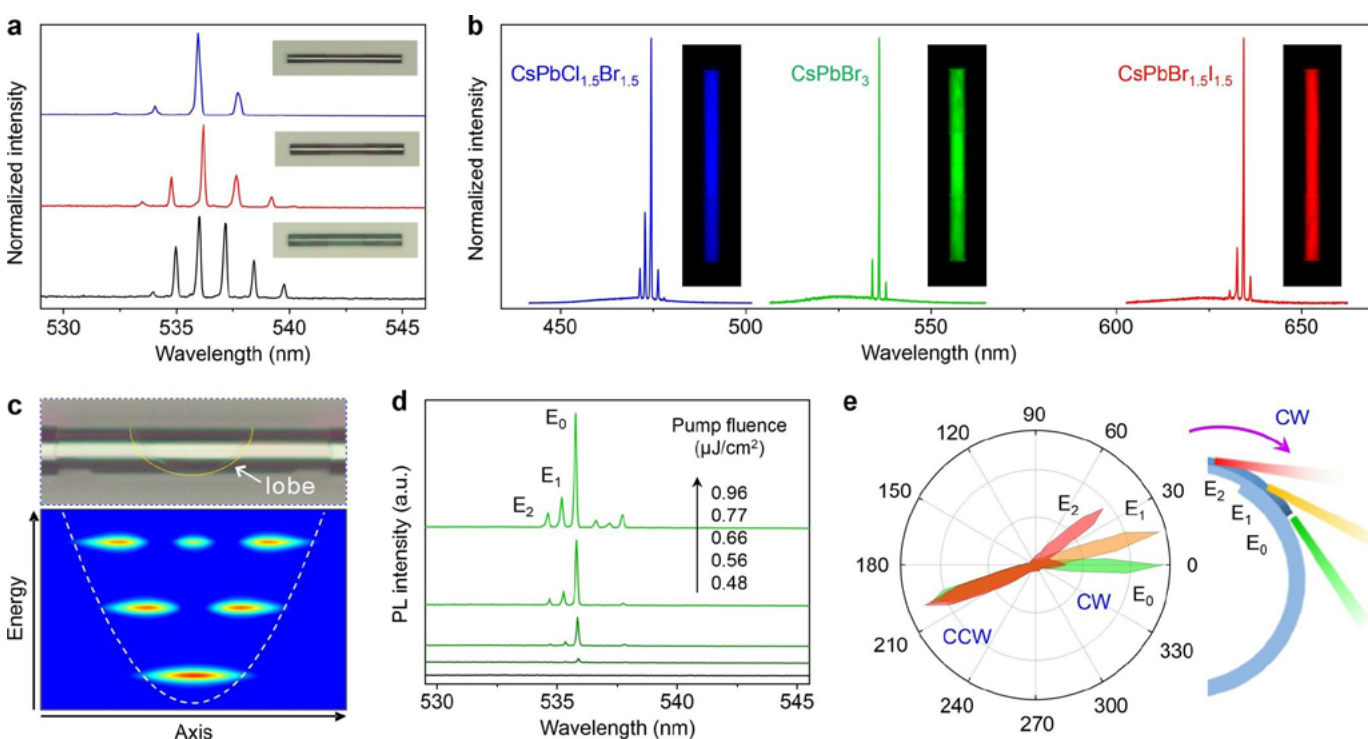
Leibniz Program of the German Research Foundation
 Würzburg-Dresden Cluster of Excellence on Complexity and Topology in Quantum Matter - ct.qmat.

Cooperations

- ¹ Institute of Chemistry, Chinese Academy of Sciences, China
- ² Jinagsu University, China
- ³ Harbin Institute of Technology, Shenzhen, China
- ⁴ TU Chemnitz, Germany

Abb. 3: a,b) Laserspektren der Perowskit-Mikroröhrchen mit unterschiedlichen Größen und Zusammensetzungen. c) Berechnete Feldverteilungen axialer Moden in einem mit einem Flügel modifizierten Mikroröhrchens. d) Emissionsspektren des flügelmodifizierten Perowskit-Mikroröhrchens unter verschiedenen Pumpflüssen. e) Normierte Fernfeld-Emissionsintensitäten der axialen Lasermoden.

Fig. 3: a,b) Lasing spectra of the perovskite microtubes with different sizes and compositions. c) Calculated field distributions of axial modes in a lobe-modified microtube. d) Emission spectra of the lobe-modified perovskite microtube under different pump fluences. e) Normalized far-field emission intensities of the axial laser modes.

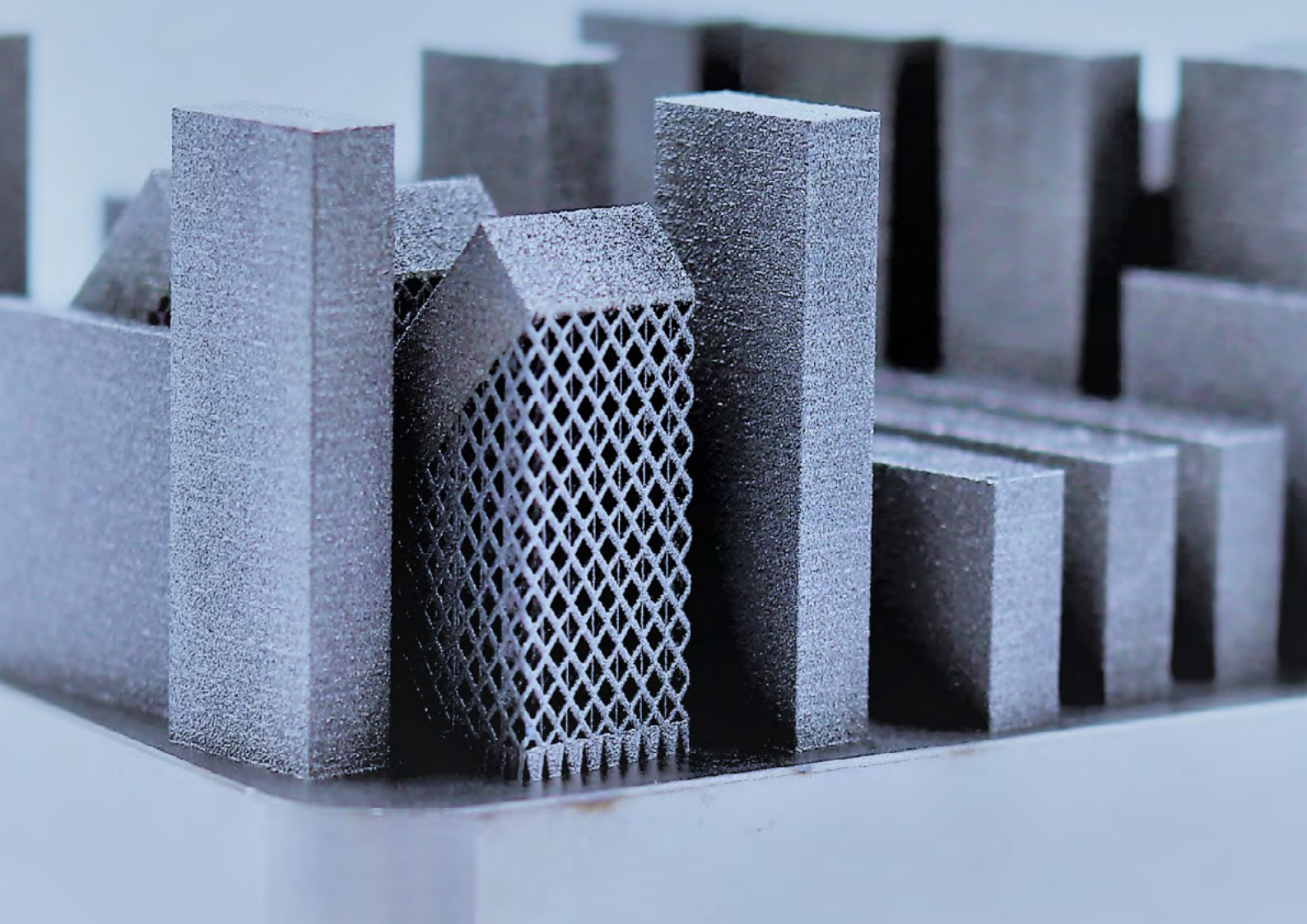


FORSCHUNGSGEBIET 4:

Vom Material zum Produkt

RESEARCH AREA 4:

Towards Products



Vom Material zum Produkt

Das Forschungsgebiet 4 umfasst Materialsysteme, deren Eigenschaften im Hinblick auf konkrete Anwendungen, Prototypen und Produkte optimiert werden. Dies geschieht in der Regel in enger Zusammenarbeit mit Industriepartnern. Forschungsergebnisse, die wirtschaftliche Bedeutung haben können, werden frühzeitig patentrechtlich geschützt. Eine große Zahl nationaler und internationaler Patente belegt die Praxisrelevanz dieser Themen.

Ein typisches Beispiel sind akustische-Oberflächenwellen-Bauelemente. Diese werden als Frequenzfilter zur Auswahl von Signalübertragungskanälen und Sensoren verwendet. Sie bestehen aus einem piezoelektrischen Einkristallchip, auf dem elektrische in akustische Signale und wieder zurück umgewandelt werden. Das IFW hat auf diesem Gebiet wichtige Innovationsbeiträge geleistet, die direkten Einfluss auf die Produkte haben, z. B. die Verbesserung der Temperaturstabilität und der elektromechanischen Anregung durch Aufbringen eines speziellen Dünnenschichtmaterials.

Weitere Projekte in diesem Forschungsgebiet betreffen Materialien für biomedizinische Anwendungen, Legierungen für hochfeste Werkstoffe, Nanomembranen für flexible magnetoelektronische Bauelemente und Demonstratoren für die Anwendung von Hochtemperatursupraleitern.

Towards Products

This research area comprises materials whose physical, mechanical and chemical properties are to be optimized with respect to certain applications, prototypes and products. Usually this is achieved in close cooperation with partners from industry. In the case that scientific results are of economic importance intellectual property rights are secured. A large number of national and international patents and a high degree of licensing indicate their practical relevance.

A typical example are surface acoustic waves components. These are used in sensors and as frequency filters for the channel selection in signal transition. They consist of a piezo-electric single crystal chip which transforms electric signals in acoustic ones and back. The IFW has contributed a number of innovations in this field, for example a considerable improvement of temperature stability and of electro-mechanical excitation by a special thin film material. Further projects in this research area concern materials for bio-medical applications, alloys for high-strength materials, nanomembranes for flexible electronic devices and demonstrators for the application of high-temperature superconductors.

Environmentally friendly cathode materials for cost-effective Lithium-ion batteries

Mohamed A. A. Mohamed, Mikhail V. Gorbunov, Daria Mikhailova, Bernd Büchner, Martin Valldor¹, Silke Hampel, Nico Gräßler

Lithiumreiche Antiperowskite gelten als umweltfreundliche, kostengünstige und ungiftige Alternative für Lithium-Ionen-Batterieanwendungen. Diese neuartigen Kathodenmaterialien basieren zu 100 Prozent auf umweltverträglichen Bestandteilen (Abb. 1) und verzichten auf das umweltkritische Element Cobalt, das noch in den allgegenwärtigen Lithium-Ionen-Batterien enthalten ist. Im Gegensatz zu den derzeitigen kommerziellen Kathoden weisen die lithiumreichen Antiperowskite eine reversible Multi-Elektronen-Funktionalität auf, die zu Batterien mit hoher Energiedichte führt. Allerdings leiden sie im Moment noch unter einer schlechten zyklischen Stabilität, was ihre Anwendung erschwert. In unseren Studien zeigen wir am Beispiel der Lithium-Eisen-Schwefel-Sauerstoff-Verbindung ($\text{Li}_2\text{Fe}\text{SO}_4$), dass die strukturellen und elektrochemischen Eigenschaften durch eine anionische Substitution des Schwefels (S) durch Selen (Se) eingestellt werden können.
(> Fokus Nachhaltigkeit, Seite 15)

Lithium-rich antiperovskites are considered as environmentally friendly, low-cost and non-toxic alternatives for lithium-ion battery applications. These novel cathode materials are based 100 percent on environmentally compatible components (Fig. 1) and do not contain the environmentally critical element cobalt, which is still found in the ubiquitous lithium-ion batteries. In contrast to current commercial cathodes, lithium-rich antiperovskites exhibit reversible multi-electron functionality, resulting in batteries with high energy density. However, at the moment they still suffer from poor cycling stability, which complicates their application. In our studies, we show on the material iron the lithium-iron-sulfur-oxygen compound ($\text{Li}_2\text{Fe}\text{SO}_4$) that the structural and electrochemical properties can be tuned by anionic substitution of sulfur (S) by selenium (Se).
(> Focus Sustainability, page 15)

Abb. 1: Kostengünstige und ungiftige Inhaltsstoffe: Lithiumoxid (weiß), Eisen (grau) und Schwefel (gelb) sind die Bestandteile für das neuartige Kathodenmaterial ($\text{Li}_2\text{Fe}\text{SO}_4$).
Fig. 1: Cost-effective and non-toxic raw materials: lithium oxide (white), iron (gray) and sulfur (yellow) are the constituents for the novel cathode material ($\text{Li}_2\text{Fe}\text{SO}_4$).



Lithium-rich antiperovskite cathodes

Lithium-ion batteries have become an essential part of everyday life, whether in smartphones, laptops, or electric cars. Continuous technological progress requires an increase in battery performance while taking sustainable production and recycling into account. In this context, the cathode material plays a crucial role. Current commercial cathodes, such as layered LiCoO_2 , layered $\text{LiNi}_{1/3}\text{Mn}_{1/3}\text{Co}_{1/3}\text{O}_2$, olivine LiFePO_4 , and spinel LiMn_2O_4 , have some disadvantages yet despite extensive optimizations [1]. More specifically, all these cathodes have a limitation of one electron transfer in the redox processes, which restricts their gravimetric capacities and energy density. Therefore, lithium-rich materials are considered an attractive option. The approach of multi-electron redox processes for Li-rich materials can be realized either by (i) successive redox of transition metal cations or (ii) redox involving both transition metal cations and anions [2, 3]. Recently, a novel class of Li-rich antiperovskite cathodes with a general formula $(\text{Li}_2\text{TM})\text{ChO}$ ($\text{TM} = \text{Fe}, \text{Mn}, \text{Co}; \text{Ch} = \text{S}, \text{Se}$) was discovered in 2017 [4, 5]. These antiperovskite cathodes display a multi-electron storage merit with reversible transfer of 1.2 Li^+ per formula unit. Furthermore, they offer other advantages such as reasonable working voltage ($\sim 1.2 - 3$ V) and 3-dimensional (3D) Li^+ diffusion with low diffusion barrier (~ 0.32 eV) [6]. Among the antiperovskite cathodes, the $(\text{Li}_2\text{Fe})\text{SO}$ composition exhibits one of best reported electrochemical performance with an average discharge capacity ~ 285 mAh g $^{-1}$ at 0.1C and a high rate capability (~ 200 mAh g $^{-1}$ at 1C). However, this compound suffers from poor cycling stability at current rates below 1C and low capacity recovery at 0.1C after only 50 cycles (< 80 %) [7]. To improve the electrochemical performance of $(\text{Li}_2\text{Fe})\text{SO}$, the anion substitution of S to Se presented here is an important approach for its future application.

Effect of anionic substitution on structural stability

With an increasing Se content of the $(\text{Li}_2\text{Fe})\text{S}_{1-x}\text{Se}_x\text{O}$ solid solutions the compounds show higher thermal stability as well as higher stability in moist air. The Goldschmidt tolerance factor (t) is a predictor for the structural stability of antiperovskites based on the degree of mismatch between the constituent

ions [8]. The calculated factor (t) confirms that the structural stability increases with higher Se content, which is attributed to the larger ionic radius of Se^{2-} (1.84 Å) compared to S^{2-} (1.7 Å).

Electrochemical studies

The multi-stage redox processes of the solid solutions were characterized by cyclic voltammetry (CV) (see Figure 2). The three-step oxidation is composed of cationic ($\text{Fe}^{2+}/\text{Fe}^{3+}$) and anionic ($\text{S}^{2-/\text{0}}$ and $\text{Se}^{2-/\text{0}}$) processes. Based on previous XPS measurements for $(\text{Li}_2\text{Fe})\text{SO}$ [7], the oxidation peak at 3 V is attributed to partial oxidation of sulfide (S^{2-}) to elemental sulfur (S^0). Similarly, the oxidation peak at ~ 2.9 V for $(\text{Li}_2\text{Fe})\text{S}_{0.9}\text{Se}_{0.1}\text{O}$ corresponds to a partial oxidation of S^{2-} to S^0 , while the other two peaks at 2.1 and 2.5 V are expected to be a two-stage oxidation of Fe^{2+} to Fe^{3+} . Interestingly, the first oxidation peak at around 2.1 V, for the composition with $x(\text{Se}) = 0.1$, shifts to higher potentials with increasing Se content, while the second oxidation peak at 2.55 V is nearly independent on the Se content, as shown in Figure 2.

In contrast, as the Se content increases, the intensity of the anionic oxidation peak grows while its position shifts to a lower potential. This implies that either (i) Se facilitates the oxidation of S^{2-} or (ii) Se^{2-} is also oxidized at lower potentials, and the peaks partially overlap in the voltammogram. However, the second scenario seems to be more likely, because Se substitution at the S-site in $\text{Li}_2\text{FeS}_{2-y}\text{Se}_y$ solid solutions was found to increase the energy of frontier states and thus decrease the anion oxidation potential [9]. This reduction in anion oxidation potential was attributed to the participation of $4p$ orbital of Se in the density of states at the expense of S $3p$. Separated peaks due to S^{2-} and Se^{2-} oxidations were not observed in our CV data, suggesting that complete mixing of the anionic states occur instead of having two independent oxidations. This result highlights the role of anionic substitution on controlling the redox potentials.

The influence of Se incorporation in the $(\text{Li}_2\text{Fe})\text{SO}$ cathode on the electrochemical performance and cycling stability is shown in Figure 3. In general, no linear dependence of the Se content on the electrochemical properties can be derived. In particular, the capacity value and capacity retention

upon cycling depend on the relative atomic percentages between S and Se. Replacing a small amount of S (10 at. percent) in $(\text{Li}_2\text{Fe})\text{SO}$ with Se decrease the specific discharge capacity, but is not sufficient to stabilize the performance in terms of capacity retention/recovery compared to $(\text{Li}_2\text{Fe})\text{SO}$. Further increasing of Se content resulted in improved capacity accompanied with promising cycling stability, especially at low current rates (< 1C) as seen for $(\text{Li}_2\text{Fe})\text{S}_{0.7}\text{Se}_{0.3}\text{O}$. This composition exhibited an average discharge capacity of 245 mAh g⁻¹ at 0.1C, which is similar to that for $(\text{Li}_2\text{Fe})\text{SO}$. However, it shows better cycling stability in terms of capacity retention at low current rates and a capacity recovery of ~100 percent at 0.1C rate after 50 cycles at different C rates. Samples with Se contents $x > 0.3$ display promising capacity recovery, but with lower average capacity at all current densities compared to $(\text{Li}_2\text{Fe})\text{S}_{0.7}\text{Se}_{0.3}\text{O}$. Therefore, various *in situ* and *ex situ* techniques were used to explore the origin of its superior performance of $(\text{Li}_2\text{Fe})\text{S}_{0.7}\text{Se}_{0.3}\text{O}$ material. *Operando* XRD measurements indicated a higher structural stability during cycling for $(\text{Li}_2\text{Fe})\text{S}_{0.7}\text{Se}_{0.3}\text{O}$ compared to unsubstituted $(\text{Li}_2\text{Fe})\text{SO}$. Furthermore, X-ray absorption spectroscopy (XAS) confirmed

that the multielectron capability originates from the contribution of the cation (Fe) and anions (S/Se) in the redox processes.

Conclusions

Understanding the multi-electron redox mechanisms of Li-rich antiperovskites is a key to improving electrochemical performance. In particular, the anionic redox process in $(\text{Li}_2\text{Fe})\text{SO}$ was accompanied by partial irreversible oxidation of S^{2-}/S^0 and consequent confining decreased structural stability [7]. Here we showed that the anion redox function is tunable by anionic substitution of S by Se. The Se-content in $(\text{Li}_2\text{Fe})\text{S}_{1-x}\text{Se}_x\text{O}$ play a significant role in enhancing structure stability and improving the capacity recovery. $(\text{Li}_2\text{Fe})\text{S}_{0.7}\text{Se}_{0.3}\text{O}$ displayed the best electrochemical performance among all compositions. In previous studies, we have shown that partial cationic substitution of Fe by Mn has an additional stabilizing effect [10]. The specific combination of cationic and anionic substitution will provide environmentally friendly Li-rich antiperovskites with optimized compositions for practical application in Li-ion batteries.

Abb. 2: Cyclovoltammogramme für die Serie $(\text{Li}_2\text{Fe})\text{S}_{1-x}\text{Se}_x\text{O}$ mit $x = 0.1, 0.3, 0.5, 0.7, 0.9$.
Fig. 2: Cyclic voltammograms for the series $(\text{Li}_2\text{Fe})\text{S}_{1-x}\text{Se}_x\text{O}$ where $x = 0.1, 0.3, 0.5, 0.7, 0.9$.

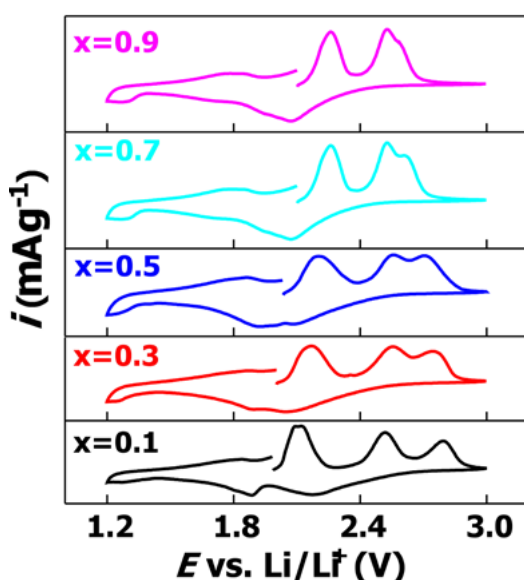
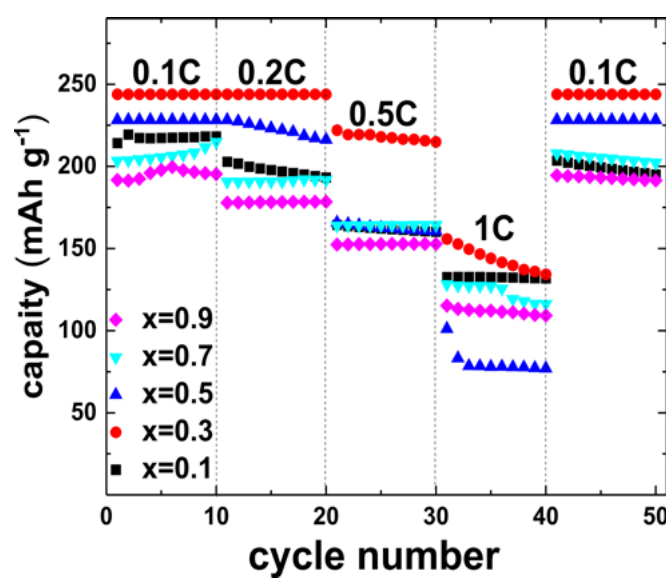


Abb. 3: Entladekapazitätserhaltungsprofil bei verschiedenen Stromstärken als Funktion der Zyklenzahl für die Serie $(\text{Li}_2\text{Fe})\text{S}_{1-x}\text{Se}_x\text{O}$ mit $x = 0.1, 0.3, 0.5, 0.7, 0.9$.
Fig. 3: Discharge capacity retention profile at different current rates as a function of cycle number for the series $(\text{Li}_2\text{Fe})\text{S}_{1-x}\text{Se}_x\text{O}$ where $x = 0.1, 0.3, 0.5, 0.7, 0.9$.



Published in

Tuning the electrochemical properties by anionic substitution of Li-rich $(\text{Li}_2\text{Fe})\text{S}_{1-x}\text{Se}_x\text{O}$ cathodes for Li-ion batteries, M. A. A. Mohamed et. al., *J. Mater. Chem. A* 9, (2021), 23095

References

- [1] D. Deng, *Energy Sci. Eng.* 3 (2015) 385
- [2] J. Lee et al., *Nature* 556 (2018) 185
- [3] K. Luo et al., *Nat. Chem.* 8 (2016) 684
- [4] K. Lai et al., *J. Am. Chem. Soc.* 139 (2017) 9645
- [5] K. Lai et al., *Inorg. Chem.* 57 (2018) 13296
- [6] Z. Lu et al., *J. Mater. Chem. A* 6 (2018) 5185
- [7] D. Mikhailova et al., *ACS Appl. Energy Mater.* 1 (2018) 6593
- [8] Y. Sun et al., *J. Am. Chem. Soc.* 141 (2019) 5640
- [9] A. Martinolich et al., *Chem. Mater.* 33 (2021) 378
- [10] M. Gorbunov et al., *Inorg. Chem.* 59 (2020) 15635

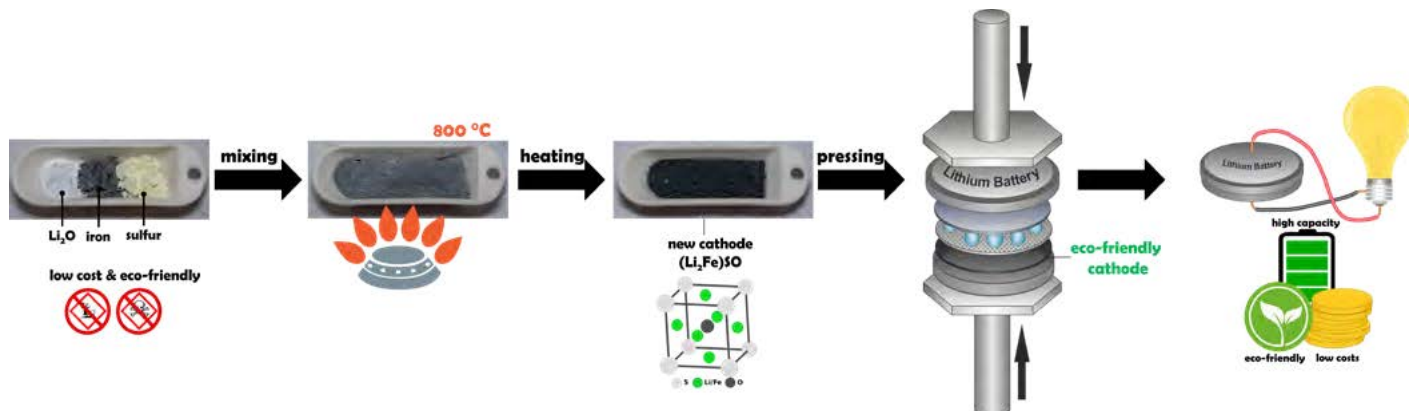
Funding

European Social Fund (ESF), Sächsische Aufbaubank (*LUKSIAK*, Project-ID: 100350438).

Cooperation

¹ Department of Chemistry, University of Oslo, Norway

Abb. 4: Schematische Darstellung der Herstellung und Verwendung von neuartigen Kathodenmaterialien aus dem Projekt *LUKSIAK*: Nach dem Mischen der kostengünstigen und ungiftigen Ausgangsstoffe erfolgt die Umsetzung bei einer Temperatur von 800 °Celsius zu dem neuartigen Kathodenmaterial. Im nächsten Schritt wird die Li-Ionen-Knopfzelle durch Zusammenpressen der Kathode und der einzelnen Komponenten hergestellt. Grafik: Nico Gräßler
Fig. 4: Schematic illustration of the production and use of novel cathode materials from the *LUKSIAK* project: After mixing the low-cost and non-toxic starting materials, the reaction takes place at a temperature of 800 °Celsius to form the novel cathode material. In the next step, the Li-ion button cell is produced by pressing the cathode and the individual components together. Graphic: Nico Gräßler



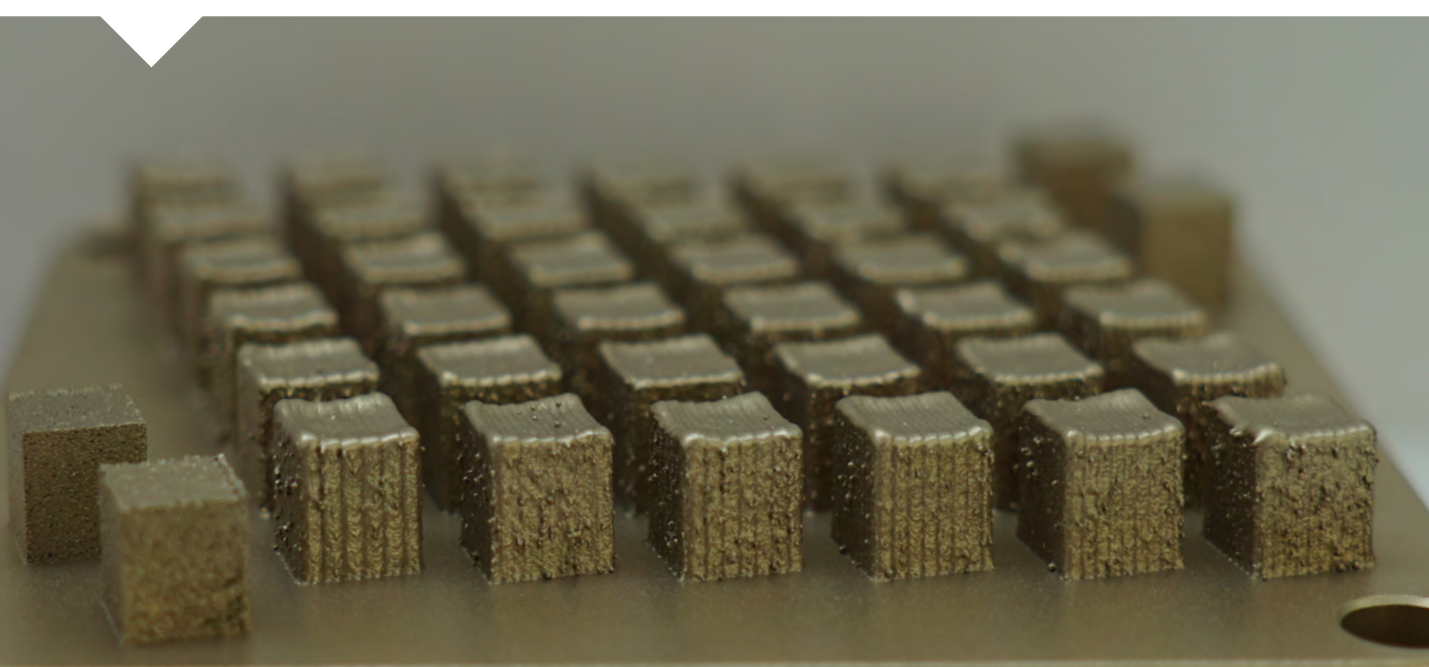
Laser powder bed fusion of ductile Cu-Al-Mn shape memory alloys - From general processing to functional parts

Tobias Gustmann, Nazim Babacan¹, Thomas Gemming, Uta Kühn, and Julia Hufenbach

Additive Fertigungstechnologien, wie das Laser-Strahlschmelzen, stellen wesentliche Treiber für die digitale Transformation, nachhaltige Prozessketten und On-Demand-Produktion dar [1]. Dies bezieht sich nicht nur auf Nischenanwendungen, sondern wird beispielsweise in Teilen der Luftfahrt sowie in der Medizintechnik angewendet. Das Verfahren kommt ohne den Einsatz von Werkzeugen oder Formkörpern aus und überzeugt durch eine ortsungebundene, flexible Fertigung und große Designfreiheit. Um das Potential des Strahlschmelzens für die industrielle Anwendung auszuschöpfen, bedarf es eines prozessangepassten Materialportfolios. Am IFW Dresden werden daher maßgeschneiderte Konstruktions- und Funktionswerkstoffe entwickelt und analysiert. Ein Beispiel stellt das Strahlschmelzen einer Kupfer-Aluminium-Mangan-Formgedächtnislegierung dar (Abb. 1), die sich als Alternative zu sehr kostspieligen NiTi-Basis-Legierungen etabliert hat.

Additive manufacturing technologies, viz. laser powder bed fusion (LPBF), play a significant role in digital transformation, sustainable process chains, and production on demand [1]. This holds for niche and main applications in the, e.g., medical engineering, or aerospace sector. The process does not require the use of tools or molds and is convincing due to its flexible production and great design freedom. The potential of the process can be unlocked if the material portfolio is constantly extended. In this field, researchers at the IFW Dresden are contributing in terms of advanced structural and functional material designs. One example is the processing of a Copper-Aluminium-Manganese shape memory alloy (Fig. 1) as an alternative to rather costly NiTi-based alloys.

Abb. 1: Cu-Basis-Formgedächtniskörper nach dem Laser-Strahlschmelzen (Infrarotlaser) mit hoher Aufbaurate (mittige Probenreihen).
Fig. 1: Cu-based shape-memory parts fabricated via laser powder bed fusion (infrared laser source) with increased built-up rates (sample rows in the center).



Flexible processing of novel alloys in a unique laser powder bed fusion laboratory

The LPBF process manifests unique manufacturing conditions for metal parts through layer-by-layer melting of predefined areas of an applied powder bed (Fig. 2a). The processing of thin powder layers on a massive substrate plate in combination with small melt volumes results in relative high cooling rates (approximately 10^6 K/s [2]). In addition, local remelting effects can further interact with the material. Thus, the process as a whole and, in particular, the applied process parameters have a strong impact on the microstructure and material properties. A key aspect in LPBF of novel materials is the final part quality, viz. porosity, which can be relatively high in contrast to conventional manufacturing [2, 3]. This can lead to early part failure. Therefore, a systematic approach to optimize the process for every material and a careful handling of the powders, depending on their quality, at all stages is needed. At the IFW Dresden, researchers can rely on a state-of-the-art lab infrastructure for the fabrication of LPBF parts. Depending on the machine setup, quantities being smaller than a volume of 100 ml up to a mass of several hundred kilograms of powder can be used for sample preparation and prototyping.

Depending on the weldability, additional adjustments of the process, viz. preheating the powder bed (200 to 650 °Celsius), have to be considered for novel alloys to fulfill further requirements. Here, several mobile IFW device modules, which were developed together with the Research Technology Department both for powder handling and preheating during processing, are available and allow an efficient processing of hard-to-weld and rather costly and exotic materials. The capabilities of the LPBF laboratory at the IFW Dresden also include a “Top Hat” laser source for advanced processing. This particular dual laser setup has been installed in 2020 and was updated with a permanent filter for safe and sustainable processing in 2021. “Top Hat” lasers are usually applied in welding and joining technologies. Due to their homogeneous energy density profile and increased beam diameter, alloys can be efficiently processed at much higher laser powers and layer thicknesses (higher rippled surfaces), which dramatically boosts

the built-up rate by a factor of two to ten. The first results imply promising results and the research in this field will be intensified in the near future.

Tailoring the shape memory properties of a Cu-Al-Mn shape memory alloy

In the past five to ten years, the LPBF process has attracted considerable attention for producing shape memory alloys (SMAs) [3, 4]. Regarding SMAs as functional materials, they significantly benefit from the versatility of LPBF. For instance, the recurring energy dissipated in the material during processing dictates the cooling rate and with it the microstructure, viz. grain size. Since important properties like transformation temperatures (TTs) of SMAs correlate with these parameters, LPBF can be considered as a powerful tool to fabricate near-net-shaped parts with a directly adjusted transformation and mechanical behavior. In addition, the relative high cooling rates also lead to a suppression of the precipitation of brittle phases which is seen as one of the major drawbacks regarding conventional manufacturing of, e.g., Ni-free Cu-Al-Mn shape memory alloys. Hence, the purpose of a recent study, as part of an Alexander von Humboldt project (fellow: N. Babacan), was to explore the potential of a Cu-SMA ($\text{Cu}_{71.6}\text{Al}_{17}\text{Mn}_{11.4}$, see powder in Fig. 2b) processed via LPBF.

Firstly, the effect of the processing parameters on the density was evaluated. Secondly, the microstructure, as well as the mechanical performance, were investigated. It has to be emphasized that LPBF of Cu-SMAs was intensively studied in the past five to eight years at the IFW Dresden. Alloys with increased TTs (high-temperature shape memory alloys – HT-SMAs) were investigated [3]. The processability of ductile ternary alloys (low degree of ordering in the austenite [5]) with Al contents of about 17 at. percent and TTs below room temperature was examined for the first time. The gained experiences in the field of Cu-based HT-SMAs were, therefore, a useful fundamental base. Specimens with 11 mm height and 5 mm diameter have been fabricated to obtain a suitable process window in which part density remains constant irrespective of the energy input. Pre-defined laser powers and scanning speeds have been also transferred to the processing of thinner-walled

geometries (Fig. 2c) in order to find the best fit between geometric-specific part quality and desirable material properties.

Based on the applied parameter variations and the comparison of all density values, one reference setup has been identified as a promising candidate for the manufacturing of both, near-net-shaped as well as complex designed and filigree lattice structures (Fig. 2d) [6]. The density of various parts produced in several batches remained very stable and revealed only a negligible number of residual pores (Fig. 2e). These findings are promising and special to Cu-SMAs because the processing of other Cu alloys, or pure Cu, is by far way more limited due to the higher reflectivity for infrared lasers.

An investigation of cast and additively manufactured samples revealed that the microstructure of specimens fabricated via LPBF is fully austenitic which is related to the process-specific high cooling rates. Thus, thermal post-processing of the material in contrast to the conventionally produced samples (austenite and unfavorable α phase) was not needed. These findings, in addition, directly reflected in the transformation behavior and the corresponding TTs which often dictate the conditions for a possible application. The measurement curves of the LPBF parts were smooth and the martensite-to-austenite

transformation finished at around -30 °Celsius. The transformation of the as-cast specimen was either not measurable or of a jerky nature (heat-treated) showing a decreased austenite-finish (A_f) temperature (-47 °Celsius). Lower A_f temperatures can be a critical factor for mechanical loading/unloading scenarios at room temperature. It limits the application temperature range and promotes local plastic deformation with respect to the applied load. To better clarify the influence of the processing on the mechanical behavior with respect to the obtained microstructure and transformation characteristics, experiments under quasi-static loading (Fig. 3a) as well as tests using an incremental loading/unloading approach (Fig. 3b) were performed. At least two samples of each condition have been tested. The controlled compression experiments until part failure served as a fundamental base to measure the general deformability depending on the microstructures and to pre-monitor the superelastic regime (stress-induced martensitic transformation, arrow in Figure 3a). A relatively large deformability has been observed for both sample states. This confirmed the general findings that are published for this particular type of alloy and clearly showed that Cu-Al-Mn materials can be used for shape-memory

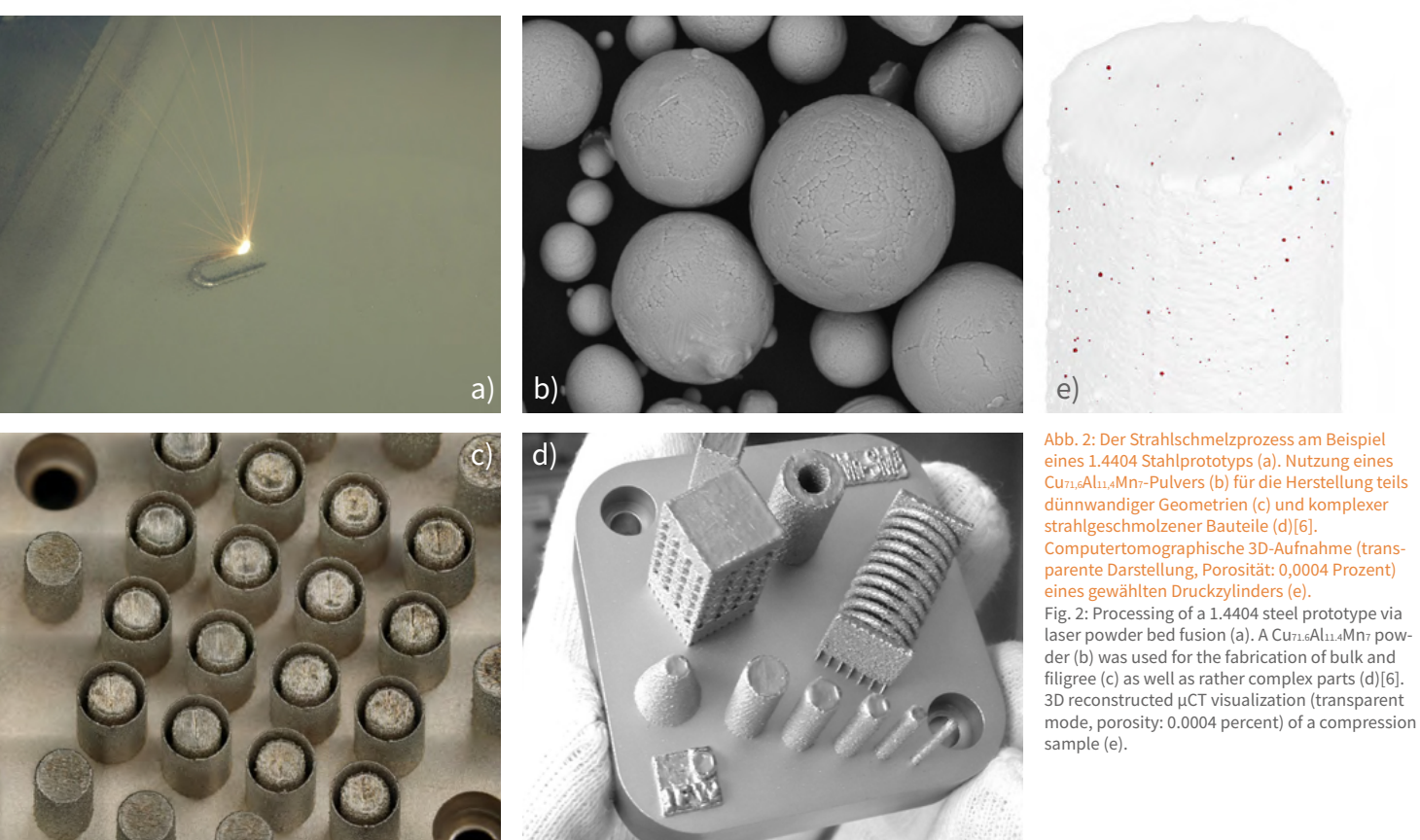


Abb. 2: Der Strahlgeschmelzprozess am Beispiel eines 1.4404 Stahlprototyps (a). Nutzung eines Cu_{71,6}Al_{11,4}Mn₇-Pulvers (b) für die Herstellung teils dünnwandiger Geometrien (c) und komplexer strahlgeschmolzener Bauteile (d)[6]. Computertomographische 3D-Aufnahme (transparente Darstellung, Porosität: 0,0004 Prozent) eines gewählten Druckzylinders (e).

Fig. 2: Processing of a 1.4404 steel prototype via laser powder bed fusion (a). A Cu_{71,6}Al_{11,4}Mn₇ powder (b) was used for the fabrication of bulk and filigree (c) as well as rather complex parts (d)[6]. 3D reconstructed µCT visualization (transparent mode, porosity: 0.0004 percent) of a compression sample (e).

purposes where ductility is key. However, large deviations occurred for the cast specimens under dynamic loading/unloading. This is specific to the relative coarse-grained and equiaxed microstructure (high anisotropy, critical grain boundary triple junctions). In contrast, the relative fine-grained and homogeneous microstructure of the LPBF specimens (inset in Fig. 3b) led to a more promising mechanical response. For instance, the increased yield stresses (star in Fig. 3a) of the detwinned martensite implied a much higher resistance against dislocation slip. Hence, a higher shape recovery rate is often measured even for strain values above 5 percent which is clearly shown in Figure 3b). Interestingly, LPBF samples in the as-built state, viz. without any thermal stabilization of the martensitic transformation, performed best. This offers great potential in terms of reducing overall process costs. In combination with fine-tuning the martensitic transformation in-situ during processing, or low-temperature (LT) direct aging, unique and affordable shape-memory parts with locally adjusted material properties are imaginable. Thus, further studies in the aforementioned field will be tackled to overcome final hampering factors and to be able to directly manufacture pronounced columnar-grained structures with excellent superelasticity.

References

- [1] D. Gu, et al., *Science* 372 (2021) 932
- [2] J. P. Oliveira, et al., *Mater. Des.* 193 (2020) 108762
- [3] T. Gustmann, et al., *Shape Mem. Superelasticity* 3 (2017) 24
- [4] J. van Humbeeck, *Shape Mem. Superelasticity* 4, (2018) 309
- [5] R. Kainuma, et al., *Metall. Mater. Trans.* 27A (1996) 2187
- [6] N. Babacan, et al., *Mater. Des.* 203 (2021) 109625

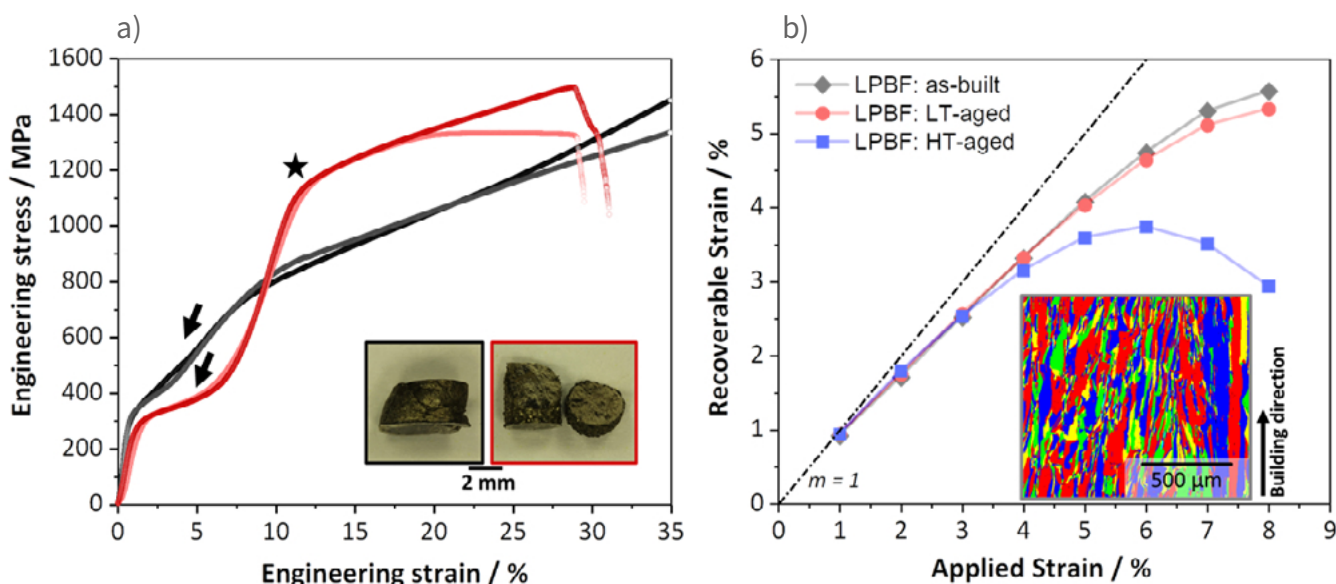
Funding

Alexander von Humboldt-Stiftung (AvH):
 Project title: “*Modulating functionality in selectively laser melted Cu-Al-Mn and Fe-Mn-Al-Ni shape memory alloys*”

Cooperation

¹Department of Mechanical Engineering, Sivas University of Science and Technology, Turkey

Abb. 3: Mechanisches Verhalten von Guss- (wärmbehandelt) und Strahlschmelzproben bis zum Versagen (a). Der Bildeinschub zeigt die gestauchten Probenstücke der jeweiligen Probenzustände. Übersicht des superelastischen Rückverformungsverhaltens an Raumtemperatur als Funktion der aufgebrachten Stauchung (b).
 Fig. 3: Compression behavior of heat-treated cast and as-built LPBF samples until fracture (a). The insets highlight the leftovers of the tested specimens. Compressive superelastic response of as-built and heat-treated (LT: low-temperature, HT: high-temperature) LPBF reference samples at room temperature (b).



Additive manufactured low modulus Ti-Nb with tailored microstructure for load-bearing bone implants

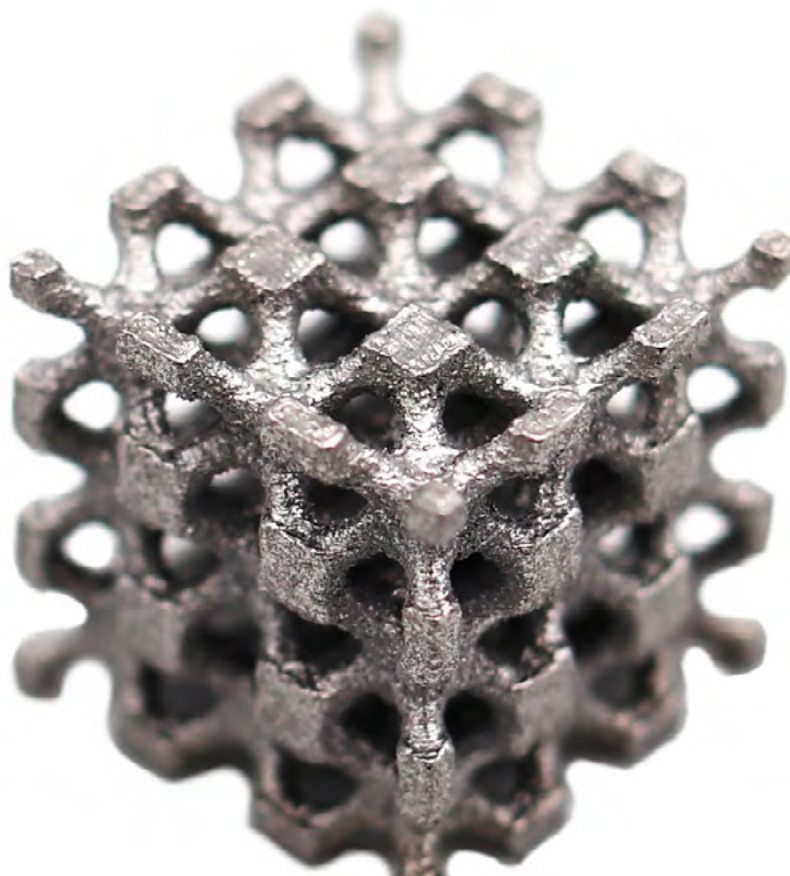
Stefan Pilz, Tobias Gustmann, Uta Kühn, Annett Gebert

Im Fokus unserer Forschung an biokompatiblen Materialien für Knochenimplantate stehen Beta-Legierungen von Titan und Niob, kurz: β -Ti-Nb Legierungen. Diese Materialien führen mit ihrer niedrigen E-Moduln zu einer verringerten Implantatsteifigkeit und tragen damit zu einem verbesserten Heilungsverlauf bei (Vermeidung von stress-shielding-Effekten). Additive Herstellungsverfahren wie Laser Powder Bed Fusion (LPBF) erlangen vor allem für neue Implantatdesigns zunehmend an Bedeutung. Wir präsentieren einen innovativen Ansatz zur Einstellung richtungsabhängiger sehr niedriger E-Moduln für die Legierung β -Ti-42Nb mit anisotropem Gefüge, das durch optimale LPBF Prozessparameter erhalten wurde. Es konnte eine E-Modulreduktion um etwa 30 Prozent im Vergleich zum isotropen Legierungszustand erzielt werden. Das eröffnet neue Möglichkeiten zur Herstellung von Knochenimplantaten, die optimal den mechanischen Belastungsbedingungen angepasst sind.

Biocompatible β -Ti-Nb alloys are in focus of our research on bone implant materials as their low Young's moduli can effectively reduce implant stiffness and thus, reduce stress shielding. Additive manufacturing technologies, e.g. laser powder bed fusion (LPBF), gain rapidly growing importance due to a great potential to fabricate new implant designs. We present an innovative approach for achieving orientation-dependent extremely low Young's moduli of β -Ti-42Nb via an anisotropic microstructure adjustment by identification of suitable LPBF parameters. A modulus reduction by around 30 percent compared to that of the isotropic alloy state was obtained. This paves the way to fabricate bone implants which are optimally adapted to applied mechanical loading.

Abb. 1: Gitterstruktur aus einer Ti-Nb Legierung hergestellt mittels Laser Powder Bed Fusion (LPBF). Die Gitterstruktur hat eine Seitenlänge von 12 Millimetern.

Fig. 1: Lattice structure of a low modulus Ti-Nb alloy fabricated by laser powder bed fusion (LPBF). This lattice structure has a side length of 12 millimeters.



New metallic implant materials with high biocompatibility and low Young's modulus

Currently, load-bearing bone implants in orthopedics and trauma surgery are made of titanium or alloys such as Ti-6Al-4V, 316L stainless steel and CoCr alloys. Despite their worldwide acceptance as high-performance implants in clinical use, those types reveal some drawbacks specifically at long-term implantation conditions. One problem is the release of harmful alloying elements, such as Al, V, Cr, Co, Ni species, due to wear or corrosion which can lead to serious complications and additional diseases. Therefore, implant materials consisting of only highly biocompatible elements are demanded. Another important clinical complication is bone resorption as consequence of stress shielding. It is caused by the high stiffness of currently used implants in comparison to the adjacent bone. Thereby, most of the physical loading is transferred by the implant and bypasses the surrounding bone thus, diminishing a mechanical stimulation of bone growth. As bone is a living tissue, it remodels dynamically by generation and resorption of bone tissue depending on the applied mechanical loading. An altered load transfer caused by a stiff implant leads to an "under-loading" of the bone compared to its natural state and as consequence, to bone loss and a reduced bone density. This reduction of bone stock can result in implant loosening or fracture of the weakened bone which causes too many cases of early revision surgery. The problem of stress shielding can mainly be attributed to the high Young's modulus values of the currently used alloys (120-220 GPa) when compared to healthy bone (10-30 GPa). It becomes even more severe in case of systemically diseased bone, e.g. in case of osteoporosis. To overcome the issues of limited biocompatibility and stress shielding, intense research is done to develop alloys with more cyto-compatible composition and with significantly lower Young's modulus values. Ti-(40-45wt. percent)Nb alloys are promising candidates to fulfill these requirements [1]. They show a superior corrosion behaviour and very low metal release rates, yielding excellent cytocompatibility which can be further adapted by chemical surface modifications [2]. Furthermore, they exhibit Young's modulus values as low as 60-65 GPa in isotropic solution-treated states due to

their β -type (body centred cubic) crystal structure. This is already around half the value of clinically used Ti-6Al-4V (120 GPa). Importantly, those can even be further reduced by taking advantage of the crystallographic orientation dependence of the Young's modulus. For example, the Young's modulus values of a Ti-45Nb single crystal vary from around 91 GPa along the <111> crystal direction, to 69 GPa along the <110> direction to only 40 GPa along the <001> crystal direction (Figure 2). Therefore, a single crystalline Ti-Nb implant with a <001> orientation along the main loading direction would be favorable to further markedly reduce the implant stiffness and in consequence, the stress-shielding problem. But until now, industrial processes to fabricate large Ti-Nb single crystals are not established and would be very cost intensive. An emerging technique that can create highly <001>-textured implant species is laser powder bed fusion (LPBF).

Adjusting the Young's modulus of a Ti-Nb alloy by laser powder bed fusion

LPBF, also known as selective laser melting (SLM), is an advanced additive manufacturing technology, that uses a laser beam to selectively melt metal powder in a layer-by-layer process. It offers the possibility to fabricate patient specific implants and to realize new implant designs that are not feasible with conventional manufacturing technologies and has therefore, attracted increasing interest in research and selected technology branches [3]. Furthermore, LPBF offers the opportunity to control the local microstructure and texture and therefore, the local mechanical properties of parts by applying different processing parameters [4]. This paves the way to fabricate implants (e.g., hip stems) that can be locally adapted to the applied mechanical loading. Usually process parameters such as the scanning speed and laser power or adjusted exposure strategies (e.g., vector rotation per layer, applied scanning pattern) are used to control the microstructure during LPBF processing. The size and the profile of the applied laser beam is an important, not often recognized feature that defines the microstructure of LPBF-processed specimen. Most of the available industrial LPBF systems are equipped with one ore multiple infrared

lasers with a near Gaussian intensity distribution and a beam diameter smaller than 100 µm. These configurations have two main limitations due to process instabilities at high laser powers: (1) ejection of spatters and (2) the increase of the build-up rate is limited. To overcome these issues high-power laser sources (around 1000 W) with a top hat intensity profile and an increased spot size were developed. Unlike the typical Gaussian intensity profile, the top hat profile has a flat region at the center, and a narrow “transfer region” at the edges of the beam where the energy declines to zero. A very strong $<001>$ texture development parallel to the building direction in combination with epitaxial grain growth is reported for specimen fabricated with a top hat laser. Such a microstructure would be beneficial for the fabrication of load-bearing implants with a reduced stiffness along the main loading direction. We have therefore conducted a comparative study with both types of laser sources and analyzed their influence on the microstructure and the mechanical properties of a novel β -type Ti-42Nb alloy.

Both beam profiles result in different solidification and cooling conditions and therefore, in substantial

differences in the microstructures (Figure 3). For the Gaussian laser, the complex and inhomogeneous heat flow during the process leads to a grain size in the range of 200 µm and only a very weak texture. By means of a top hat laser, a highly oriented and more uniform heat flow towards the substrate plate is realized, that results in a highly anisotropic microstructure, with a very strong $<001>$ texture parallel to the building direction and highly elongated grains (mm-range). Based on the crystallographic orientation dependence of the Young's modulus, such a microstructure should result in a strong elastic anisotropy with a low Young's modulus along parallel to the building direction. That assumption was confirmed by simulations based on the experimentally determined texture data as well as tensile tests that were conducted for selected loading directions. Here, a Young's modulus as low as 44 GPa was measured parallel to the building direction, which corresponds to a reduction of over 30 percent compared to the values measured for the nearly isotropic Gaussian reference samples (around 68 GPa) and the ones reported in literature for LPBF processed Ti-42Nb (e.g., 62 GPa). In contrast, a high

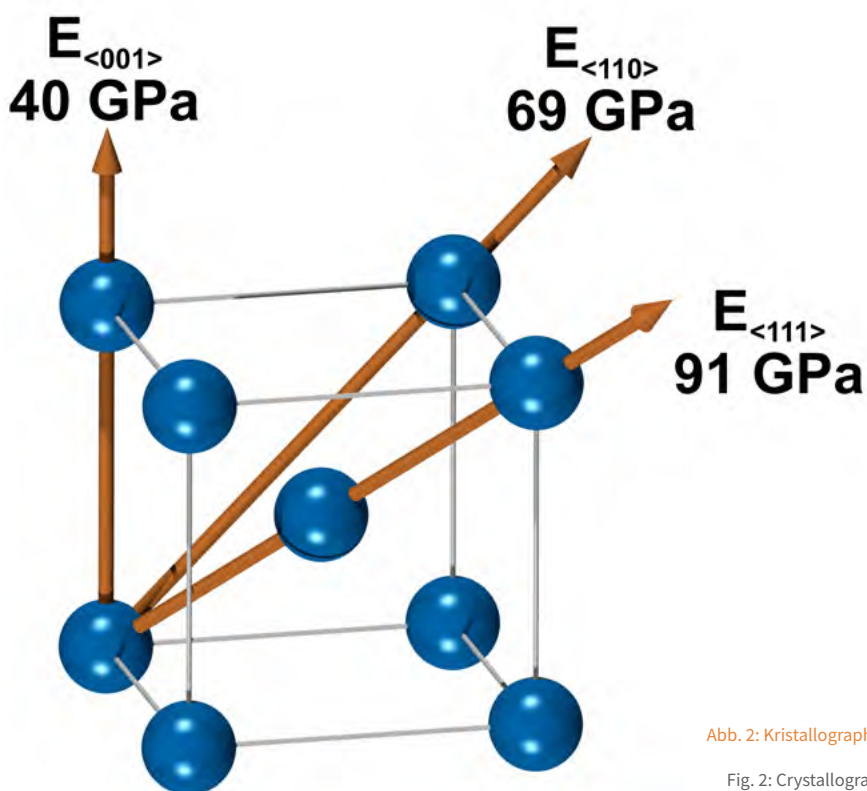


Abb. 2: Kristallographische Orientierungsabhängigkeit des E-Moduls der kubisch raumzentrierten Elementarzelle der Legierung Ti-45Nb.
Fig. 2: Crystallographic orientation dependence of the Young's modulus of the body centered cubic Ti-45Nb unit cell.

Young's modulus of 79 GPa is determined at an angle of 45° illustrating the high elastic anisotropy of the microstructure.

The obtained results reveal the unique capability of a top hat laser configuration to fabricate β -Ti-Nb parts with an adapted very low Young's modulus along the LPBF building direction. This new approach is a breakthrough towards the envisioned production of patient-specific implants with tailored mechanical properties for the reduction of stress-shielding effects. By applying a so-called Hull-Core-Strategy, that means combining a top hat (core: adapted part properties, very high build-up rates) as well as a Gaussian (hull: high precision and low surface roughness) laser, the fabrication of near-net-shape parts as well as sophisticated implant geometries, like implementation of lattices, becomes also possible.

Acknowledgements:

The authors thank M. Zimmermann and F. Günther from TU Dresden for a fruitful cooperation.

References

- [1] A. Reck et al., Mater Sci Eng A 761 (2019)
- [2] R. Schmidt et al., Mater Sci Eng C 108 (2020)
- [3] J. Ni et al., Mater Today Bio 3 (2019)
- [4] M. Otto et al., Metals 11 (2021)

Funding

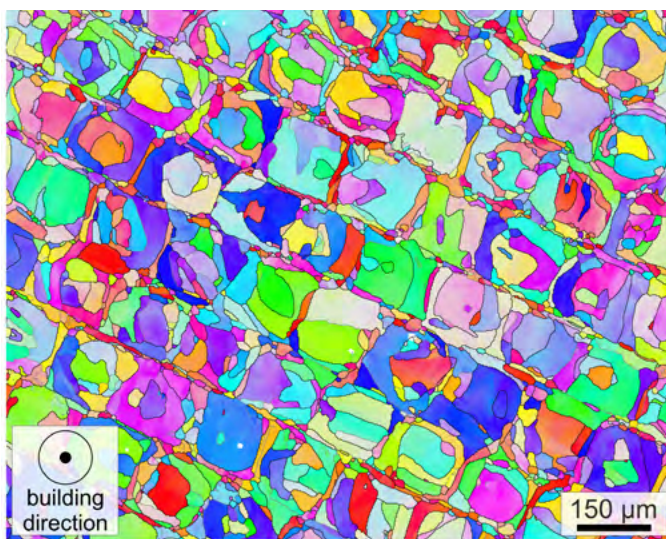
German Research Foundation

Cooperations

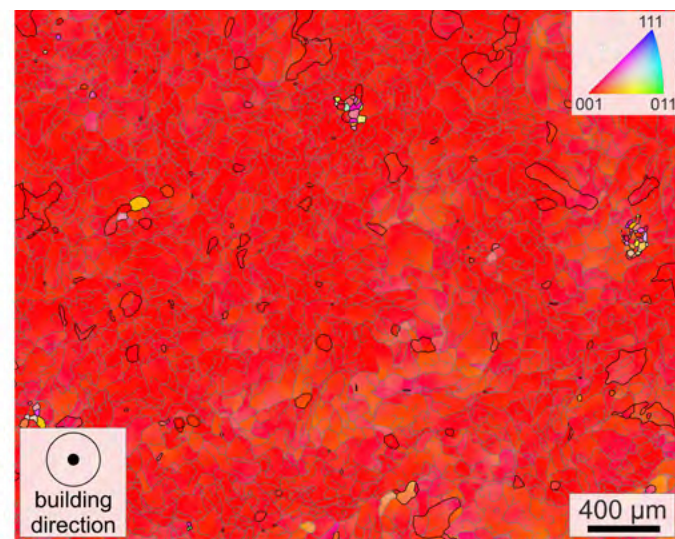
TU Dresden, Germany
Fraunhofer Institute for Material and Beam Technology IWS, Germany
University of Münster, Germany
Taniobis GmbH, Germany

Abb. 3: Inverse Polfigur-Karten von Ti-42Nb Proben, welche mittels Gauß- und Top-Hat-Laser hergestellt wurden. Die mittels Top-Hat-Laser hergestellten Proben zeigen dabei eine starke <001>-Textur parallel zur Baurichtung.
Fig. 3: Inverse pole figure (IPF) mappings of Ti-42Nb specimens processed with a Gaussian and a top hat laser configuration. For samples processed with a top hat laser configuration a strong <001> texture along the building direction is visible.

Gaussian laser



top hat laser



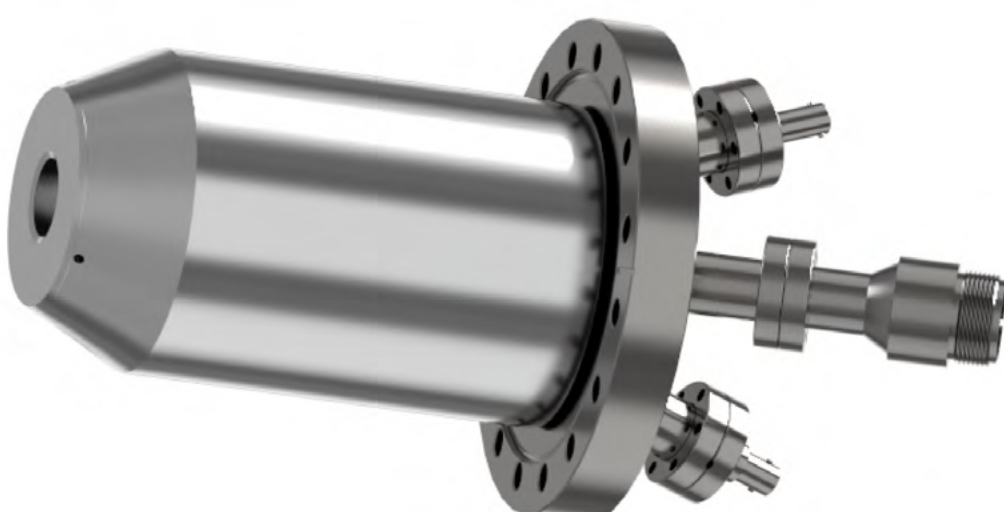
Elite electrons

Sergey Borisenko, Alexander Fedorov, Andrii Kuibarov, Saicharan Aswartham, Sabine Wurmehl, Bernd Büchner

Die elektronische Struktur spielt eine immer bedeutendere Rolle bei der Entwicklung neuartiger Quantenmaterialien. Die experimentelle Bestimmung dieser elektronischen Struktur war bisher sehr aufwändig und erfordert immer noch erhebliche Ressourcen. Das IFW Dresden hat eine neuartige Technologie entwickelt und patentiert, die es ermöglicht, die wichtigsten Eigenschaften des Elektronenverhaltens mit einem Bruchteil der verwendeten Zeit und Kosten im Vergleich zu den herkömmlichen Techniken zu ermitteln. Die Technologie wurde in einem Prototyp-Spektrometer implementiert. Derzeit vertreibt das IFW-Spin-off-Unternehmen *Fermiologics* erfolgreich eine kommerzielle Version des Geräts.

Electronic structure plays an increasingly important role in the development of novel quantum materials. Until now, the experimental determination of the electronic structure has been very laborious and still requires considerable resources. IFW Dresden has patented a novel technology that allows the determination of the most important properties of the electron behavior with a fraction of the time and cost compared to conventional techniques. The technology has been implemented in a prototype spectrometer, and currently an IFW spin-off company *Fermiologics* is successfully marketing a commercial version of the device.

Abb. 1: FeSuMa® 1.0 Elektronenspektrometer hergestellt von Fermiologics im IFW Dresden. Die 200-mm-Version dieses Geräts würde auf diese Seite passen. Dieses einfache und kompakte Design ist ein bedeutender Fortschritt gegenüber herkömmlichen halbkugelförmigen Analysatoren. Bild: Fermiologics
Fig. 1: FeSuMa® 1.0 electron spectrometer produced by Fermiologics in IFW Dresden. 200mm version of this device would fit on this page. This simple and compact design is a significant advance over conventional hemispherical analyzers. Image: Fermiologics



Everything that surrounds us depends on the movement of electrons. This motion holds atoms together and makes the existence of materials possible. The energy of only about 3 milligrams of electrons is sufficient to propel Tesla Roadster hundreds of kilometers over a period of hours [1]. This is because only a fraction of all electrons, namely those with the highest energies, determine most of the physical properties of a material, such as the ability to conduct electric current, reflect light, generate electromagnetic waves, magnetism, plasticity, and so on. Knowing exactly how these elite electrons behave would help us to better understand existing materials, improve them and design new ones.

One cannot describe the motion of every single electron, but it seems that the ones we are interested in just want a certain momentum in each direction. In theory, each metal at absolute zero temperature can be uniquely characterized by a Fermi surface - locus of endpoints of exactly such momenta vectors brought to the common origin. It is this, essentially three-dimensional construct, a kind of ID of the material, which is sufficient to derive many of its physical properties.

Angle-resolved photoemission spectroscopy (ARPES) is in principle capable of determining Fermi momenta, but so far only small parts of the 3D Fermi surfaces have been explored experimentally in detail. The main reason for this is that the experimental apparatus is still quite sophisticated and determining a single Fermi vector with high precision takes a relatively long time. Our new methodology is precisely designed to measure the 3D Fermi surfaces and allows the 2D slices of them to be seen live on the PC screen. A high-resolution 3D mapping can then be performed within tens of minutes. Surprisingly, the most technologically complicated element of our experimental setup has been known since the sixties of the last century.

Humanity has been aware of electric charges for a long time, but the first trajectories of electrons, were observed and photographed by Wilson in his famous cloud chamber just over a hundred years ago [2]. Well, those were the electrons emitted spontaneously from a radioactive material, but

how can one learn about electrons inside stable matter? This year is the anniversary of Einstein being awarded the Nobel Prize in Physics for explaining the photoelectric effect - a great scientific discovery whose importance can hardly be overestimated. It also provided the answer to our question - electrons can be ejected from the sample by ultraviolet light! Moreover, measuring the energies and momenta of such photoelectrons, one can derive the corresponding values inside the material by using the fundamental conservation laws. In particular, those photoelectrons, having the largest kinetic energies are our elite electrons.

It is the direction of the ejected photoelectrons, which became better visible in subsequent photographs published by Wilson [3], that attracted the attention of Arthur Compton. Although the author himself remarked that "The cathode rays appear to start in all directions..." [3], Compton noticed that electrons are emitted at a certain angle [4]. This event can be seen as the birth of ARPES, as later Compton and others became directly interested in the angular distribution of photoelectrons using Wilson's chamber and made groundbreaking contributions to the field. It is therefore not a surprise that both gentlemen shared Nobel Prize in 1927.

Cloud chambers were used to study electron trajectories until the 1930s, when the first channel multipliers based on secondary electrons were invented [5]. From then on, even a single electron could be detected because it produced an avalanche of secondary electrons, resulting in a noticeable current spike that can be picked up by common equipment. It was then realized that the performance of such multipliers is not a function of the channel length or the channel diameter separately, but only a function of their ratio [6]. Thus, almost an arbitrary reduction of size is possible. The first operational microchannel plate (MCP), an array of millions of miniature electron multipliers oriented parallel to one another, has been built in the beginning of sixties [7].

MCPs, being able to detect a two-dimensional distribution of photoelectrons, are intensely used in different types of ARPES analyzers until today. However, in order to determine 3D Fermi surface,

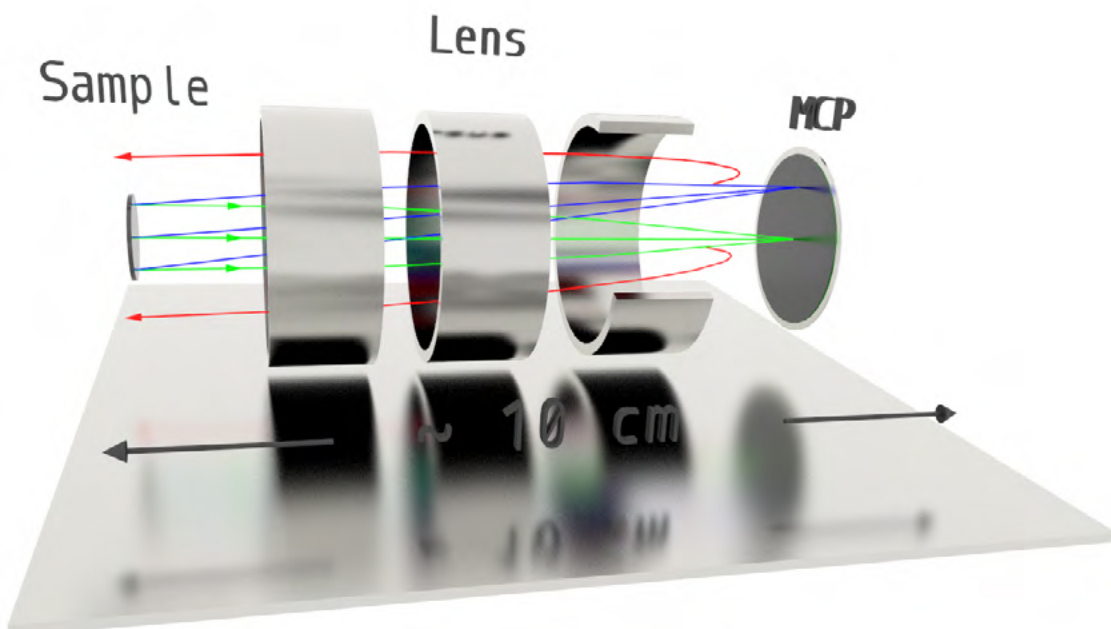
one needs to select photoelectrons having highest kinetic energy and count them in all directions. The directions corresponding to the local maxima in the angular distribution would be our sought-after Fermi momenta. This procedure has to be then repeated for a range of photon energies, since a single $h\nu$ allows probing only a sphere of particular radius in the momentum space. The smaller the step with which the photon energies are sampled, the denser the coverage of the momentum space with concentric spheres of different radius. In other words, one has to record photocurrent as a function of four variables - photon energy, kinetic energy and two angles defining the direction. But MCP allows to count electrons as a function of only two of them.

Nowadays, among the many different types of electron analyzers, the hemispherical ones have become the most popular. Their nontrivial schematic drawings even became associated with the term "ARPES", which you can easily check by typing these letters into your browser. However, this approach is based on the parallel detection of only one of the angles and kinetic energy, i.e. MCP records intensity distribution as a function of angle and kinetic energy, thus probing only a narrow stripe in

momentum space. Sampling another dimension in angular space requires many more measurements and leads to an anisotropic angular resolution, let alone full 3D mapping. There are other methods that use pulsed radiation and/or gratings as energy filters, but their efficiency with respect to measurements of 3D Fermi surfaces is even lower. As a consequence, only 2D Fermi surface maps or interpolations are available in the literature and our knowledge about the essentially three-dimensional ID of a given material remains strongly limited.

Recently, we proposed a novel technique [8] that simplifies the whole process and makes 3D Fermi surfaces easily accessible with high resolution. We use an electronic lens that focuses all photoelectrons that have left the surface at a certain angle to a single point directly on MCP, as shown in the Figure 1 with green and blue beams. In this way, we capture a more intuitive for angle-resolved photoemission two-dimensional angular distribution of intensity at once. The key novelty here is that we use the same MCP to select kinetic energies. Since we are only interested in the electrons with the largest kinetic energies, the only task is to filter out the electrons with lower kinetic energies. This is done simply by applying a negative retarding potential to the MCP

Abb. 2: Einfache ARPES. Die Methode ist schematisch dargestellt. Die Elektronen stammen von der Probenoberfläche. Die grünen Strahlen entsprechen der normalen Emission. Blaue Strahlen stellen Elektronen dar, die in einem Winkel von 10° in der vertikalen Ebene emittiert werden. Die roten Strahlen sind die Elektronen mit niedrigerer kinetischer Energie aus beiden Strahlen, die durch das Bremsfeld abgelenkt werden. Drei Zylinder stellen die Elektronenlinse dar. MCP ist der positionsempfindliche Detektor.
Fig. 2: Simple ARPES. Schematics of the method is shown. Electrons originate at the sample surface. Green rays correspond to normal emission. Blue rays represent electrons emitted at 10° angle in the vertical plane. Red rays are the electrons having lower kinetic energies from both beams, deflected by the retarding field. Three cylinders represent the electron lens. MCP is the position-sensitive detector.



front. The result is that the slower electrons (red beams in the Figure 1) do not reach the detector and we get a live image of a 2D section of the Fermi surface on the MCP. One can now successively take such images by varying the photon energies and plot only local maxima as a function of all three momentum components [9]. An example of such a dataset is shown in Figure 2 - this is the first truly high-resolution 3D Fermi surface map of TiTe₂ [10]. Electric vehicles, smartphones and skyscrapers are mostly made of metallic materials, each with a unique Fermi surface. Quantum technologies, including computing, are convincingly entering our everyday lives and require novel quantum materials that can be created through electronic structure design. We hope that similar to the progress in the transition from photography to cinematography, our technique will make material architecture in momentum space realistic.

Acknowledgement

SVB is grateful to BMWi for the support within the WIPANO project. The work is supported by BMBF via UKRATOP program.

References

- [1] <https://www.tesla.com/blog/weighty-matters-involving-electrons>
- [2] C T R Wilson, Proc R Soc London, Ser A, 85, 285-288 (1911)
- [3] C T R Wilson, Proc R Soc London, Ser A, 87, 277-292 (1912)
- [4] A H Compton, Bull Natl Res Count (US), 4, 1-56 (1922)
- [5] P. T. Farnsworth, Electron Multiplier, U.S. Patent N. 1, 969, 399 (1930)
- [6] J. L. Wiza, Nucl. Instrum. Methods 162, 587-601 (1979)
- [7] W. C. Wiley and C. F. Hendee, IRE Trans. Nucl. Sci. NS-9, 103 (1962)
- [8] Patent: S. Borisenko, DE102017130072, US11133166B2
- [9] This interactive animation visualizes the method in more details: <https://webdemo.3dit.de/ifw/detektor/>
- [10] S. Borisenko et al. preprint arXiv:2105.15055

Cooperations

Fermiologics, Dresden, Germany
 Department of Physics and Astronomy,
 Interdisciplinary Nanoscience Center (iNANO),
 Aarhus University, Denmark
 Kyiv Academic University, Ukraine
 Helmholtz-Zentrum Berlin für Materialien und
 Energie, BESSY II, Germany
 Max Planck Institute for Solid State Research, Germany
 Institute of Condensed Matter Physics, Ecole
 Polytechnique Fédérale de Lausanne, Switzerland

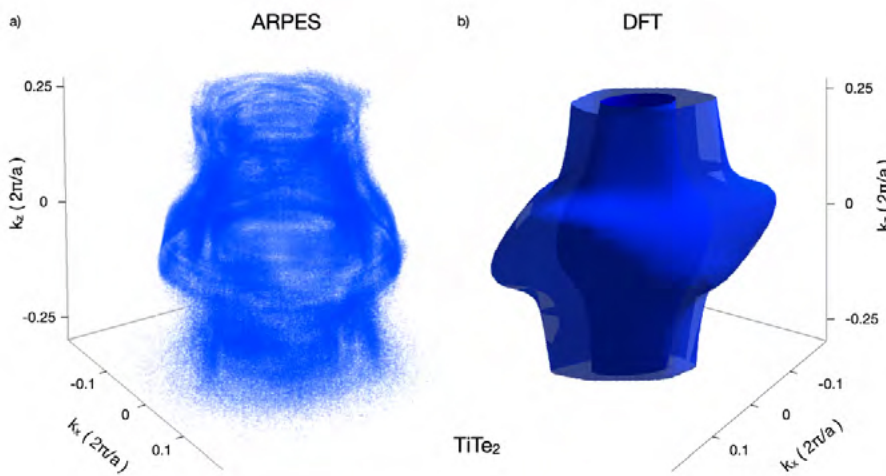


Abb. 3: Dreidimensionale Fermi-Fläche von TiTe₂
 a) Ein Voxelgramm der Photoemissionsintensität, aufgenommen mit dem FeSuMa-Analysator und Synchrotronlicht. Photonenergien zwischen 14 und 34 eV werden in 0,2 eV-Schritten abgetastet. Dargestellt sind Voxel innerhalb des normalisierten Intensitätsintervalls zwischen 0,012 und 0,020. Die Gesamtzahl der Punkte des zugrunde liegenden Datensatzes beträgt 1,71924e+07. Die durchschnittliche Intensität liegt bei 0,007, das absolute Maximum bei 0,041. b) Berechnete Fermi-Fläche von TiTe₂ im gleichen Impulsvolumen.

Fig. 3: Three-dimensional Fermi surface of TiTe₂
 a) A voxelgram of photoemission intensity recorded using FeSuMa analyzer and synchrotron light. Photon energies between 14 and 34 eV are scanned with 0.2 eV/step. Voxels within normalized intensity interval between 0.012 and 0.020 are shown. Total number of points of the underlying dataset is 1.71924e+07. Average intensity is 0.007, absolute maximum is 0.041. b) Calculated Fermi surface of TiTe₂ within the same momentum volume.



Trustees

Ministerium für Wissenschaft, Kultur und Tourismus

Executive Board

Administrative Director
Juliane Schmidt

Labor Council
Head: Mario Bloeck

Admin. Project Management
Friederike Jaeger

Legal Department
N. N.

Internal Audit and Compliance
Stefan Leipnitz

Safety and Environment
Uwe Schmiel

Institute for Integrative Nanosciences
Prof. Dr. Rudolf Schäfer (temp.)

Magnetic Microstructures and Devices
Prof. Dr. Rudolf Schäfer
Dr. Volker Neu
Dr. Andy Thomas

Quantum and Topological Photonics
Dr. Libo Ma
Dr. Caspar Hopfmann

Micro- and NanoBiomedical Engineering
Dr. Mariana Medina-Sánchez¹

Institute for Theoretical Solid State Physics

Prof. Dr. Jeroen van den Brink

Theoretical Solid State Physics
Prof. Dr. Jeroen van den Brink

Quantum Chemistry
Dr. Liviu Hozoi

Topological States of Interacting Matter
Dr. Ion Cosma Fulga⁵

Computational Methods for Correlated Materials
Dr. Oleg Janson³

Numerical Solid State Physics and Simulation
PD Dr. Manuel Richter

Finance and Controlling
Juliane Schmidt

Finance and Controlling
Dirk Rehn

Funding and Cooperation
Carsten Glück

Research Technology
Prof. Dr. Dirk Lindackers

Electrical Engineering
Karsten Peukert

Mechanical Engineering
Dr. Ralf Voigtlander

Information Technologies
Thomas Fichte

Building- and Facilitymanagement
Andreas Völker

Administrative Services
Friederike Jaeger

Human Resources
Michael Stritzke

Purchase and Disposal
Kristin Schwencke

Library
Jana Sonnenstuhl

Zahlen und Fakten 2021

Das IFW Dresden ist eines der größten Forschungsinstitute Sachsen und Mitglied der Leibniz-Gemeinschaft. Als Leibniz-Institut mit gesamtstaatlicher Bedeutung wird das IFW gleichermaßen vom Bund und dem Land Sachsen gefördert. Wir unterhalten enge Kooperationen mit Universitäten, anderen außeruniversitären Forschungseinrichtungen und Partnern aus der Industrie auf nationaler und internationaler Ebene. Neben dem wissenschaftlichen Auftrag ist die Ausbildung von Nachwuchs im wissenschaftlichen, technischen und administrativen Bereich ein wichtiger Bestandteil unserer Arbeit.

Sowohl Chancengleichheit als auch Familienfreundlichkeit sind erklärte Ziele des IFW Dresden. Im Jahr 2021 lag der Frauenanteil in wissenschaftlichen Positionen bei 29 Prozent und der Anteil von Frauen in wissenschaftlichen Führungspositionen bei 23 Prozent. Wir unterstützen unsere Beschäftigten dabei, Familienleben und berufliche Anforderungen in Einklang zu bringen. Seit dem Jahr 2007 ist das IFW Dresden mit dem "audit berufundfamilie" zertifiziert.

Facts und Figures 2021

IFW is one of the largest research institutes in Saxony and a member of the Leibniz Association. As a Leibniz Institute of national importance, the IFW is supported by the federal government and the state of Saxony. We maintain national and international cooperations with universities, other research institutions and industrial partners. In addition to the scientific mission, the training of the scientific, technical and administrative staff is an important part of our work.

Equal opportunities and family friendliness are declared goals of IFW Dresden. In 2021, the proportion of women in scientific positions was 29 percent and the proportion of women in scientific management positions 23 percent. We support our employees in reconciling family life and professional requirements. IFW Dresden has been certified with the "*audit berufundfamilie*" since 2007.



Finanzierung

Financing

Institutionelle Förderung durch Bund und Länder

Institutional funding by the federal government and the federal states

37,5 Mio. EUR

Eingeworbene Drittmittel

Third party funding

10,6 Mio. EUR

davon/ including:

Deutsche Forschungsgemeinschaft/ German Research Foundation: **6,1 Mio. EUR**

Leibniz-Gemeinschaft/ Leibniz Association: **0,5 Mio. EUR**

Bund und Freistaat Sachsen/ Federal Government and State of Saxony: **1,9 Mio. EUR**

Europäische Union/ European Union: **1,6 Mio. EUR**

Industrie/ Industrial contact: **0,2 Mio. EUR**

Stiftungen und andere Geldgeber/ Foundations and other donors: **0,3 Mio. EUR**

Beschäftigte

Personnel

Gesamtzahl der Beschäftigten: 31.12.2021

Personnel total: 31.12.2021

509

davon/ including:

Wissenschaftliches Personal/ scientific staff: **316**

Technisches Personal/ technical staff: **119**

Verwaltungspersonal/ administrative staff: **55**

Auszubildende/ apprentices¹⁾: **19**

Doktorand*innen/ doctoral students: **126**

Stipendiat*innen/ scholarship recipients: **47**

Gastwissenschaftler*innen/ guest scientists²⁾: **52**

zusätzlich betreute Doktor- Diplom- u. Masterarbeiten/

supervised PhD's and undergraduate students without contract: **20**

¹⁾ 6 verschiedene Ausbildungsberufe sowie Student*innen der Berufsakademie/ 6 different training occupations and students of the training academy

²⁾ Eingebunden in die IFW-Forschung, über Forschungskooperationen finanziert / Integrated in the IFW research, financed by research cooperations

Kuratorium Board of Trustees

Dr. Babett Gläser

Sächsisches Staatsministerium für Wissenschaft,
Kultur und Tourismus, Germany
Vorsitzende / Chair

Dr. Peter Schroth

Bundesministerium für Bildung und Forschung,
Germany
(bis Juli 2021/ up to July 2021)

Ingo Höllein

Bundesministerium für Bildung und Forschung,
Germany
(ab Juli 2021 / since July 2021)

Prof. Dr. Gerhard Rödel

Technische Universität Dresden, Germany

Prof. Dr. Manfred Hennecke

Berlin, Germany

Wissenschaftlicher Beirat Scientific Advisory Board

Prof. Dr. Mark Golden

Universiteit van Amsterdam, Netherlands
Vorsitzender / Chair

Prof. Dr. Robert H. Blick

Universität Hamburg, Germany

Prof. Dr. Andrey Chubukov

University of Minnesota, USA

Prof. Dr. Judith Driscoll

University of Cambridge, United Kingdom

Prof. Dr.-Ing. Horst Hahn

Karlsruhe Institute of Technology (KIT), Germany

Prof. Dr. David Johnson

University of Oregon, USA

Dr. Yves Küsters

Siemens AG, Germany

Prof. Dr. Nini Pryds

Danmarks Tekniske Universitet, Denmark

Prof. Dr. Roberto De Renzi

Università di Parma, Italy

Dr. Jügern Rapp

Robert Bosch GmbH, Germany

Prof. Dr. Maria-Roser Valenti

Goethe-Universität Frankfurt am Main,
Germany

Prof. Dr. Artur Zrenner

Universität Paderborn, Germany

Auszeichnungen Awards

Prof. Dr. Bernd Büchner

Aufnahme in die Nationale Akademie der Wissenschaften der Ukraine als ausländisches Mitglied für den Bereich Physik der Supraleitung / Election as a foreign Member of the National Academy of Sciences of Ukraine in Physics of Superconductivity

Prof. Dr. Jeroen van den Brink

Wissenschaftsscout für Theoretische Physik der Kondensierten Materie im Henriette Herz-Scouting-Programm der Humboldt-Stiftung / Science Scout for Condensed Matter Theoretical Physics in the Humboldt Foundation's Henriette Herz Scouting Program

Ina Jasmin Hill

VDI Hochschulpreis für die hervorragende Bachelorarbeit zum Thema "Microstructural and mechanical characterisation of biodegradable FeMn-based alloys for implantat applications" / VDI University Award for the outstanding bachelor thesis on the topic of "Microstructural and mechanical characterisation of biodegradable FeMn-based alloys for implantat applications"

Interne Auszeichnungen Internal Awards

Dr. Vineeth K. Bandari

Tschirnhaus-Medal of the IFW for excellent PhD theses

Dr. Daniel Dzekan

Tschirnhaus-Medal of the IFW for excellent PhD theses

Dr. Sebastian Selter

Tschirnhaus-Medal of the IFW for excellent PhD theses

Rufe

Call on Professorships

Dr. Jiri Orava

Jan Evangelista Purkyně University in Ústí nad Labem

Prof. Dr. Oliver G. Schmidt

Fudan-University Shanghai

TU Dresden Young Investigator TU Dresden Young Investigator

Dr. Aliaksei Charnukha, Dr. Cosma Fulga, Dr. Caspar Hopfmann, Dr. Oleg Janson, Dr. Axel Lubk

Stipendien Scholarships

Im Jahr 2021 waren 47 Stipendiat*innen am IFW Dresden tätig. Darunter waren 13 Geförderte von der Alexander von Humboldt-Stiftung, 6 Geförderte vom Deutschen Akademischen Austauschdienst DAAD und 18 Geförderte vom China Scholarship Council.

In 2021, 47 scholarship holders worked at IFW Dresden. Among them were 13 fellows of the Alexander von Humboldt Foundation, 6 fellows of the German Academic Exchange Service DAAD and 18 fellows of the China Scholarship Council.

Publikationen Publications

Im Jahr 2021 haben IFW-Wissenschaftler*innen 406 referierte Zeitschriftenartikel veröffentlicht, eine beträchtliche Anzahl von ihnen in sehr renommierten Zeitschriften.

In 2021, IFW scientists have published 406 refereed journal articles, a considerable number of them in high impact journals.

Eine ausführliche Publikationsliste ist auf unserer Homepage verfügbar:
A detailed list of publications is available on our homepage:
<https://www.ifw-dresden.de/research/publications>

Wissenschaftliche Konferenzen Scientific Conferences

March 26	3. UKRATOP-Workshop, online
May 25 - 27	Nature-Conference <i>Microrobots and Nanorobots for Biotechnology</i> , online
September 13 - 14	International Conference <i>Frustrated Magnetism and Topology</i> , IFW Dresden
October 10 - 14	BIOREMIA-Workshop <i>Science Communication and Presentation Skills</i> , Dresden
October 14	Farewell-Colloquium for Prof. Dr. Oliver G. Schmidt
October 14 - 15	SAW Symposium

Scan and find our
publications



Geistiges Eigentum / Patente

Intellectual Properties / Patents

Zum 31. Dezember 2021 hielt das IFW 90 Patente in Deutschland und 75 internationale Patente.
By 31 December 2021, the IFW holds 90 patents in Germany and 75 international patents.

Erteilte Patente

Patent grants

DE 10 2011 084 434.1 (11118 DE)

15.03.2021

Verfahren und Vorrichtung zur Messung von Kraftgradienten bei der Kraftmikroskopie
invented by Thomas Mühl, Julia Körner

DE 10 2011 088 360.6 (11134 DE)

10.11.2021

Resonanzdetektor
invented by Daniil Karnaushenko, Denys Makarov, Larysa Baraban, Oliver G. Schmidt

DE 10 2013 201 845.2 (11302 DE)

02.09.2021

Seltenerdmetallfreie permanentmagnetische Materialien
invented by Hannes Stummer, Sabine Wurmehl, Bernd Büchner

US 15/115380 (11402 US)

04.05.2021

Verfahren zur Herstellung der Beweglichkeit von immobilen Zellen
invented by Oliver G. Schmidt

DE 10 2015 204 112.3 (11503 DE)

20.04.2021

Biologisch abbaubare Eisenbasislegierungen und ihre Verwendung
invented by Julia Kristin Hufenbach, Uta Kühn, Annett Gebert, Jürgen Eckert

DE 10 2015 205 443.8 (11506 DE)

27.05.2021

Anodenmaterial für Lithium-Ionen-Batterien
invented by Maik Scholz, Rüdiger Klingeler, Marcel Haft, Sabine Wurmehl, Silke Hampel, Franziska Hammerath, Bernd Büchner

US 15/986399 (11526 US) 20.07.2021

Aufgerollte Energiespeicherbauelemente und Verfahren zu ihrer Herstellung
invented by Oliver G. Schmidt

DE 10 2015 224 938.7 (11528 DE)

15.06.2021

Verfahren und Vorrichtung zur Ermittlung von Kraftfeldern, Kraftfeldgradienten, Materialeigenschaften oder Massen mit einem System aus gekoppelten, schwingungsfähigen, balkenartigen Komponenten
invented by Christopher Reiche, Thomas Mühl, Julia Körner

EP 3 526 160 (11612 EP/EP/FR/GB)

DE 50 2017 011 190.4 (11612 EP/DE)

11.08.2021

Verfahren zur Herstellung mindestens eines dreidimensionalen Bauelementes zur uni-, bi-, tri- oder multidirektionalen Messung und/oder Generierung von Vektorfeldern und dreidimensionales Bauelement zur uni-, bi-, tri- oder multidirektionalen Messung und/oder Generierung von Vektorfeldern
invented by Daniil Karnaushenko, Dmitriy Karnaushenko, Oliver G. Schmidt

US 16/107431 (11613 US)

28.12.2021

DE 2017 214 638.9 (11613 DE)

23.08.2021

Dreidimensionale Mikro-Bauelemente und Verfahren zu ihrer Herstellung

invented by Daniil Karnaushenko, Dmitriy Karnaushenko, Oliver G. Schmidt

EP 3 487 622 (11618 EP/EP/CH/FR/GB)

DE 50 2017 010 856.3 (11618 EP/DE)

07.07.2021

Vorrichtung für die Mikrofluidik

invented by Andreas Winkler, Stefan Harazim

DE 10 2017 126 803.0 (11624-2 DE)

26.10.2021

US 16/461668 (11624 US)

27.07.2021

Vorrichtung und Verfahren zur Umwandlung thermischer Energie in elektrische Energie

invented by Kai Sellschopp, Sebastian Fähler, Anja Waske

DE 10 2017 211 592.0 (11626 DE)

05.11.2021

Verfahren zur Herstellung omniphober Oberflächen

invented by Julia Linnemann, Jakob Sablowski, Simon Unz, Michael Beckmann, Lars Giebel

DE 10 2017 130 072.4 (11715 DE)

20.05.2021

US 16/771705 (11715 US)

28.09.2021

Impulsauflösendes Photoelektronenspektrometer und Verfahren zur impulsauflösenden Photoelektronenspektroskopie

invented by Sergey Borisenko

DE 10 2018 110 730.7 (11813 DE)

02.12.2021

Verfahren, Vorrichtung und Anordnung zur Filtration magnetischer Partikel

invented by Anja Waske, Stefanie Hartmann

DE 10 2020 118 363.1 (12009 DE)

05.08.2021

Einrichtung zur Nutzung von thermischer Energie mit einem Formgedächtnismaterial

invented by Sebastian Fähler, Bruno Neumann

DE 10 2020 118 370.4 (12011 DE)

04.11.2021

Vorrichtung und Verfahren zur Umwandlung thermischer Energie in elektrische Energie

invented by Sebastian Fähler, Dietmar Berger, Daniel Dzekan, Anja Waske, Bruno Neumann

Patentanmeldungen

Priority patent applications

EP 21 184 069.9 (11922 EP)

06.07.2021

Verfahren zur Herstellung eines magnetokalorischen Drahts, magnetokalorischer Draht und dessen Verwendung

invented by Jens Freudenberg, Maria Krautz

EP 21 191 538.4 (12019 EP)

16.08.2021

Implantatwerkstoff und dessen Verwendung

invented by Julia Kristin Hufenbach, Martin Otto, Birgit Paul, Uta Kühn, Ulrich Rößler, Annett Gebert

PCT/EP2021/086691 (12022 PCT)

20.12.2021

Wälzlager für den Einsatz in temperaturwechselnder Umgebung und deren Verwendung

invented by Danny Baumann, Alexander Horst

PCT/EP2021/086696 (12023 PCT)**20.12.2021**

Biegeelastische Wellenkupplung

*invented by Danny Baumann, Alexander Horst***DE 10 2021 105 120.7 (12031 DE)****03.03.2021**

Speicher für Vorrichtungen zur additiven Fertigung von Bauteilen

*invented by Tobias Gustmann, Uwe Biscop***DE 10 2021 111 085.8 (12110 DE)****29.04.2021**

Vorrichtung und Verfahren zur Umwandlung thermischer Energie in mechanische Energie

*invented by Deepak Kamble, Dharshan Barkur, Sebastian Fähler***DE 10 2021 110 168.9 (12113 DE)****21.04.2021**

Verfahren zum Speichern und zur Anwendung von Flüssigwasserstoff

*invented by Dirk Lindackers, Hagen Schmidt, Jens Morgenstern, Christoph Haberstroh, Paul Sass***DE 10 2021 118 719.2 (12114 DE)****20.07.2021**

Vorrichtung und Verfahren zur elektrischen Charakterisierung von Eigenschaften von Stoffen, Baugruppen und/oder Bauteilen in einer Umgebung mit hoher Temperatur

*invented by Thomas Windisch, Hagen Schmidt, Robert Weser, Uwe Biscop***DE 10 2021 132 706.7 (12115 DE)****10.12.2021**

Mikronadeln und Verfahren zu ihrer Herstellung

*invented by Eric Eisner, Daniil Karnaushenko, Oliver G. Schmidt***Gebrauchsmusteranmeldungen**

Utility model applications

DE 20 2021 106 789.6 (22127 DE)**14.12.2021**

Schildartiges Bauelement für Vorrichtungen zur additiven Fertigung von Bauteilen

*invented by Tobias Gustmann, Uwe Biscop***DE 20 2021 106 791.8 (22128 DE)****14.12.2021**

Pulverspeicher für Vorrichtungen zur additiven Fertigung von Bauteilen

*invented by Tobias Gustmann, Uwe Biscop***Markenanmeldungen**

Trademark applications

DE 30 2021 114 604.2 (32117 DE)**27.08.2021**

Wortmarke HyLiq

DE 30 2021 114 605.0 (32123 DE)**27.08.2021**

Wort-/Bildmarke HyLiq

DE 30 2021 100 895.2 (31918 DE)**22.02.2021**

Wort-/Bildmarke DRESDA

Dissertationen

PhD Theses

Gizem Aslan Cansever

Effect of Impurities, Off-Stoichiometry and Site-Disorder on Structural and Magnetic Properties of Transition Metal Oxides Induced by Different Synthesis Conditions, TU Dresden

Vineeth Kumar Bandari

Towards Smart Motile Autonomous Robotic Tubular Systems (S.M.A.R.T.S), TU Chemnitz

Vasilii Dubrovin

Effects of non-covalent interactions on electronic structure and anisotropy in Ln-based SMMs: theoretical studies, TU Dresden

Le Feng

The Magnetic Properties and Microstructure of Hot Extruded MnAl-C-Based Alloys, TU Dresden

Selma Franca

Higher-order topological superconductors, TU Dresden

Tianbing He

Powder metallurgy of shape memory bulk metallic glass composites: synthesis, properties and deformation mechanism, TU Dresden

Sepideh Izadi

Processing and characterization of nanoparticle-based bulk quantum materials, TU Dresden

Valentin Labracherie

Electrical transport in nanostructures of the Weyl semimetal WTe₂, TU Dresden, Université Grenoble Alpes

Michaela Lammel

Advancing 3D Spintronics: Atomic Layer Deposition and Yttrium Iron Garnet Thin Films, TU Dresden

Piotr Lepucki

Development of self-assembled, rolled-up microcoils for nuclear magnetic resonance spectroscopy, TU Dresden

Fei Li

On-Chip 3D Interdigital Micro-Supercapacitors with Ultrahigh Areal Energy Density, TU Chemnitz

Zichao Li

Skyrmion-hosting B20-type MnSi films on Si substrates grown by flash lamp annealing, TU Dresden

Dijana Milosavljevic

Electronic structure calculations and microscopic modelling of complex structure property relations, TU Dresden

Gyuhyeon Park

Magneto-thermoelectric effects in magnetic metallic thin-films, TU Dresden

Francesco Scaravaggi

Electronic correlations and nematicity in 122 and 1111 Fe-based superconductors, TU Dresden

Sebastian Schimmel

Aufbau und Performance eines 30mK-Rastertunnelmikroskops und Untersuchungen zum Einzelmolekülmagnet Dy₂₂ScN@C₈₀ auf Substratoberflächen, TU Dresden

Lauritz Ule Schnatmann

Thermoelectric properties of SrSi Weyl semimetals, TU Dresden

Stefan Schwabe

Multikalorischer Effekt von Mn₃Ga-basierten Schichten auf ferroelektrischen Substanzen, TU Dresden

Sebastian Selter

Crystal growth, Structure and Anisotropic Magnetic Properties of Quasi-2D Materials, TU Dresden

Aoyu Tan

Magneto-transport Properties of Antiferromagnetic Topological Insulators MnBi₂Te₄ and MnBi₄Te₇, TU Dresden, Université Grenoble Alpes

Georgios Velkos

Magnetic studies on lanthanide-based endohedral metallofullerenes, TU Dresden

Bruno Weise

Untersuchung des martensitischen Phasenübergangs in der multifunktionalen Heusler-Legierung Ni-Co-Mn-Al, TU Dresden

Jonas Zehner

Untersuchung magneto-ionischer Effekte für elektrisch, schalbare, magnetische Domenenstrukturen, TU Dresden

Studentische Abschlussarbeiten Graduation theses

Syed Muhammad Abbas

Sn-based intermetallics as anodes for Li-ion batteries, Masterarbeit, TU Chemnitz

Carsten Albert

Entwicklung eines Leitfadens zur Erstellung von Begleittexten mit Interpretationshilfen für Exponate zur Quantenmechanik, Staatsexamen, TU Dresden

Benjamin Buchholz

Evaluation of the Breit-Hartree Contribution to the total energy of open atomic shells, Bachelorarbeit,
Universität der Bundeswehr, Hamburg

Syed Adeel Bukhari

Development and characterisation of PDMS, with varying degrees of cross-linking, to improve its viscoelastic and adhesive properties at cryogenic temperatures, Masterarbeit, TU Dresden

David Castellanos Robles

Soft microrobots made by droplet microfluidics, Masterarbeit, TU Chemnitz

Arthur Delan

Herstellung und Charakterisierung von supraleitenden Übergangsmetallnitriden, Bachelorarbeit, TU Dresden

Nora Fernandez Navas

Preparation of nanoporous gold nanowires from AuCu alloys as materials for biosensors, Masterarbeit, TU Chemnitz

Ruben Dario Gonzalez Betancourt

Magneto thermal transport study of antiferromagnetic MnTe thin films, Masterarbeit, TU Dresden

Yaqian Guo

High-throughput screening of collinear antiferromagnets for spintronic applications, Masterarbeit, TU Darmstadt

Ina Jasmin Hill

Microstructural and mechanical characterization of biodegradable Fe-Mn-C alloys for implant applications,
Bachelorarbeit, Hochschule Rhein-Waal

Julius Kohler

Effect of rotary swaging and heat treatment on microstructure and mechanical properties of a near- β Ti-₁₃Nb-₁₃Zr alloy, Masterarbeit, TU Dresden

Sanjeev Vishal Kota

On-demand generation of airborne droplets by means of surface acoustic waves, Masterarbeit, TU Chemnitz

Anncharlott Kusber

Photoelektronenspektroskopie an Eisen(II)-Phthalocyanin-Schichten, Bachelorarbeit, TU Dresden

Congcong Liu

Oxide und Sulfide von Eisen und Cobalt als Compositelektroden für Metall-Ionen-Batterien, Masterarbeit, TU Dresden

Bhumika Patel

Micro-acoustic liquid atomizer for application-relevant demonstrations, Masterarbeit, TU Dresden

Vira Shyta

Topological London theory and bosonization duality in anisotropic topological antiferromagnets, Masterarbeit, Kyiv Academic University

Kilian Srowik

Elektronenspinresonanzspektroskopie an magnetischen Van-der-Waals Verbindungen, Bachelorarbeit, TU Dresden

Zhengxing Zhou

Korrelation der lokalen und globalen Orientierungsverteilung in BaHfO₃ dotierten supraleitenden YBa₂Cu₃O_{7-x}-Schichten auf metallischen Teplaten, Diplomarbeit, TU Dresden

Yucheng Zhu

Energy storage devices based on Cu nanowires, Masterarbeit, TU Chemnitz



Materialforschung

für die Technologien von übermorgen



Impressum Imprint

Annual Report 2021

Herausgegeben durch das:
Leibniz-Institut für Festkörper- und
Werkstoffforschung Dresden
Helmholtzstraße 20, 01069 Dresden, Germany

www.ifw-dresden.de

Inhaltliche Verantwortung:
Prof. Dr. Bernd Büchner

Redaktion und Gestaltung:
Patricia Bäuchler

Bildnachweise:
IFW Dresden, sofern nicht anders angegeben

Druck:
ARNOLD group, Großbeeren

Dresden, Februar 2022





SACHSEN Dieses Institut wird mitfinanziert durch Steuermittel auf der Grundlage des von den Abgeordneten des Sächsischen Landtags beschlossenen Haushaltes.

